

國立交通大學

電子工程學系 電子研究所碩士班

碩 士 論 文

應用於數位電視廣播系統之通道等化器設計



Channel equalizer for DVB-T/H System

學生：馬英豪

指導教授：李鎮宜 教授

中華民國九十五年七月

應用於數位電視廣播系統之通道等化器設計

Channel equalizer for DVB-T/H System


研究生：馬英豪

Student：Ying-Hao Ma

指導教授：李鎮宜

Advisor：Chen-Yi Lee

國立交通大學
電子工程學系 電子研究所 碩士班
碩士論文



A Thesis
Submitted to Institute of Electronics
College of Electrical Engineering and Computer Science
National Chiao Tung University
in Partial Fulfillment of the Requirements
for the Degree of
Master of Science
in

Electronics Engineering

July 2006

Hsinchu, Taiwan, Republic of China

中華民國九十五年七月

應用於數位電視廣播系統之通道等化器設計


學生：馬英豪

指導教授：李鎮宜 教授

國立交通大學

電子工程學系 電子研究所碩士班

摘要



數位電視的發展為未來一大趨勢，在本論文中，我們將會介紹通道估測演算法以及在 2005 年 6 月，我們使用 0.18 微米製程實現了數位電視廣播系統基頻接收器的晶片設計。系統架構設計是根據歐規數位電視地面廣播系統的規格，以及考量通道非理想特性狀況。我們提出可適應性調整估測器的權重係數在時變通道中可達到降低雜訊干擾的效應。此外，通道響應使用散佈領航碼作二維通道響應的內插，我們分析多種多項式內插方法於不同通道下的效能。在硬體架構下，複數除法器佔了通道等化器大部分的硬體花費以及功率消耗，所以此處我們提出複數除法器的改善架構，在此架構可以有效率的降低硬體花費及功率消耗。可節省原本 90.5% 的硬體花費以及 59.9% 的功率花費。

Channel equalizer for DVB-T/H System

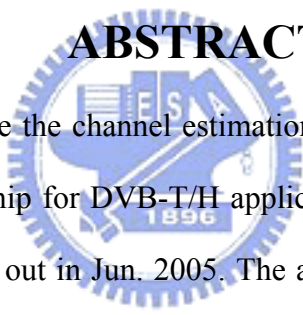
Student : Ying-Hao Ma

Advisor : Dr. Chen-Yi Lee

Institute of Electronics Engineering

National Chiao Tung University

ABSTRACT

The logo of National Chiao Tung University is a circular emblem with a gear-like border. Inside the circle, there is a stylized representation of a building or a shield with the letters 'NCTU' and the year '1896' at the bottom. The logo is semi-transparent and overlaid on the abstract text.

In this thesis, we introduce the channel estimation algorithm for DVB-T/H system, and COFDM basedband receiver chip for DVB-T/H applications. This chip is implemented with 0.18 μ m cell library and tapped out in Jun. 2005. The architecture is established according to the standard and several channel impairments. We propose the adaptive channel estimator for pilot signal which can average out the noise effects under portable environments. Furthermore, the channel response is estimated by means of two-dimension interpolation of scattered pilots. We analyze several polynomial interpolation methods under channels specified by standards. In architecture part, we can find the complex division is dominant the equalizer in cost and power. So we proposed the improved architecture for simplified the division architecture which hardware can be saved by 90.5% and power saved by 59.9% in divider itself.

誌 謝

從大四推徵進實驗室以來，Si2 這個大家庭已經與我共度了兩年多的時光。在這裡不但學到了許多專業知識，為人處事方面更是受益良多。

能完成這本論文，我最感謝的，是 李鎮宜教授這兩年多以來不厭其煩的指導與研究方向的指引，讓我在研究遇到挫折或困難時，得以重新找到突破瓶頸的方法。此外，也要感謝 李鎮宜教授為實驗室提供完善的研究設備，使我的研究得以順利完成。

在這裡，也要特別感謝 DVB group 的黎峰學長、昱偉學長、陳元老兒大夥一起努力 tape out 的那段不眠不休的日子真的很有趣，快速的拉近了彼此的距離跟感情，感謝大家這兩年來的腦力激盪與相互討論，不但使我在相關的研究領域有所精進，更學習到團隊合作的可貴。尤其是昱偉不只在功課以及其他方面幾乎都給了我很多寶貴意見跟實際的支持，讓我感到相當窩心的感動及感謝。還有可靠的 YY 以及三師兄，凶狠的 meeting 的砲火攻勢，讓我每次都很感挫折但卻覺得收穫良多。

還要感謝與我同居的家豪、侯康、阿龍，在這兩年內，我們一起經歷過許多風風雨雨，有歡笑沒有淚水，有你們的陪伴，使我這兩年的碩士生涯充滿了多彩多姿的回憶。

最後，我要由衷的感謝我的父母及家人，感謝你們多年來的栽培及細心，讓我能順利完成碩士的學業。僅將此論文獻給你們，以表達我最深的感激。

Contents

CHAPTER 1 . INTRODUCTION.....	1
1.1 MOTIVATION	1
1.2 INTRODUCTION TO DVB-T/H SYSTEM.....	2
1.3 ORGANIZATION OF THIS THESIS.....	7
CHAPTER 2 . CHANNEL ESTIMATION ALGORITHMS	8
2.1 INTRODUCTION TO CHANNEL ESTIMATION	8
2.2 MOTIVATION	10
2.3 CHANNEL ESTIMATOR FOR PILOT SIGNAL	11
2.4 TRANSFORM DOMAIN PROCESSING.....	15
2.5 INTERPOLATION PROCESS.....	18
2.5.1 <i>Interpolation in time domain</i>	19
2.5.2 <i>Interpolation in frequency domain</i>	22
CHAPTER 3 . CHANNEL EQUALIZATION ALGORITHMS.....	26
3.1 INTRODUCTION TO CHANNEL EQUALIZATION	26
3.2 MOTIVATION	27
3.3 PROPOSED DIVISION SCHEME	27
CHAPTER 4 . SIMULATION AND PERFORMANCE ANALYSIS	33
4.1 SIMULATION PLATFORM.....	33
4.2 CHANNEL MODEL.....	36
4.2.1 <i>Multipath Fading Channel Model</i>	36

4.2.2	<i>Mobile channel model</i>	38
4.2.3	<i>Doppler spectrum types</i>	40
4.2.4	<i>Additive White Gaussian Noise (AWGN)</i>	43
4.2.5	<i>Carrier Frequency Offset and Sampling Clock Offset model</i>	44
4.3	PERFORMANCE ANALYSIS	44
4.3.1	<i>Interpolation in frequency domain</i>	45
4.3.2	<i>Interpolation in time domain</i>	51
4.3.3	<i>Transform domain processing</i>	53
4.3.4	<i>Channel estimator for pilot signal</i>	55
CHAPTER 5. ARCHITECTURE AND IMPLEMENTATION		62
5.1	DESIGN METHODOLOGY	62
5.2	ARCHITECTURE OF THE DVB-T/H BASEBAND RECEIVER[28]	63
5.3	ARCHITECTURE OF CHANNEL EQUALIZER	67
5.3.1	<i>Channel estimation architecture</i>	67
5.3.2	<i>Channel equalization architecture</i>	70
CHAPTER 6. CONCLUSION AND FUTURE WORK		75
BIBLIOGRAPHY		76

List of Figures

FIG. 1.1 FUNCTIONAL BLOCK DIAGRAM OF DVB-T SYSTEM.....	3
FIG. 1.2 BLOCK DIAGRAM OF DVB-H CODEC AND TRANSMITTER.....	5
FIG. 2.1 TIME VARIANT CHANNEL FREQUENCY RESPONSE.....	9
FIG. 2.2 PILOT PATTERN IN DVB-T/H SYSTEMS	10
FIG. 2.3 CHANNEL ESTIMATION FUNCTION BLOCK DIAGRAM.....	11
FIG. 2.4 THE FILTER DIAGRAM.....	12
FIG. 2.5 THE MODIFIED FILTER DIAGRAM	13
FIG. 2.6 THE TIME VARIANT CFR AT 1 ST PILOT SUBCARRIER WITH DOPPLER.....	14
FIG. 2.7 BLOCK BASED ESTIMATOR MODEL & THE DYNAMIC CHANNEL MODEL.....	14
FIG. 2.8 ADAPTIVE WEIGHT FILTER AT EACH PILOT SUB-CARRIER	14
FIG. 2.9 THE RELATIONSHIP OF CFR AND NOISE.....	16
FIG. 2.10 THE CFR OF RAYLEIGH CHANNEL @ AWGN 25dB.....	16
FIG. 2.11 THE FLOW DIAGRAM	17
FIG. 2.12 THE 2X1D INTERPOLATION PROCESSING	19
FIG. 2.13 1 ST -ORDER PREDICTIVE INTERPOLATION IN TIME DOMAIN.....	20
FIG. 2.14 LINEAR INTERPOLATION IN TIME DOMAIN	21
FIG. 2.15 POLYNOMIAL INTERPOLATION IN FREQUENCY DOMAIN	22
FIG. 3.1 THE FORMAT (M, N) STRUCTURE.....	28
FIG. 3.2 THE BITS PRESENTATION OF DIVISION.....	28
FIG. 3.3 THE STATE DIAGRAM.....	29
FIG. 3.4 THE FLOW OF THE STATE 1	30
FIG. 3.5 THE FLOW OF THE MAIN FUNCTION IN STATE 2	31

FIG. 3.6 TIMING DIAGRAM.....	32
FIG. 4.1 OVERALL DVB-T/H PLATFORM.....	33
FIG. 4.2 THE BASEBAND RECEIVER DESIGN	35
FIG. 4.3 FUNCTIONAL BLOCKS OF INNER RECEIVER.....	35
FIG. 4.4 CHANNEL MODEL OF DVB-T/H SYSTEM.....	36
FIG. 4.5 CHANNEL RESPONSE OF RAYLEIGH AND RICEAN (K=10DB) CHANNEL.....	38
FIG. 4.6 TU6 MODEL	39
FIG. 4.7 DOPPLER SPREAD MODEL.....	40
FIG. 4.8 RAYLEIGH DOPPLER SPECTRUM GENERATOR	42
FIG. 4.9 RAYLEIGH FADING DOPPLER SPECTRUM BY JAKE’S MODEL.....	42
FIG. 4.10 RICE FADING DOPPLER SPECTRUM BY JAKE’S MODEL	43
FIG. 4.11 MSE OF DIFFERENT FREQUENCY INTERPOLATOR IN GAUSSIAN CHANNEL	46
FIG. 4.12 MSE OF DIFFERENT FREQUENCY INTERPOLATOR IN RICEAN CHANNEL	47
FIG. 4.13 MSE OF DIFFERENT FREQUENCY INTERPOLATOR IN RAYLEIGH CHANNEL	48
FIG. 4.14 COMPARISON DIFFERENT FREQUENCY INTERPOLATOR IN DYNAMIC CHANNEL.....	51
FIG. 4.15 DIFFERENT TIME INTERPOLATOR UNDER RAYLEIGH CHANNEL	52
FIG. 4.16 DIFFERENT TIME INTERPOLATOR UNDER TU6 CHANNEL	53
FIG. 4.17 PERFORMANCE BETWEEN DIFFERENT R UNDER RAYLEIGH CHANNEL	54
FIG. 4.18 PERFORMANCE BETWEEN DIFFERENT R UNDER TU6 CHANNEL.....	55
FIG. 4.19(A) PERFORMANCE UNDER STATIC RICEAN CHANNEL.....	57
FIG. 4.19(B) PERFORMANCE UNDER RICEAN CHANNEL WITH 70HZ DOPPLER.....	57
FIG. 4.20(A) PERFORMANCE UNDER STATIC RAYLEIGH CHANNEL	58
FIG. 4.20(B) PERFORMANCE UNDER RAYLEIGH CHANNEL WITH 70HZ DOPPLER.....	58
FIG. 4.21(A) PERFORMANCE UNDER TU6 CHANNEL WITH 10HZ DOPPLER.....	59
FIG. 4.21(B) PERFORMANCE UNDER TU6 CHANNEL WITH 30HZ DOPPLER	59
FIG. 4.21(C) PERFORMANCE UNDER TU6 CHANNEL WITH 150HZ DOPPLER	60

FIG. 5.1 PLATFORM-BASED DESIGN METHODOLOGY	63
FIG. 5.2 ARCHITECTURE OF THE DVB-T/H BASEBAND RECEIVER	65
FIG. 5.3 POWER PROFILING.....	65
FIG. 5.4 CHIP PHOTO	66
FIG. 5.5 THE ARCHITECTURE FOR 2X1D LINEAR INTERPOLATION CHANNEL EQUALIZATION	68
FIG. 5.6 $E[N^2/X^2]$ ESTIMATION BY CONTINUOUS PILOTS	69
FIG. 5.7 $E[D^2]$ ESTIMATION BY PREVIOUS 3 SAMPLES	69
FIG. 5.8 ARCHITECTURE FOR PROPOSED ESTIMATION	70
FIG. 5.9 HARDWARE ARCHITECTURE FOR PROPOSED CHANNEL EQUALIZATION	71
FIG. 5.10 PROPOSED ARCHITECTURE FOR 12 CYCLE	72
FIG. 5.11 PROPOSED ARCHITECTURE FOR 6 CYCLE	72
FIG. 5.12 TIMING DIAGRAM.....	73



List of Tables

TABLE 1-1 PARAMETERS FOR 8MHZ CHANNEL IN DVB-T STANDARD	4
TABLE 1-2 PARAMETERS FOR 8MHZ CHANNEL IN DVB-H STANDARD.....	6
TABLE 2-1 STORAGE REQUIREMENTS FOR INTERPOLATION IN TIME DOMAIN	22
TABLE 2-2 THE COEFFICIENTS LIST	25
TABLE 2-3 THE COEFFICIENTS RELATIONSHIP	25
TABLE 3-1 THE PARAMETER RELATIONSHIP IN STATE2	31
TABLE 4-1 TYPICAL URBAN RECEPTION (TU6) CHANNEL MODEL	39
TABLE 4-2 RURAL AREA RECEPTION (RA6) CHANNEL MODEL	40
TABLE 4-3 COMPARISON ON PERFORMANCE AND COST UNDER RAYLEIGH CHANNEL MODEL	52
TABLE 4-4 COMPARISON ON PERFORMANCE AND COST UNDER TU6 CHANNEL MODEL	53
TABLE 4-5(A) COMPARISON ON PERFORMANCE BETWEEN DIFFERENT B.....	60
TABLE 4-5(B) COMPARISON ON PERFORMANCE BETWEEN DIFFERENT B.....	61
TABLE 4-5(C) COMPARISON ON PERFORMANCE BETWEEN DIFFERENT B.....	61
TABLE 5-1 CHIP SUMMARY	66
TABLE 5-2 COEFFICIENTS TABLE FOR C1 AND C2	70
TABLE 5-3 SYNTHESIS AND GATE-LEVEL SIMULATION RESULTS	74
TABLE 5-4 COMPARISONS FOR COST AND POWER.....	74

Chapter 1 .

Introduction

In this chapter, we will describe the motivation of this research first. Introduction to the DVB-T/H standard will be made later. Finally, the organization of this thesis will be listed in the end of this chapter.

1.1 Motivation

Orthogonal frequency division multiplexing is a multicarrier transmission technique which uses parallel data transmission and frequency division multiplexing and was drawn firstly in 1960s [1-2]. Because of the high channel efficiency, OFDM is wildly applied in the new generation wireless access systems such as digital broadcasting systems [3-4] and wireless local area network [5-6].

In wireless communications, the receiver systems have to compensate the channel effects. Therefore, the channel equalizer and FEC techniques are exploited the system performance. The channel equalizer is used to recover original signal under non-perfect channel environment. In practical, the statistics of channel frequency response are not known, and time variant. In DVB-T/H system, we base on the pilots arrangement to estimate the channel and to compensate the non-perfect channel effects. Because of the DVB-T/H is (2K/4K/8K) point-modulation, which data in each OFDM is quite large. So different methods of collecting data for estimating the channel statistics will cost a lot of memory requirements. In DVB-H systems, the mobile issue is added. So the channel effects will degrade the performance seriously. This is a big challenge for defense the Doppler effects.

The objective of this thesis is to design a low complexity channel equalizer scheme, and performance of proposed method can defense about 70Hz Doppler effects under practical hardware cost.

1.2 Introduction to DVB-T/H system

Digital Video Broadcasting-Terrestrial (DVB-T) has been subjected to technical discussion for many years and undoubtedly been shown as a great success in delivering high quality digital television by terrestrial means [3]. DVB-T standard has been produced by European Telecommunication Standard Institute (ETSI) in Aug, 1997. It has been applied in many countries around the world such as Taiwan. Although the DVB-T reception can be applied in mobile environment, the ability of reception for handheld terminals is still not good enough because of its high operation power. Therefore, Digital Video Broadcasting-Handheld (DVB-H) was also proposed based on the DVB-T technology to provide broadcast services for handheld devices such as PDAs or mobile phones [7]. The detailed concepts of DVB-T and DVB-H will be illustrated later.

The transmission system of the DVB-T standard is shown in Fig. 1.1. It contains the blocks for source coding, outer coding and interleaving, inner coding and interleaving, mapping, OFDM modulation, and frame adaptation, respectively. In the case of two-level hierarchy, the functional block diagram of the system must be expended to include the modules shown in dashed line. After the MPEG2 transport multiplexer, a Reed-Solomon (RS) shortened code (204,188, t=8) and a convolutional byte-wise interleaving with depth I=12 shall be applied to generate error protected packets. As Fig. 1.1 shows, the outer interleaver is followed by the inner coder. This coder is designed for a range of punctured convolutional codes, which allows code rates of 1/2, 2/3, 3/4, 5/6, and 7/8. If two-level hierarchical transmission is used, each of two parallel inner codes has its own code rate. Afterward, the

inner interleaver is block based bit-wise interleaving. The constellation mapping for OFDM subcarriers operates with various modes after the inner interleaver. The constellation modes are QPSK, 16-QAM, 64-QAM, non-uniform 16-QAM, and non-uniform 64-QAM, respectively. The transmission channel bandwidth is 6MHz, 7MHz, and 8MHz, respectively.

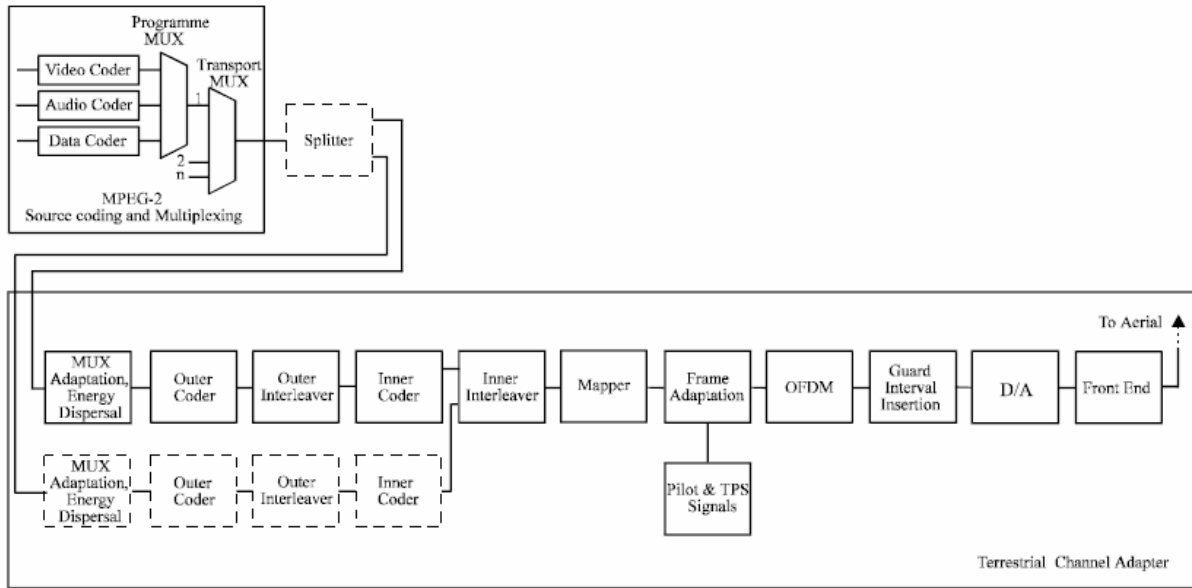


Fig. 1.1 Functional Block diagram of DVB-T system

The DVB-T system uses OFDM technique with various transmission parameters. The parameters for 8MHz channel bandwidth in DVB-T standard are listed in Table 1-1. Two modulation modes are defined: a 2k mode and an 8k mode. The 2k mode is suitable for short distance transmission and high speed mobile reception because of its short symbol duration and wide subcarrier spacing. On the contrary, the 8k mode is suitable for long distance transmission and deep multipath spread. Other parameters such as code rate, constellation mode, and guard interval length can also be decided properly according to the broadcasting channel condition of the local area.

An OFDM frame consists of 68 OFDM symbols and four frames constitute a super-frame. In addition to the transmitted data, an OFDM symbol contains several kinds of reference signals for synchronization and channel estimation such as scattered pilots,

continual pilots, and TPS (Transmission Parameter Signaling) pilots. Scattered pilots are inserted every 12 subcarriers and have an interval of three subcarriers in the next adjacent symbol. Continual pilots locate at fixed subcarrier index which contain 177 for 8k mode and 45 for 2k mode, respectively. Both scattered pilots and continual pilots are transmitted at boosted power level of 16/9 whereas the data subcarriers are normalized to 1, and modulated according to the PRBS (Pseudo Random Binary Sequence) sequence $(X^{11}+X^2+1)$. The TPS pilots are used for signaling parameters related to transmission scheme, i.e. to channel coding and modulation. The TPS pilots are defined over 68 consecutive OFDM symbols and transmitted in parallel on 17 TPS subcarriers for 2k mode and 68 for 8k mode. Each OFDM symbol conveys one TPS bit which is differentially encoded in every TPS subcarrier. The TPS information contains frame number, constellation, hierarchy, code rate, guard interval, FFT mode, and BCH error protection code, respectively. Unlike continual and scattered pilots, TPS pilots are transmitted as the normal power level of 1 with DBPSK modulation.

Table 1-1 Parameters for 8MHz channel in DVB-T standard

Parameter	8k mode	2k mode
Number of subcarriers K	6817	1705
Value of carrier number K_{min}	0	0
Value of carrier number K_{max}	6816	1704
FFT size N	8192	2048
Symbol duration T_U	896 μ s	224 μ s
Subcarrier spacing $1/T_U$	1.116KHz	4.464KHz
Spacing between K_{min} and K_{max}	7.61MHz	7.61MHz
Guard interval N_g/N	1/4, 1/8, 1/16, 1/32	1/4, 1/8, 1/16, 1/32

The DVB-H technology is a spin-off of the DVB-T standard. It is large extent compatible to DVB-T but takes into account the specific properties of the addressed

terminals- small, lightweight, portable, battery-powered devices in mobile environment. Unlike the DVB-T transport stream adopted from the MPEG2 standard, the DVB-H system is IP (Internet Protocol)-based, therefore the outer DVB-H interface is the IP interface. The IP data are embedded into the transport stream by means of the MPE (Multi Protocol Encapsulation) frame, an adaptation protocol defined in the DVB Data Broadcasting Specification [8]. One MPE frame contains one or more IP datagrams and has a maximum number of 1024 rows and a constant number of 255 columns. The block diagram of DVB-H codec and transmitter is as shown in Fig. 1.2.

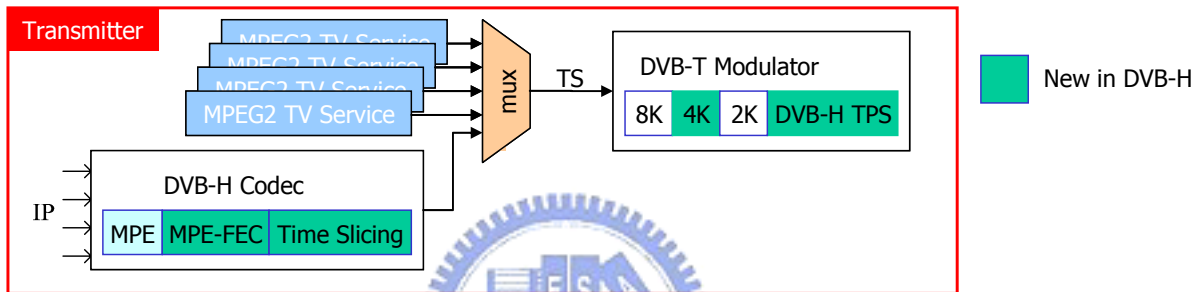


Fig. 1.2 Block diagram of DVB-H codec and transmitter

As we can see the DVB-H codec is composed of the MPE, MPE-FEC, and time slicing. In order to satisfy the low power issue in battery-powered terminals, a time-multiplexed transmission of different service is exploited. This technique, called time slicing, allows for selective access to desired data and results in a large battery power saving effect. The burst duration of time slicing is in the range of several hundred ms whereas the off-time may amount to several seconds. The lead time for power-on and resynchronization is assumed to be less than 250ms. Depending on the duty/turn-off ratio, the resulting power saving may be more than 90%. For mobile channels reception and long delay spread conditions, an enhanced error protection scheme on the link layer is needed. This scheme is called MPE-FEC and employs powerful channel coding and time interleaving. The MPE-FEC scheme consists of an RS code in conjunction with an extensive block interleaving. The RS (255, 191, 64) code is utilized to perform MPE-FEC error protection. Besides, a virtual block interleaving effect is

also performed by reading from and writing to the MPE frame in column direction whereas coding is applied in row direction.

As for the physical layer, the DVB-H is compatible with the DVB-T standard except some additional points. First, the DVB-H provides new TPS pilots which exploit the reserved TPS subcarriers defined in the DVB-T standard. The new contents of the TPS pilots provide the information about MPE-FEC and time slicing. Besides, an additional OFDM transmission mode and a new symbol interleaving method within the inner interleaver, 4k mode and in-depth interleaving, are also provided by the new TPS pilots. DVB-H provides an intermediate 4k mode with 4096-point FFT in the OFDM modulation. The 4k mode represents a compromise solution between the 2k and 8k mode to satisfy long distance transmission and mobile reception. The in-depth interleaving allows the symbol interleaver operates at 8k interleaving length while the 2k or 4k mode is applied to improve the interleaving performance. Besides, the DVB-H also supports 5MHz transmission channel bandwidth. The parameters for 8MHz channel bandwidth in DVB-H standard are listed in Table 1-2.

Table 1-2 Parameters for 8MHz channel in DVB-H standard

Parameter	8k mode	4k mode	2k mode
Number of subcarriers K	6817	3409	1705
Value of carrier number	0	0	0
Value of carrier number K_{min}	6816	3408	1704
FFT size N	8192	4096	2048
Symbol duration T_U	896 μ s	448 μ s	224 μ s
Subcarrier spacing $1/T_U$	1.116KHz	2.232KHz	4.464KHz
Spacing between K_{min} and	7.61MHz	7.61MHz	7.61MHz
Guard interval N_g/N	1/4, 1/8, 1/1	1/4, 1/8, 1/1	1/4, 1/8, 1/1
	6, 1/32	6, 1/32	6, 1/32

1.3 Organization of This Thesis

This thesis is organized as follows. In chapter 2, the signal models and the detailed algorithms of the proposed channel estimation scheme will be introduced. In chapter 3 we propose the modified architecture scheme. The simulation result and performance analysis will be discussed in chapter 4. Chapter 5 will introduce the design methodology, improved architecture of the proposed design and the chip summary of DVB-T/H [28]. Conclusion and future work will be given in chapter 6.



Chapter 2 .

Channel Estimation Algorithms

In this chapter, we introduce the signal model and the effect of time variant channel in DVB-T/H system first. The algorithms of channel estimation in different categories will be illustrated in later sections. Some comparison and discussion between developed and the proposed algorithms are also made.

2.1 Introduction to channel estimation

OFDM is a bandwidth efficient signal scheme for digital communications. In OFDM systems, it has received a lot of interest in mobile communication research lately. For wideband mobile communication systems, the radio channel is usually frequency selective and time variant. Furthermore, the channel transfer function of radio channel appears unequal in both frequency and time domains. Therefore, a dynamic estimation of the channel is necessary for the demodulation of OFDM signals. In wideband mobile channels, the pilot-based signal correction scheme has been proven a feasible method for OFDM systems. Most channel estimation methods for OFDM transmission systems have been developed under assumption of a slow fading channel, where the channel transfer function is assumed stationary within one OFDM data block. In practice, the channel transfer function of a wideband radio channel may have significant changes even within one OFDM data block. Therefore, it is preferable to estimate channel characteristic based on the pilot signals in each individual OFDM data block.

The major goal of channel estimation is to estimate the channel frequency response (CFR)

on the subcarrier. $h_l(n) = h(n, t) = \sum_i h_i(t) \cdot \delta(n - \tau_i)$ This equation is comprised of the actual channel impulse response (CIR) and the transmission filter. The transmitted signal is $s_l = \frac{1}{N} \sum_{k=0}^{N-1} X_{l,k} e^{j2\pi k \frac{n}{N}}$, so the received signal is $y_l(n) = h_l(n) \otimes s_l(n)$. The \otimes operator is convolution, and l means that it is the l th symbol. For the moment, we assume the channel to be constant during the transmission of one OFDM symbol denoted by $h_l(n)$. Furthermore, when the convolution operation in time domain transfers to frequency domain it becomes a multiplication operation. So the demodulated data symbol in frequency domain can be shown by $Y_{l,k} = FFT(y_l(n)) = H_{l,k} \cdot X_{l,k}$, and the $H_{l,k}$ is the channel frequency response.

$$H_{l,k} = FFT(h_l(n)) = \sum_{n=0}^{N-1} h_l(n) e^{-j2\pi \frac{kn}{N}} \quad (2-1)$$

For time variant channel environments, the CFR will vary as time and frequency. It is illustrated in Fig.2.1. The channel frequency response will change as time varying because of the Doppler effects. Furthermore, the multipath delay will cause the CFR with selective fading in frequency domain.

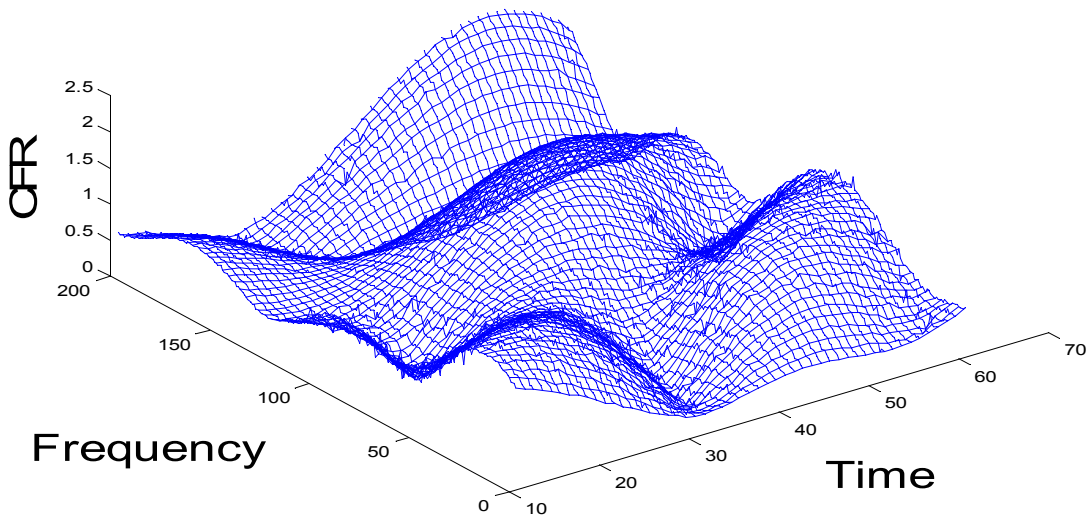


Fig. 2.1 Time variant channel frequency response

The pilot pattern is shown in Fig2.2. In DVB-T pilot carriers are transmitted together with data carriers, so that the channel transfer function is estimated both infrequency and in time. The use of pilots for estimation of the CFR is a main topic of research in OFDM system. Because of the scatted pilots the interpolation methods are adopted here too [9-11].

In this paper, the channel estimation methods for OFDM systems based on comb-type pilot sub-carrier arrangement are investigated. The channel estimation algorithm based on comb-type pilots is divided into pilot signal estimation and channel interpolation.

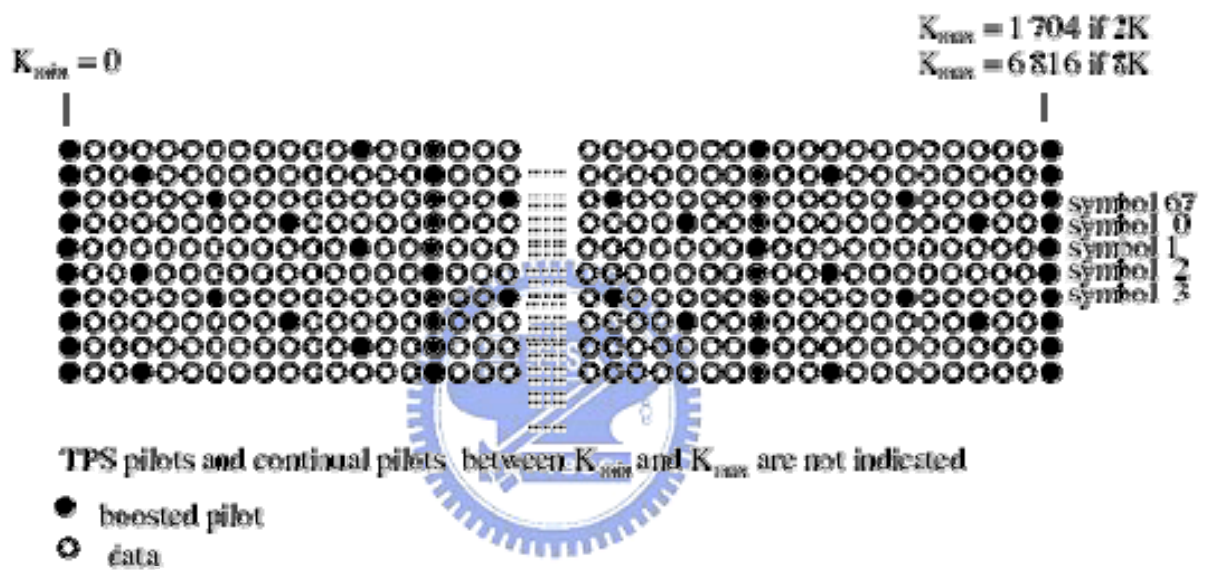


Fig. 2.2 Pilot pattern in DVB-T/H systems

2.2 Motivation

OFDM is the most prevalent modulation scheme in modern and future wireless communication systems. However, in mobile reception, a loss of sub-carrier orthogonality due to Doppler spread leads to inter-carrier interference. There are several estimation methods, like Wiener filter [9] and MMSE [12] estimator. Furthermore, there are several ICI cancellation schemes [13]. The complexity of these methods is proportional to the number of adjacent carriers which are used to cancel ICI. Besides, they have an important assumption, that the channel state information (CSI) is known. This assumption is impractical in reality,

especially during mobile environment. Here, we will propose the method which can implement efficiently and realizable methods. In following content, we will introduce the proposed channel estimation scheme.

In this paper we assume that the channel is time variant. Therefore, the channel frequency response (CFR) for present symbol should be obtained independently. The proposed channel estimation method based on pilot signals and transform domain processing is depicted in Fig. 2.3.

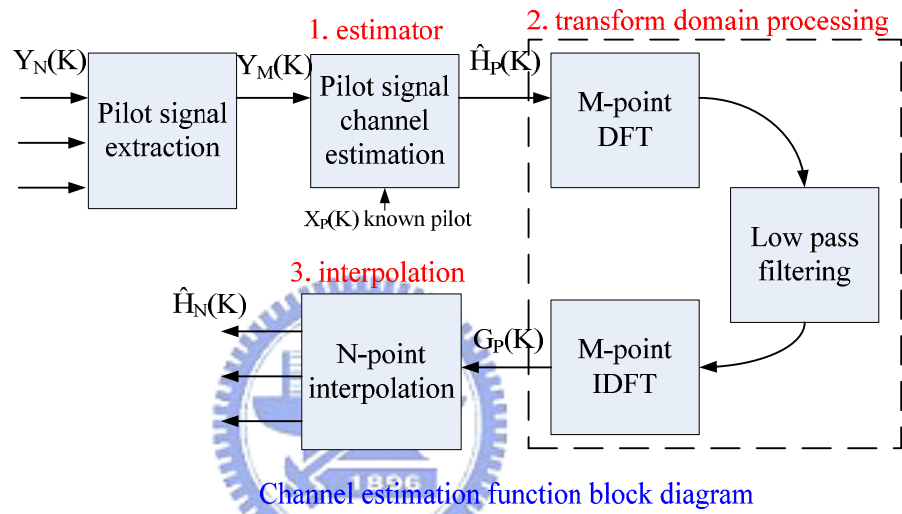


Fig. 2.3 Channel estimation function block diagram

Here we will focus on these three parts. First, the estimator can get the CFR at pilot location, and second, filtering can reduce the noise effect. Finally, we can get the CFR of whole symbol by interpolation methods. The three key points will be discussed in following.

2.3 Channel estimator for pilot signal

When we receive the receiving data $Y_N(K)$, we will extract the pilot signal $Y_M(K)$. The first key point is to get the CFR at pilot location $H_P(K)$ by $Y_M(K)$ and known pilot data $X_P(K)$. We can use LS estimator directly by $\hat{H}_p(k) = Y_M(k) / X_p(k)$. However, this estimator will be easily affected by noise. To reduce the MSE of the LS estimator, we rely on a filter method based in the LS estimator. In fact, in most slowly variant channel environment, this estimator

can get better improvement [14-16]. We propose an adaptive filter which can get better performance in slowly variant channel, and it will not degrade the performance in fast variant channel. In order to reduce the estimation error, the predicted estimated is a weighted average if the pilot-based estimate and a previous estimated. The formulation is following (2-2), where $\alpha_1=1$ and $\alpha_0=0$ initially. The filter diagram is shown in Fig.2.4.

$$\hat{H}_{l+1,k} = \alpha_{l+1}\tilde{H}_{l+1,k} + \alpha_l\hat{H}_{l,k} = \alpha_{l+1}Y_{l+1,k} / X_{l+1,k} + \alpha_l\hat{H}_{l,k}, \alpha_{l+1}, \alpha_l \in [0,1] \quad (2-2)$$

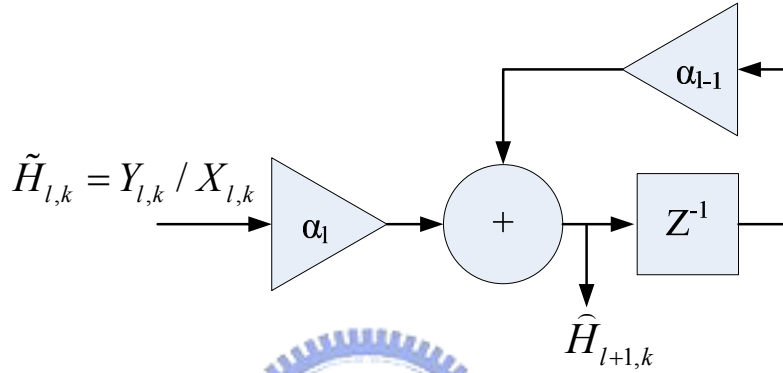


Fig. 2.4 The filter diagram

The weights α are chosen in order to minimize the MSE of the estimate. Furthermore, we propose an algorithm to decide the weights. Because of the standard, the scatter pilots is four symbols a cycle, here we use three taps FIR. The formulation becomes to (2-3), and MSE is (2-4).

$$\begin{aligned} \hat{H}_0 &= \alpha_0\tilde{H}_0 + \alpha_0\alpha_{-1}\tilde{H}_{-1} + \alpha_{-1}^2\tilde{H}_{-2} \\ &= \alpha_0(H_0 + \frac{N_0}{X}) + \alpha_0\alpha_{-1}(H_{-1} + D_1 + \frac{N_{-1}}{X}) + \alpha_{-1}^2(H_{-2} + D_2 + \frac{N_{-2}}{X}) \end{aligned} \quad (2-3)$$

$$\begin{aligned} MSE &= E(\hat{H}_0 - H_0)^2 \\ &= E[\alpha_0(H_0 + \frac{N_0}{X}) + \alpha_0\alpha_{-1}(H_{-1} + D_1 + \frac{N_{-1}}{X}) + \alpha_{-1}^2(H_{-2} + D_2 + \frac{N_{-2}}{X}) - H_0]^2 \\ &= E[(\alpha_0 + \alpha_0\alpha_{-1} + \alpha_{-1}^2 - 1)H_0 + \alpha_0\alpha_{-1}D_1 + \alpha_{-1}^2D_2 + \alpha_0\frac{N_0}{X} + \alpha_0\alpha_{-1}\frac{N_{-1}}{X} + \alpha_{-1}^2\frac{N_{-2}}{X}]^2 \end{aligned} \quad (2-4)$$

where D_i is caused by time variant channel and N_i is the AWGN noise. In MSE (2-4), we assume the CFR H_0 is much bigger than D_i and N_i . $|H| \gg |D_i|, |H| \gg \left| \frac{N_i}{X} \right|$

Under this assumption, the first term in (2-4) will dominant the MSE, so we let coefficient of

the first term equal to zero.

$$(\alpha_0 + \alpha_0\alpha_{-1} + \alpha_{-1}^2 - 1)H_0 = 0 \quad (2-5)$$

$$\alpha_0 + \alpha_0\alpha_{-1} + \alpha_{-1}^2 - 1 = 0 \quad (2-6)$$

$$\alpha_{-1} = \frac{-\alpha_0 \pm \sqrt{\alpha_0^2 - 4(\alpha_0 - 1)}}{2} = \frac{-\alpha_0}{2} \pm (1 - \frac{\alpha_0}{2}) = (1 - \alpha_0)$$

We can find the relationship between α_0 and α_{-1} is shown in (2-6).

So we define the weights

$$\alpha_0 = (1 - \beta) \quad (2-7)$$

$$\alpha_{-1} = \beta$$

So the diagram will become to Fig.2.5.

$$\hat{H}_{l+1,k} = (1 - \beta)\tilde{H}_{l+1,k} + \beta\hat{H}_{l,k} = (1 - \beta)Y_{l+1,k} / X_{l+1,k} + \beta\hat{H}_{l,k}, \beta \in [0, 1] \quad (2-8)$$

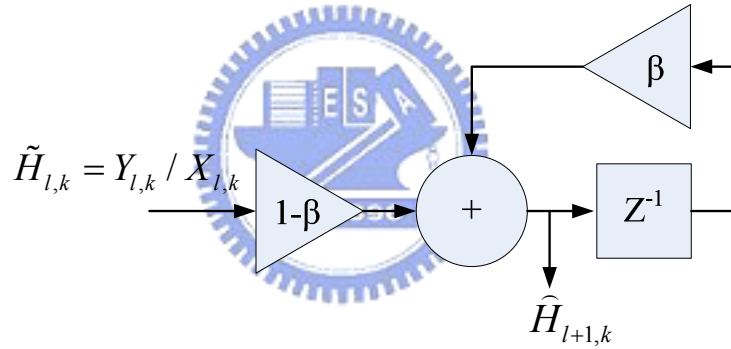


Fig. 2.5 The modified filter diagram

In Fig.2.6 we can find the time-variant CFR at someone sub-carrier in Ricean channel with different Doppler effects. CFR will change more seriously as Doppler effects increasing.

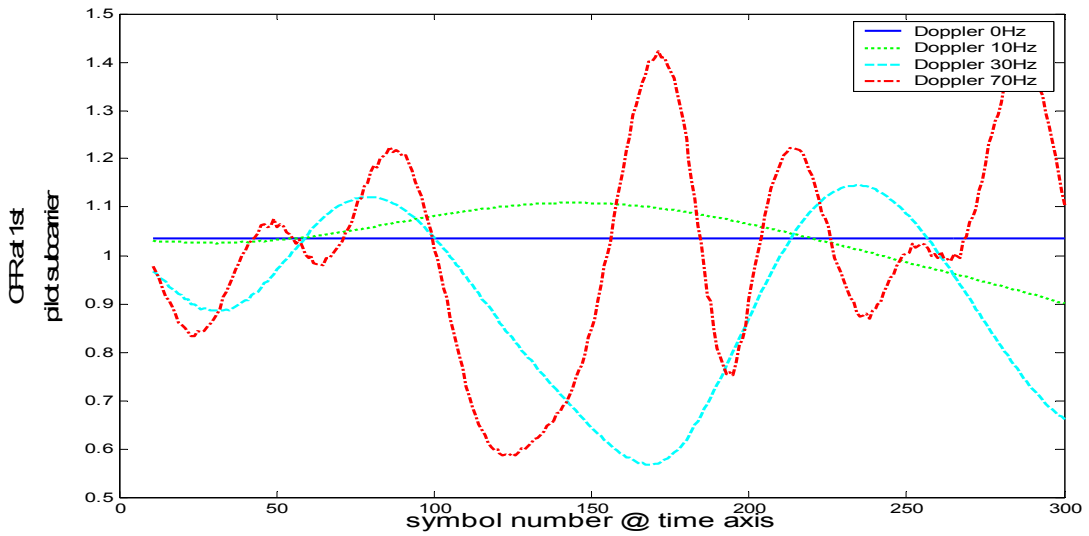


Fig. 2.6 The time variant CFR at 1st pilot subcarrier with Doppler

Fig. 2.7 shows the model we use, and we can find D_i is like linear variance. We define dynamic channel model in Fig. 2.7.

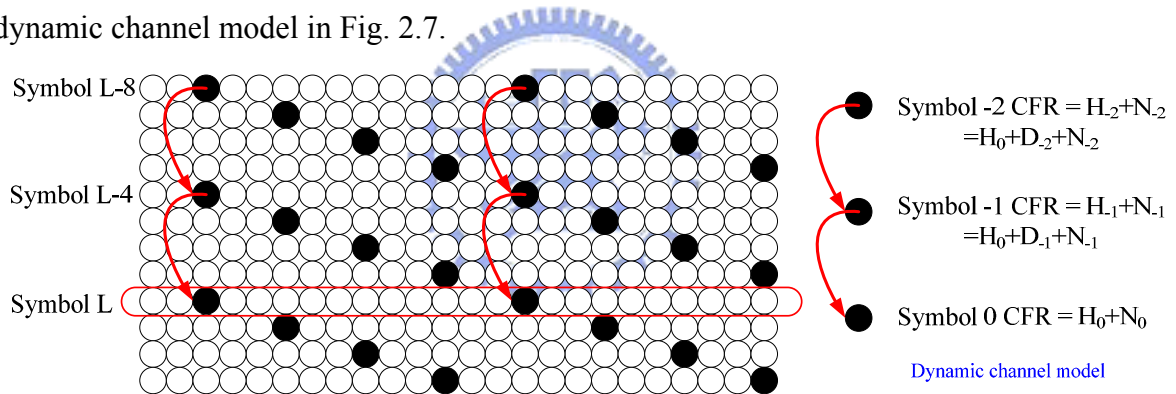


Fig. 2.7 Block based estimator model & the dynamic channel model

We can base on the MSE (2-9) to change the weight β_k at each pilot sub-carrier Fig. 2.8.

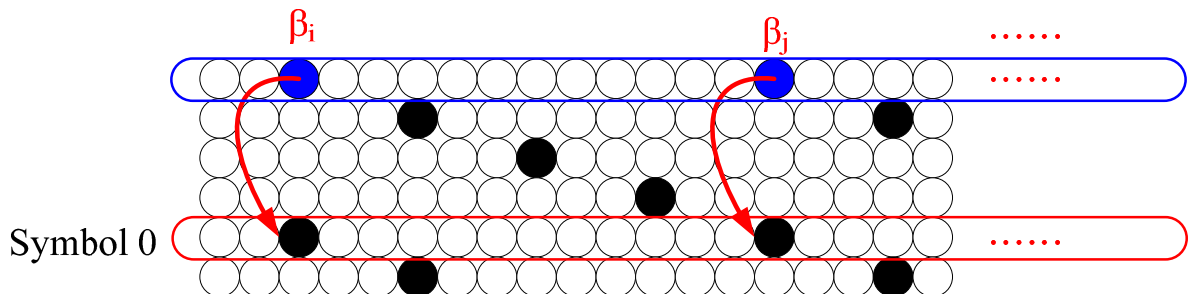


Fig. 2.8 Adaptive weight filter at each pilot sub-carrier

Because of the standard, the scatter pilots is four symbols a cycle. If we assume the $D_2=2D_1$ The MSE in (2-4) becomes to (2-9).

$$\begin{aligned}
MSE &= E(\hat{H}_0 - H_0)^2 \\
&= E(D_1(1-\beta)\beta + D_2\beta^2)^2 + E\left(\frac{N^2}{X^2}\right) \left[(1-\beta)^2 + (1-\beta)^2\beta^2 + \beta^4 \right] \\
&\xrightarrow{D_2=2D_1} E(D_1^2) [\beta^2 + 2\beta^3 + \beta^4] + E\left(\frac{N^2}{X^2}\right) [1 - 2\beta + 2\beta^2 - 2\beta^3 + 2\beta^4]
\end{aligned} \tag{2-9}$$

In this equation, we need to determine the variance of CFR in three symbols $E(D^2)$ and variance of AWGN $E(N^2/X^2)$. Furthermore, we can find first term in MSE (2-9), as Doppler effects is increasing, the $E(D^2)$ will increase too. The second term AWGN noise effect can be average out with larger β . So MSE will trade off in these two terms. We can base on the MSE equation to decide the weight of each pilot sub-carrier.

In static channel, we can find the proposed estimator can get better MSE than without filter design. The CFR variance D is equal to zero in static channel.

$$\begin{aligned}
MSE &= E(\hat{H}_0 - H_{spec})^2 = H_{spec}^2 \beta^{2n} + E\left(\frac{N_i^2}{X^2}\right) \times (1-\beta)^2 \times \frac{1-\beta^{2n}}{1-\beta^2} \\
&\xrightarrow{n=\infty} E\left(\frac{N_i^2}{X^2}\right) \times \frac{1-\beta^2-2\beta}{1-\beta^2} \leq E\left(\frac{N_i^2}{X^2}\right)
\end{aligned} \tag{2-10}$$

In static channel we can find larger β can get better performance, but in fact the channel will be time variant not only AWGN effects. Furthermore, the channel is more time dependent as the β lager. When β convergence to 0 which means the channel varying too fast over the previous estimator. We will show the simulation results and implementation method in later chapter. We can find it only needs less additional hardware cost than the existing design, but it can get better performance in the slow fading channel.

2.4 Transform domain processing

In fact, the CFR would be a smooth curve. According to this property, we use a low pass filter to reduce the high pass noise effect [11].

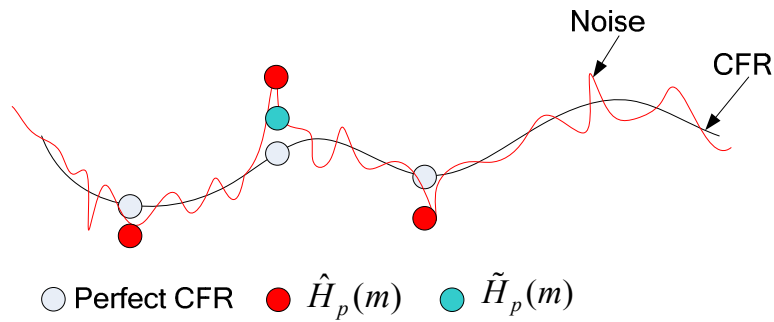


Fig. 2.9 The relationship of CFR and noise

In Fig.2.9, we can see that the relationship of CFR and noise. Because of noise we can get the red circle CFR but the perfect CFR is white circle. So the basic concept of filtering is to get a smoother CFR (blue circle) by a LPF. In theory the blue circle $\tilde{H}_p(m)$ will be closer to perfect CFR than red circle $\hat{H}_p(m)$.

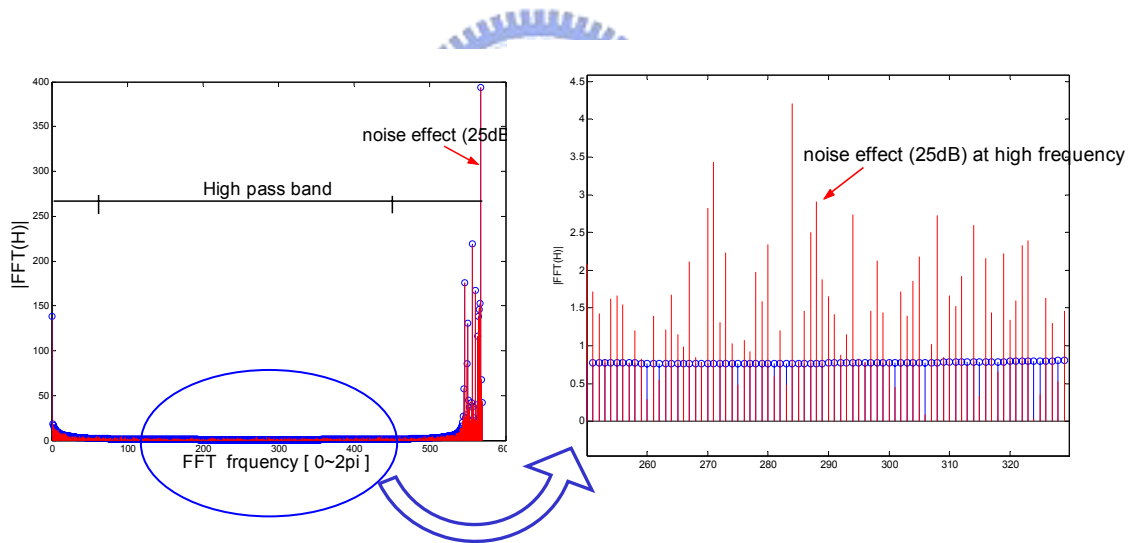


Fig. 2.10 The CFR of Rayleigh channel @ AWGN 25dB

In filtering processing, first we let the CFR through a FFT transform. The blue signal is the perfect CFR through FFT transform. The red signal is the perfect CFR add noise @ 25dB. We can see that, the energy is gathered in low pass band. In Fig.2.10 we can see the noise effect at high pass band. So we can reduce the noise in high pass band by a LPF. Fig.2.11 is the filtering process flow diagrams.

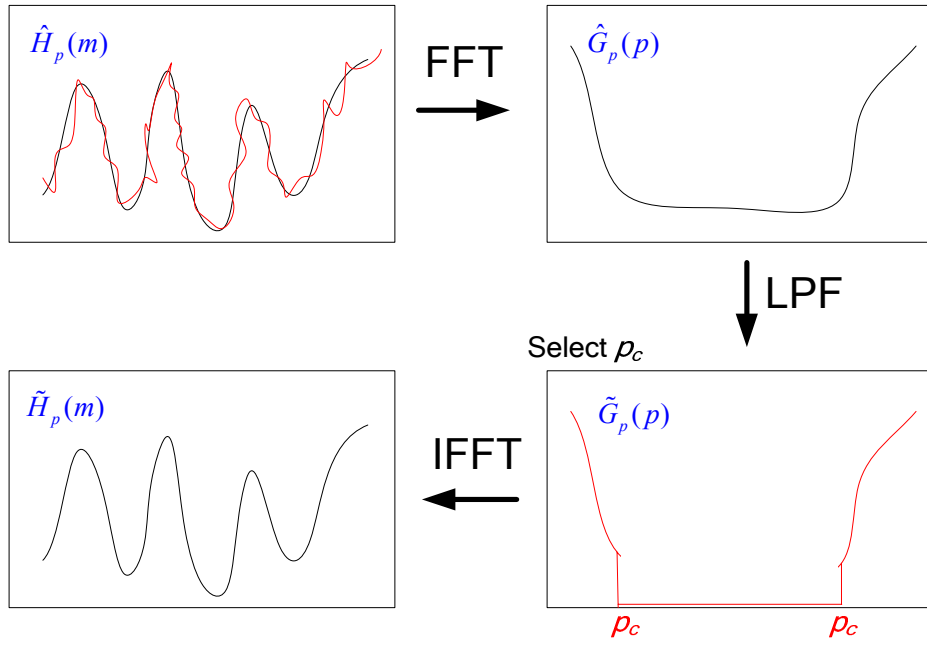


Fig. 2.11 The flow diagram

From section 2.3 we can get the estimated CFR $\hat{H}_p(m)$.

$$\hat{H}_p(m) = H_p(m) + \frac{N(m)}{X_p(m)}, m = 0, \dots, N_p - 1 \quad (2-11)$$

The noise term $N(m)/X_p(m)$ is a zero mean Gaussian random process. Variation of the true CFR $H_p(m)$ within one OFDM symbols is much slower than noise term $N(m)/X_p(m)$ with respect to index m . we can use this property to separate the two components by employing a

transform domain low-pass filter where the transform domain refers to the “frequency domain” in DFT-IDFT transformations. The transform domain representation of $\hat{H}_p(m)$

becomes $\hat{G}_p(p) = \sum_{m=0}^{N_p-1} \hat{H}_p(m) e^{-j2\pi mp/N_p}$, where $p \in [0, N_p - 1]$ is the transform domain index.

As expected the signal component $\hat{G}_p(p)$ is located at the lower frequency band (around $p=0$ and $p=N_p-1$), while the noise term is spread over the full band ($p=0, \dots, N_p-1$). The low-pass filtering can be realized by simply setting the samples in the “high pass band” to zero, that is

$$\tilde{G}_p(p) = \begin{cases} \hat{G}_p(p), & 0 \leq p \leq p_c, N_p - p_c \leq p \leq N_p - 1 \\ 0, & otherwise \end{cases}, \quad (2-12)$$

where p_c is the cutoff frequency of the filter in the transform domain. Such a low-pass

filtering reduces the noise component by an order $2p_c/N_p$. The cutoff frequency p_c of the transform domain low-pass filter is an important parameter that affects the accuracy of the channel estimation. Therefore the p_c can be determined from the following relation.

$$\frac{\sum_{p=0}^{p_c} |\bar{G}_p(p)|^2 + \sum_{p=N_p-p_c}^{p_c} |\bar{G}_p(p)|^2}{\sum_{p=0}^{N_p-1} |\bar{G}_p(p)|^2} = R, \quad (2-13)$$

where the numerator is the energy in the pass-band, the denominator represents the total energy, $R \in [0.9, 0.95]$, and $\bar{G}_p(p)$ is the average value of $\hat{G}_p(p)$ of the present data symbol and several previous ones.

2.5 Interpolation process

In DVB-T pilot carriers are transmitted together with data carriers. In block-type pilot based channel estimation, an efficient interpolation technique is necessary in order to estimate channel at data sub-carriers by using the channel information at pilot sub-carriers. Here we propose the two dimensional interpolation based channel estimation for mobile DVB-T/H reception. As we known, the 2D filtering complexity is much higher than 2x1D filtering, but the performance of 2D filtering is similar to 2x1D filtering [17-19]. Here we will separate interpolation in time domain and in frequency domain. The Fig.2.12 shows the 2x1D diagram.

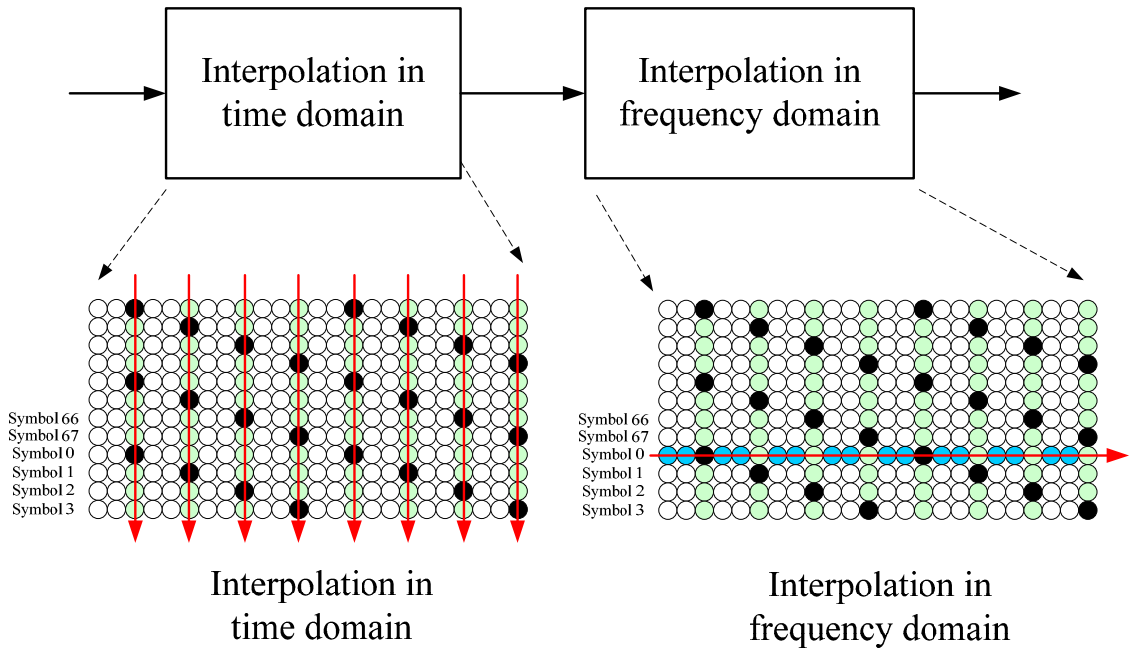


Fig. 2.12 The 2x1D interpolation processing

2.5.1 Interpolation in time domain

In time direction, the CFR is sampled at time instants $T_t = 4(T_u + T_g)$ apart. For mobile channels the correlation between these samples is determined by the bandwidth of the Jakes spectrum with a maximum Doppler frequency f_d and the residual local frequency offset Δf_k remaining after synchronization. The resulting bandwidth is $B_t = 2(f_d + \Delta f_k)$, and the interpolation is over-sampled by a factor of $r_t = \frac{T_{\max}}{T_t} = \frac{1}{B_t \cdot 4 \cdot (T_u + T_g)}$ with respect to the Nyquist sampling time T_{\max} . Interpolation is only feasible if $r_t > 1$.

For interpolation in time domain means that the casual and non-causal taps are used. For implementation aspect, we need store the non-causal data and the more latency to do operation. Furthermore, the complexity is dominated by the memory needed to provide to store the additional OFDM symbols. In other hand, in DVB-T/H systems, we can't ignore the carrier number in one OFDM symbol (1705 or 6817), and each data of subcarrier will be complex number format.

For the received carriers $C_{k,i}$, where k denotes the carrier index and i denotes the symbol

index. For CFR $\hat{H}_{k,i}$ at carriers $C_{k,i}$ to be estimated. $\hat{H}_{k,i}$ is the estimated CFR at pilot carriers where $k=12n+i*3+1$, n is an integer and $0 < n < 142$ (in 2k mode).

A. 1st-order predictive [17]

The CFR is predicted using the nearest 2 CFR by setting the CFR value equal to the extrapolate value of these 2 CFR value as Fig.2.13 shows.

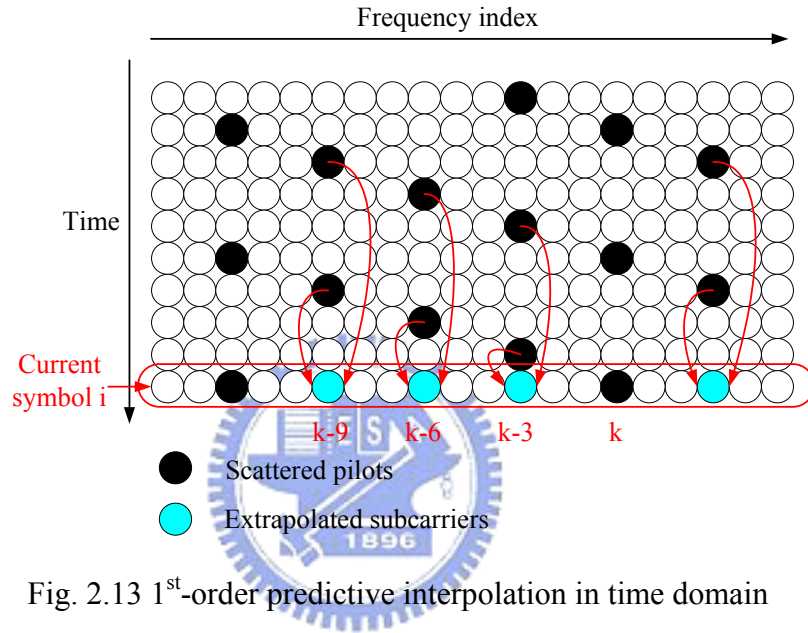


Fig. 2.13 1st-order predictive interpolation in time domain

The linear extrapolation is adopts CFR estimated at scatter pilots in the latest 7 symbols to predict the CFR of currently received symbol at those carriers.

$$\left\{ \begin{array}{l} \hat{H}_{k-3,i} = \frac{\hat{H}_{k-3,i-1} \times 5 - \hat{H}_{k-3,i-5}}{4} \\ \hat{H}_{k-6,i} = \frac{\hat{H}_{k-6,i-2} \times 6 - \hat{H}_{k-6,i-6} \times 2}{4} \\ \hat{H}_{k-9,i} = \frac{\hat{H}_{k-9,i-3} \times 7 - \hat{H}_{k-9,i-7} \times 3}{4} \end{array} \right. \quad (2-14)$$

In this scheme, the extrapolation uses pilots only on previously received symbols and currently receiving symbol, no additional storage are needed. Therefore, it only needs storage for previous CFR at pilot sub-carriers.

B. Linear interpolation

The Linear interpolation is shown in Fig.2.14

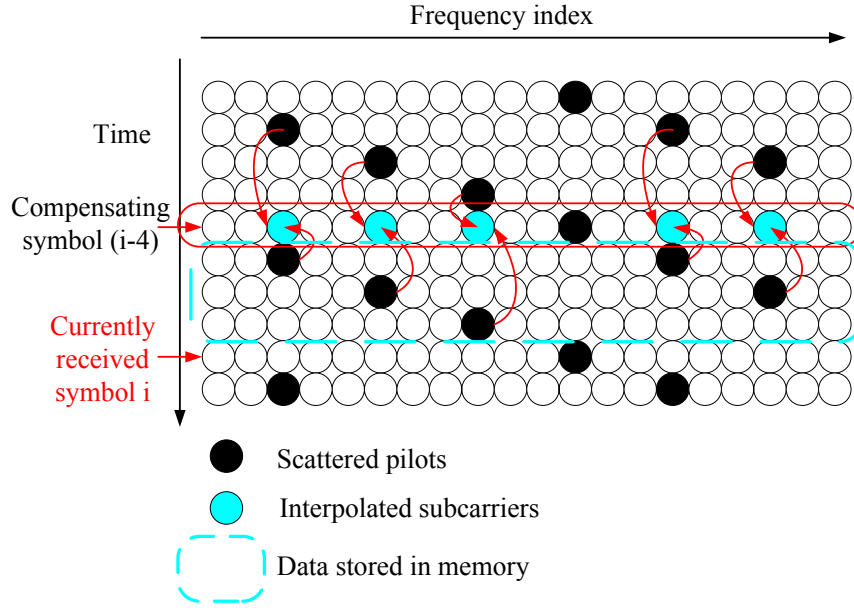


Fig. 2.14 Linear interpolation in time domain

The linear interpolation is adopts CFR estimated at scatter pilots in the latest 7 symbols to interpolate the CFR of compensating symbol at those carriers.

$$\begin{cases} \hat{H}_{k-3,i-4} = \frac{\hat{H}_{k-3,i-1} + \hat{H}_{k-3,i-5} \times 3}{4} \\ \hat{H}_{k-6,i-4} = \frac{\hat{H}_{k-6,i-2} \times 2 + \hat{H}_{k-6,i-6} \times 2}{4} \\ \hat{H}_{k-9,i-4} = \frac{\hat{H}_{k-9,i-3} \times 3 + \hat{H}_{k-9,i-7}}{4} \end{cases} \quad (2-15)$$

In this scheme, it needs storage for 3 OFDM symbols for implementation of its non-causal properties, because after compensating symbol which data didn't compensate yet. So the memory is quite large. Then, before the compensating data, it only needs storage for CFR at pilot sub-carriers.

We make comparison for the two methods in memory storages in table 2-1. Although both are two taps interpolation methods, but linear interpolation needs store more 3 OFDM symbols, and the latency is 3 OFDM symbols time.

Table 2-1 storage requirements for interpolation in time domain

	Storage requirements (2K mode)	Latency
1 st -order predictive	1138 (569*2) carriers	0 symbols
Linear interpolation	5684 (3*1705+569) carriers	3 symbols

2.5.2 Interpolation in frequency domain

After interpolation in time domain between scattered pilots, we can get estimated CFR every three subcarriers. Then, we use these sampled CFR to interpolate the whole CFR at the rest data subcarriers. Since the interpolation in time domain is done, the sample interval in frequency domain is from $12 f_c$ to $3f_c$, where f_c is the subcarrier spacing. Here, we use Linear, Parabolic, Second-order, and Cubic, four methods for interpolation in frequency domain, where $\hat{H}(k)$ is the result of the interpolation in frequency domain, k is the sub-carrier index. $H_p(m) = H(3*m)$ is the CFR after interpolation in time domain, where $3m < k < 3(m+1)$, and $\mu = k/3 - m$.

Classical polynomial interpolation of an N -point base-point set $\{t_i, x(i)\}$ can be performed by the Lagrange formulas [18-19]. It shows in Fig. 2.15.

$$y(x) = \sum_{k=0}^n \frac{\prod(x)}{(x-x_k) \prod'(x_k)} f(x_k) = \sum_{k=0}^n C_k(x) f(x_k) \quad (2-16)$$

$$C_i(x) = \frac{(x-x_0) \dots (x-x_{i-1})(x-x_{i+1}) \dots (x-x_n)}{(x_i-x_0) \dots (x_i-x_{i-1})(x_i-x_{i+1}) \dots (x_i-x_n)} \quad (2-17)$$

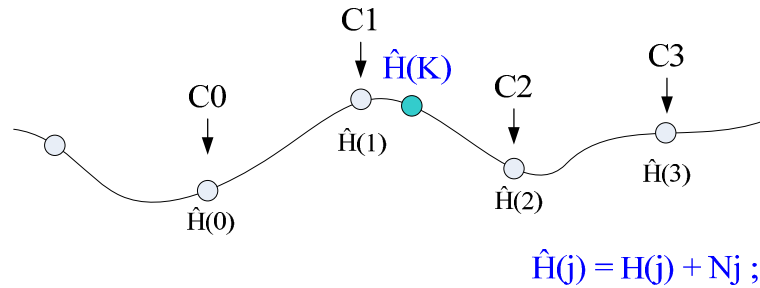


Fig. 2.15 Polynomial interpolation in frequency domain

A. Linear interpolation

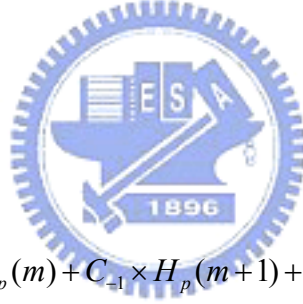
$$\hat{H}(k) = C_0 \times H_p(m) + C_{-1} \times H_p(m+1)$$

$$\text{where } \begin{cases} C_0 = 1-u \\ C_{-1} = u \end{cases} \quad (2-17)$$

B. Second-order interpolation

$$\hat{H}(k) = C_1 \times H_p(m-1) + C_0 \times H_p(m) + C_{-1} \times H_p(m+1)$$

$$\text{where } \begin{cases} C_1 = -\frac{1}{2}u + \frac{1}{2}u^2 \\ C_0 = 1-u^2 \\ C_{-1} = \frac{1}{2}u + \frac{1}{2}u^2 \end{cases} \quad (2-18)$$



C. Cubic interpolation

$$\hat{H}(k) = C_1 \times H_p(m-1) + C_0 \times H_p(m) + C_{-1} \times H_p(m+1) + C_{-2} \times H_p(m+2)$$

$$\text{where } \begin{cases} C_1 = -\frac{1}{3}u + \frac{1}{2}u^2 - \frac{1}{6}u^3 \\ C_0 = 1 - \frac{1}{2}u - u^2 + \frac{1}{2}u^3 \\ C_{-1} = u + \frac{1}{2}u^2 - \frac{1}{2}u^3 \\ C_{-2} = -\frac{1}{6}u + \frac{1}{6}u^3 \end{cases} \quad (2-19)$$

D. Parabolic interpolation

$$\hat{H}(k) = C_1 \times H_p(m-1) + C_0 \times H_p(m) + C_{-1} \times H_p(m+1) + C_{-2} \times H_p(m+2)$$

$$\text{where } \begin{cases} C_1 = -\frac{1}{2}u + \frac{1}{2}u^2 \\ C_0 = 1 - \frac{1}{2}u - \frac{1}{2}u^2 \\ C_{-1} = \frac{3}{2}u - \frac{1}{2}u^2 \\ C_{-2} = -\frac{1}{2}u + \frac{1}{2}u^3 \end{cases} \quad (2-20)$$

Here, μ is only $1/3$ or $2/3$ two kinds of values, so the taps can be calculated in advance, and save in the registers.

Next we discuss the MSE between these interpolation methods. As we know, high order interpolation will use more samples to get smother curves, and gets better performance than low order interpolation. But if we concern the noise effects, the MSE of high order interpolation will not be always better than low order interpolation. The criteria are MSE, and the formulation detail is shown in following equation (2-21).

$$\begin{aligned} MSE &= E\{|\hat{H} - H_k|^2\} = E\{|\sum_j C_j \times (H_j + N_j) - H_k|^2\} \\ &= (\sum_j C_j^2)E[N_j^2] + \sum_j C_j^2 E[H_j^2] + \sum_{i \neq j} (2C_i C_j \times E[H_i]E[H_j]) \\ &\quad - \sum_j (2C_j \times E[H_j]) \times H_k + H_k^2 \end{aligned} \quad (2-21)$$

In the same channel conditions, we can find that different interpolation methods which MSE will depend on different coefficients. The coefficients are listed on table 2-2, and the relationship is listed on table 2-3.

We can find that the first term in (2-21) will enhance the noise effect with high order interpolation in comparison of $\sum_j (C_j^2)$. In table 2-3 we can find the enhance term of each method. In the formulation, the other terms effects will be different in each interpolation method. In fact the CFR would be a smooth curve, so the higher order can get better performance without noise effects.

$$(\text{ex: } \sum_j C_j^2 E[H_j^2] + \sum_{i \neq j} (2C_i C_j \times E[H_i]E[H_j]) - \sum_j (2C_j \times E[H_j]) \times H_k)$$

However, the noise effect term $(\sum_j C_j^2)E[N_j^2]$ will be worse with higher order interpolation. So there will be a crossover in simulation with different SNR noise. We can use the equation (2-21) to determine the crossover point with different channels.

The noise term will be dominant at low SNR < crossover point, but the other term effect will be dominant at high SNR > crossover point. Then we can choose the better interpolation method for different channel cases.

Table 2-2 the coefficients list

	C0	C1	C2	C3
Average	0	0.5	0.5	0
Linear	0	0.3333	0.6666	0
Lagrange (2 order)	-0.1111	0.8889	0.2222	0
Lagrange (3 order)	-0.0617	0.7407	0.3704	-0.0494

Table 2-3 the coefficients relationship

	Average	Linear	Lagrange (2 order)	Lagrange (3 order)
$\sum(C_j^2)$	0.5	0.5555	0.8519	0.6921
$\sum 2C_i C_j$	0.5	0.4444	0.1481	0.3078
$\sum 2C_j$	2.0	2.0	2.0	2.0

Chapter 3 .

Channel Equalization Algorithms

In this chapter, we introduce the channel equalization algorithms, and we will show the critical path is the complex division operation. The division model is dominant hardware cost and power consumption in channel equalizer. So we can simplify this division model and show the results of saving hardware cost and power consumption in later sections.

3.1 Introduction to channel equalization

It is mentioned in Chapter 2. In OFDM system, it will divide the bandwidth into many subcarriers, so the channel frequency response of each subcarrier can be considered as flat fading. Therefore, the equalization for each subcarrier becomes simple in frequency domain, and it is only a one-tap equalizer to compensate the channel fading effects. In OFDM-based communication systems, the received signal $R[k]$ can be expressed by

$$R[k] = S[k] \cdot H[k] + N[k], \quad (3-1)$$

Where $S[k]$ is the transmitted signal, $H[k]$ is the CFR, and $N[k]$ is AWGN noise. The estimated signal $\hat{S}[k]$ can be obtained by dividing the estimated CFR, $\hat{H}[k]$ from channel estimation.

$$\hat{S}[k] = \frac{R[k]}{\hat{H}[k]}, \quad (3-2)$$

In related research, there was other approach via changing receiving data format to achieve divider-free method [20]. Here, we keep up the full-time complex dividing operation with new approach. We propose one new method to simplify divider complexity without transferring receiving data format. In the same time, we replace the division operation by

recurrence step based algorithm [21]. In recurrence step algorithm, it only requires an adder (subtractor) and a few registers to implement.

3.2 Motivation

In channel equalizer, it contains a complex number division. One complex division operation includes two real number divisions. As we know, the division hardware cost is proportional to square of word-lengths, but the signal bus needs sufficient digits to represent receiving signals in order to get enough accuracy. In DVB-T/H system, it will provide higher clock rate for 64Qam and Viterbi decoder. So we can reuse the hardware by raising clock rate. Furthermore, we can optimize the saturation cases and don't need to add word-length to get enough decimal fractions of the quotient. Then according to multi-cycles division, we can use the shift-subtraction structure to simplify the hardware efficiently.

In addition, the division gate count is about 62.8% of equalizer, and the cycle time of DVB-T/H systems for 8Mhz channels is about 109ns. Due to the long cycle time and the high hardware cost of long digits dividers, we propose a low cost architecture to implement the equivalent divider.

3.3 Proposed division scheme

First, we introduce the format notations. In complex divider, the equation can be expressed by:

$$\frac{a + bi}{c + di} = \frac{ac + bd}{c^2 + d^2} + \frac{bc - ad}{c^2 + d^2}i = e + fi \quad (3-3)$$

$$\text{Dynamic range: } P \in \{2^{(m_2 - n_2 - 1)} \sim -2^{(m_2 - n_2 - 1)}\} \quad (3-4)$$

$$\text{Saturation point: } \alpha = \pm 2^{(m_2 - n_2 - 1)} \quad (3-5)$$

In proposed design, the multi-cycle division, the basic concept is to separate one cycle into many cycles and get quotient by iterative subtraction. So we can simplify the divider to subtraction by hardware reuse and raising clock rate.

First, the procedure of proposed division scheme consists of three states [21]. In state 1, it will detect if the result is saturated or not. If saturation occurs, it goes to state 3, else goes to state 2. In state 2, it will do main function including subtraction operation and getting the quotient by iterations. At last, it will output the result of division in state 3. The state diagram is shown in Fig.3.3.

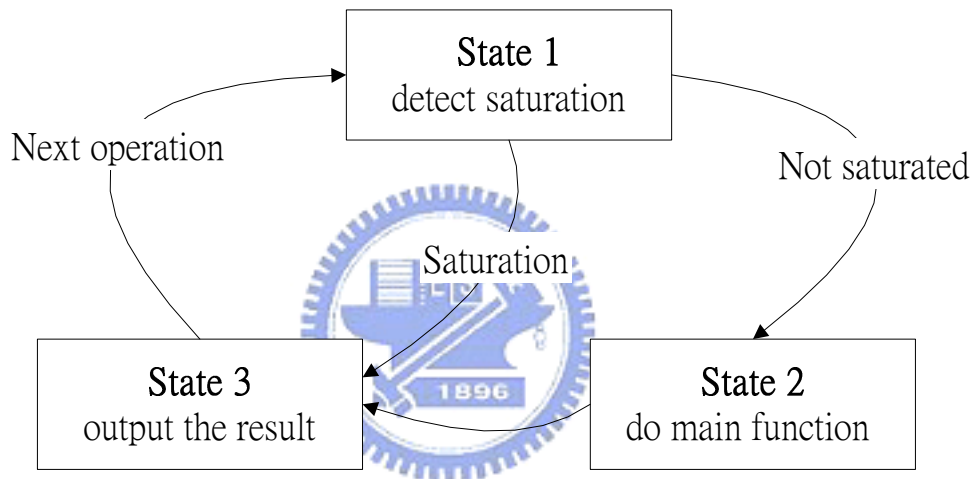


Fig. 3.3 The state diagram

As mention before, because of the format (m_2, n_2) of output so we can detect that if the result is saturated in the beginning. If the result is saturated, we can get the output immediately. In that case, other logics will be idle for power saving.

First, we define A is the minuend, B is the subtrahend, and sub is the result of subtraction. We determine the quotient by subtracting B from A. In this algorithm, the quotient can only present '1' or '0', so if A is larger than two times of B, the quotient can't represent. For this reason, we must make sure that A can not be larger than two times of B in state 2.

In state 1, first we let quotient normalize to saturation point, so we let A be the dividend after shifting (m_2-n_2-1) bits right, and let B be the divisor. The quotient will shift back at last, so it will not be affected. In this method, the relative position of dividend and divisor is

exactly to get the MSB of the quotient, and we can detect the saturation case easily. We only take one cycle for saturation detection, and we can save $(2m_1+n_2-m_2)$ cycles.

Here, A is the dividend $\gg (m_2-n_2-1)$, and B is the divisor. If A is larger than B, it will represent that the quotient is saturation, and the quotient will be the saturation point α . If A is smaller than B, it will make sure that A can not be larger than two times of B, and it will go to state 2 to get the quotient. The flow of state 1 is shown in Fig.4.

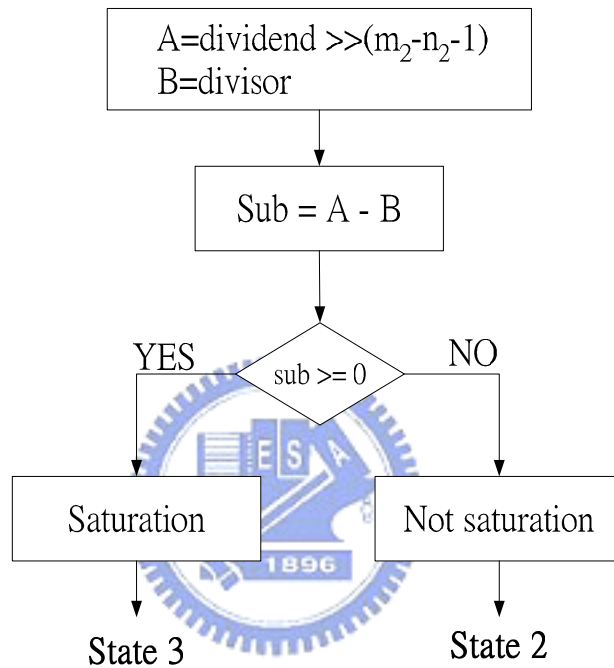


Fig. 3.4 The flow of the state 1

In state 2, we can use subtraction to determine the quotient $q[k]$ is ‘1’ or ‘0’ by binary property. Because it makes sure A can not be larger than two times of B. When $A \geq B$, the $q[k]$ will be ‘1’ else not, we can determine it by the sign bit of the subtraction result. If $A \geq B$, the sign bit of sub is ‘0’ and $q[k]$ is ‘1’, $A < B$, the sign bit of sub is ‘1’ and $q[k]$ is ‘0’. We can find $q[k]$ is the inverse of the sign bit of sub. Then, we update A by $(sub \ll 1)$ or $(A \ll 1)$ depends on the sign bit of sub to get the next bit of quotient. We can get the quotient of format (m_2, n_2) one by one bit through (m_2-1) cycles in state 2. The flow of the main function in state 2 is shown in Fig.3.5, and the relationship between parameters is listed in table 3-1.

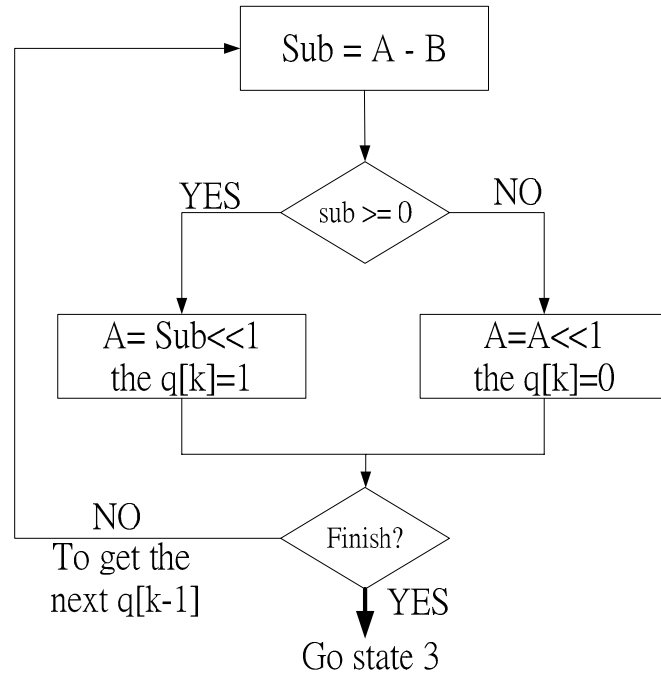


Fig. 3.5 The flow of the main function in state 2

Table 3-1 the parameter relationship in state2

	Sub >= 0	Sub < 0
Sign bit of sub	“0”	“1”
q[k]	“1”	“0”
Remainder (A)	Sub << 1	A << 1

In state 3, it is output stage. It can output the whole quotient at the last cycle of state 2, and goes to next new division operation.

Furthermore, we should determine the clock rate of this architecture which depends on the cycles of one operation. It will take m_2 cycles totally. The first cycle is for state 1 to detect if it is saturation. The following (m_2-1) cycles are for computing the (m_2-1) bits of quotient excluding sign bit. The sign bit can be determine before state 2. It will output the complete quotient stably in the last cycle. So there are m_2 cycles needed in one operation, in other word the ratio between clock rate and symbol rate is $\{1: m_2\}$. The timing diagram is shown in Fig.3.6. The hardware implementation will mention in section 5.3.2.

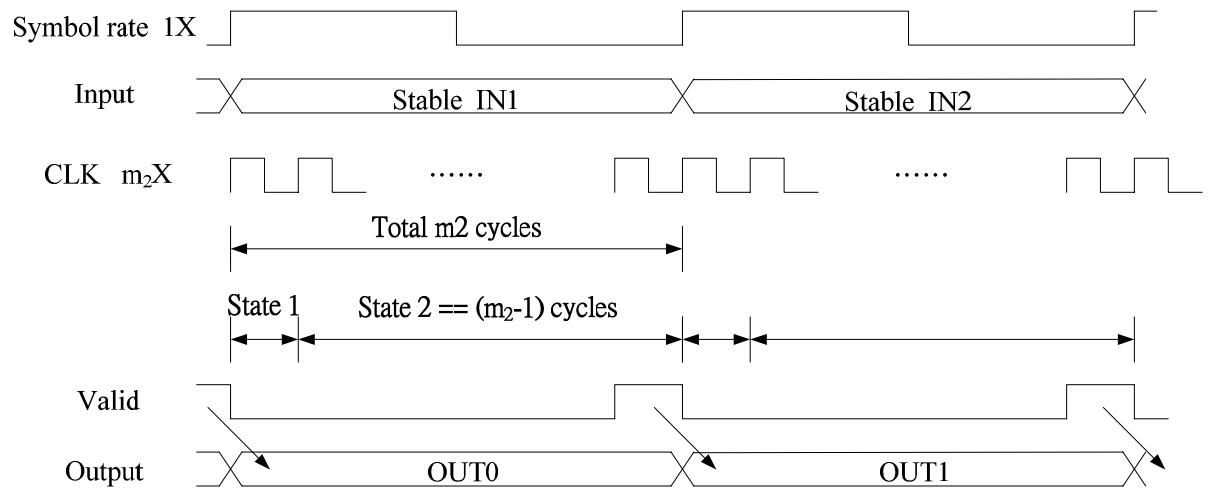


Fig. 3.6 Timing diagram



Chapter 4 .

Simulation and Performance Analysis

In this chapter, the overall simulation platform built for DVB-T/H system will be illustrated first. The channel model and some other distortion source such as Doppler delay spread and SCO model will be discussed later. Finally, the performance analysis of the proposed channel equalizer scheme and comparison with state of the art will be performed.

4.1 Simulation Platform

In order to verify the performance of the proposed channel equalizer scheme, a complete DVB-T/H baseband simulation platform is constructed in Matlab. The block diagram of the overall simulation platform is shown as Fig. 4.1.

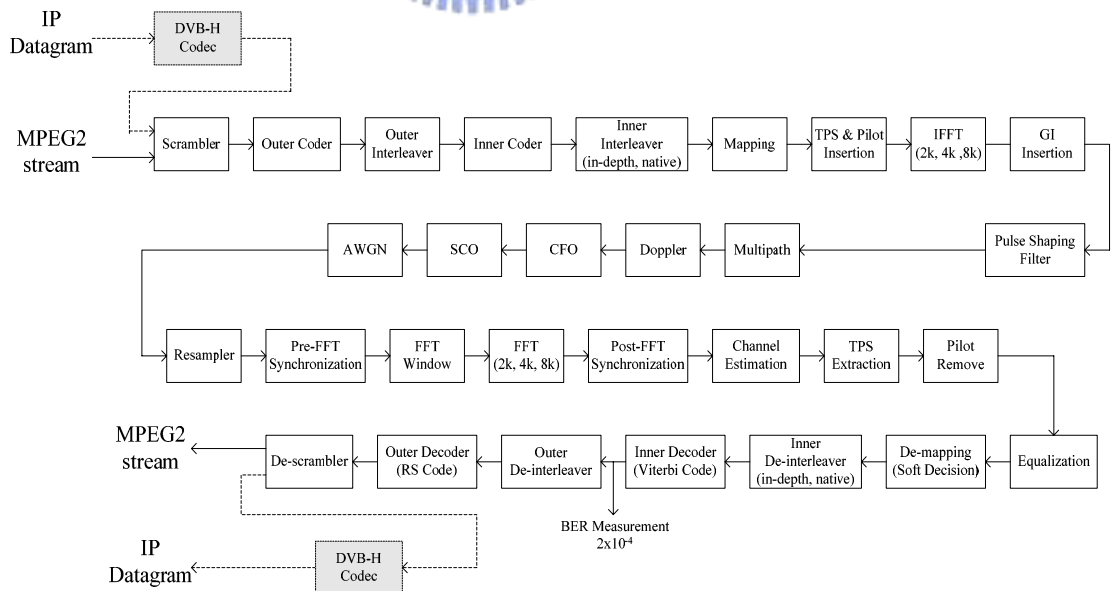


Fig. 4.1 Overall DVB-T/H platform

As shown in Fig. 4.1, the blocks with dotted line is the specific function blocks for DVB-H

system. By adding support of 4k IFFT/FFT, in-depth interleaving, and additional TPS information, the developed DVB-T system platform can share most of the function blocks with DVB-H system at the same time. The platform is composed of transmitter, channel, and receiver. A typical transmitter that receives data from MPEG2 encoder or IP datagram is completely established. The transmitter consist the full function of FEC blocks and OFDM modulation blocks. The coding rate, interleaving mode, constellation mapping mode, IFFT length, and guard-interval length are all parameterized and able to be selected while simulation. An oversampling and pulse shaping filter is added before data entering channel to simulate discrete signal as far as continuously. The oversampling rate is also parameterized and can be chosen according to the simulation accuracy. The roll-off factor of the pulse-shaping filter is chosen as a normal value $\alpha = 0.15$ because it is not defined in the DVB-T/H standard.

Various distortion models are adopted in the channel model to simulate real mobile environment such as multipath fading, Doppler spread, AWGN, CFO, and SCO. In practically, there are still some imperfect effects which contain co-channel interference, adjacent-channel interference, phase noise, and common phase error caused by imperfect front-end receiving. However, the distortion of these imperfect effects is relatively smaller compared with effective time-varying channel response caused by Doppler spread, CFO, and SCO. Therefore these effects are neglected in our simulation platform.

The baseband receiver in our system platform can be divided into inner receiver and outer receiver as Fig. 4.2 shows. The inner receiver includes all of the timing and frequency synchronization function, FFT demodulation, channel estimation, equalization, and pilot remove blocks. The outer receiver consists of other functional blocks that following the de-mapping. The transmission parameters extracted by TPS decoder such as constellation mapping mode and Viterbi code rate will be sent the relative blocks as control parameters. Besides, the extracted TPS parameter such as guard interval length and IFFT/FFT mode

should be checked all the time during online receiving to prevent synchronization error. Once TPS check fail occurs, the acquisition and tracking of inner receiver must be shut down and then restart all the synchronization schemes. As for bit-error-rate (BER) measurement, the DVB-T standard defines quasi error-free condition, which means less than one uncorrelated error event per hour, while the BER of the output of the Viterbi decoder is equal to 2×10^{-4} . Therefore, in order to verify the overall system performance, the BER after Viterbi decoder should be measured.

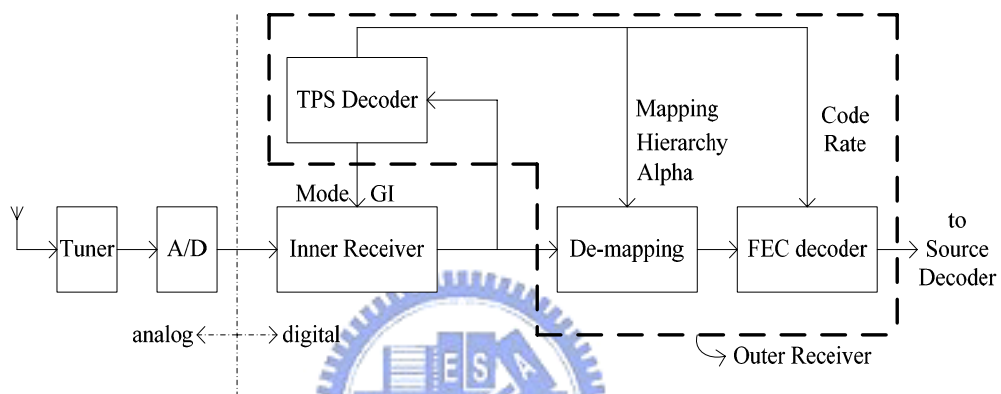


Fig. 4.2 The baseband receiver design

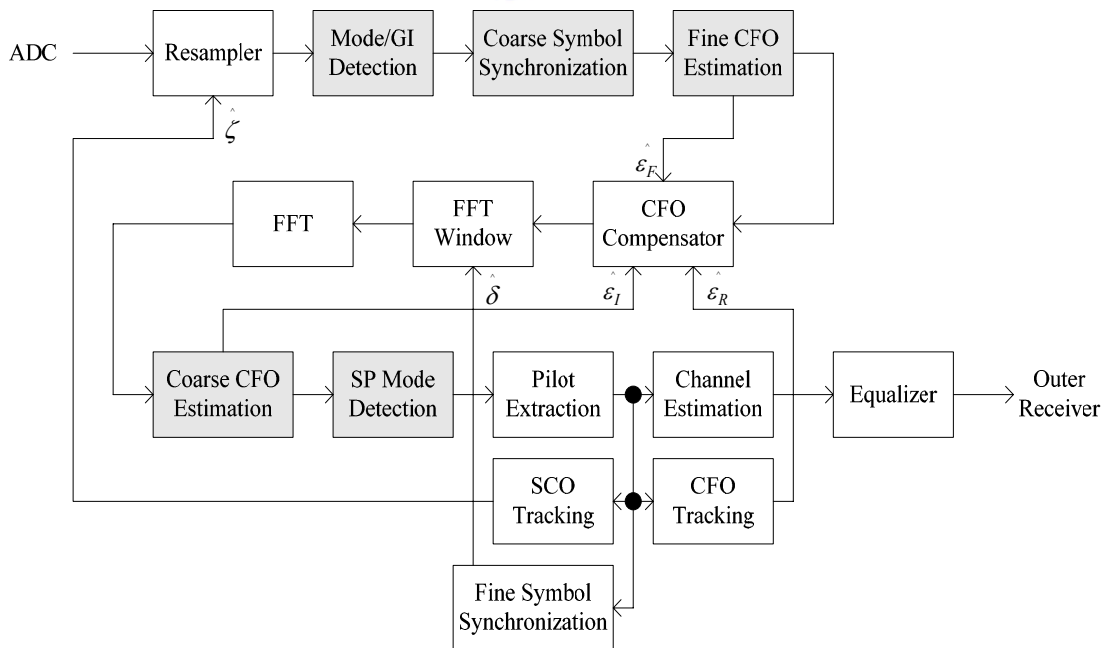


Fig. 4.3 Functional blocks of inner receiver

Fig. 4.3 shows the detail functional blocks of the inner receiver. The main functional blocks consists of symbol timing offset synchronization, carrier frequency offset synchronization, SCO synchronization, channel estimation, and equalizer, respectively. The acquisition parts (gray color) only operate in the beginning of the receiving and then are turned off when the tracking parts work, and the tracking parts works all the time until the receiver is turned off or TPS check error occurs. In this thesis, we only focus on the performance analysis of the channel estimation and equalization scheme. The detailed discussion of other functional blocks such as timing synchronization and CFO synchronization will be neglected in this work and can be found in [22].

4.2 Channel Model

The typical baseband equivalent channel model for DVB-T/H system platform is shown as in Fig. 4.4. The transmitted data will pass through multipath fading, Doppler delay spread, CFO, SCO, and AWGN in turn. The effects of co-channel interference, adjacent-channel interference, phase noise, and common phase error are neglected in our simulation. In the following sections, the detailed effect of each channel distortion will be illustrated.

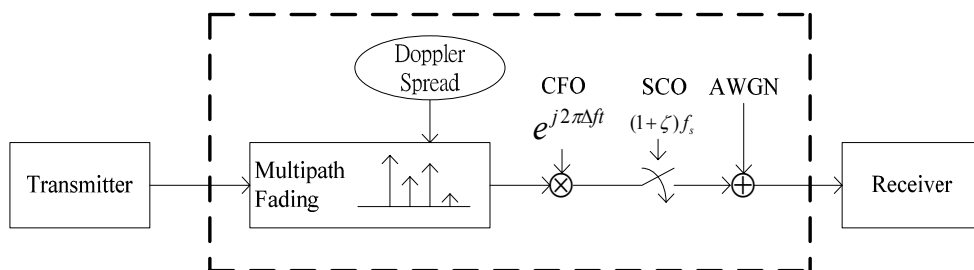


Fig. 4.4 Channel model of DVB-T/H system

4.2.1 Multipath Fading Channel Model

In wireless communication transmission, the multipath fading is caused by the reception through different paths with different time delay and power decay. In DVB-T standard, two

types of multipath fading channel model are specified [3]. The fixed reception condition is modeled by Ricean channel (Ricean factor = 10dB) while the portable reception is modeled by Rayleigh channel. The full 20-tap Ricean and Rayleigh channel was used with floating point tap magnitude and phase values with tap delay accuracies rounded to within 1/2 of duration for practical discrete simulation. The channel models can be generated from the following equations where $x(t)$ and $y(t)$ are input and output signals respectively

$$\text{Rayleigh: } y(t) = \frac{\sum_{i=1}^{20} \rho_i e^{-j\theta_i} x(t - \tau_i)}{\sqrt{\sum_{i=1}^{20} \rho_i^2}} \quad (4-1)$$

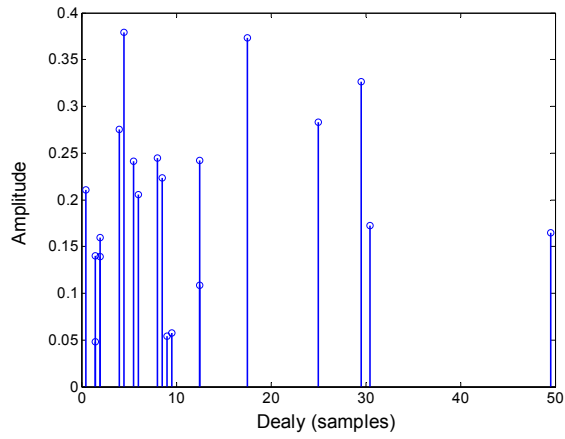
$$\text{Ricean: } y(t) = \frac{\rho_0 x(t) + \sum_{i=1}^{20} \rho_i e^{-j\theta_i} x(t - \tau_i)}{\sqrt{\sum_{i=0}^{20} \rho_i^2}} \quad (4-2)$$

where ρ_i is the attenuation of the i -th path, θ_i is the phase shift from scattering of the i -th path, and τ_i is the relatively delay of the i -th path, respectively. The detailed value of these parameters is listed in table B.1 of [3]. The rms delay of Rayleigh and Ricean channel is $1.4426 \mu s$ (about 13 samples) and $0.4491 \mu s$ (about 4 samples). From the above two equations, we can find that the major difference between Ricean and Rayleigh channel is the main path (the sight way). In Ricean channel, a main path is defined with the Ricean factor K (the ratio of the power of the direct path to the reflected path) and can be expressed as

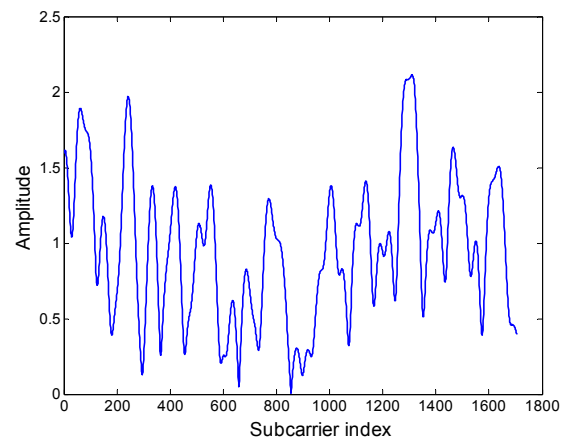
$$K = \frac{\rho_0^2}{\sum_{i=1}^{20} \rho_i^2} \quad (4-3)$$

However, there is no main path in Rayleigh channel. Hence the received signals consist of several reflected signals with similar power and bring serious synchronization error. The impulse response and frequency response of the two types of channel when $K=10\text{dB}$ are shown in Fig. 4.5. As we can see there is a significant direct path in the impulse response of the Ricean channel. In the impulse response of the Rayleigh channel, there is no any direct

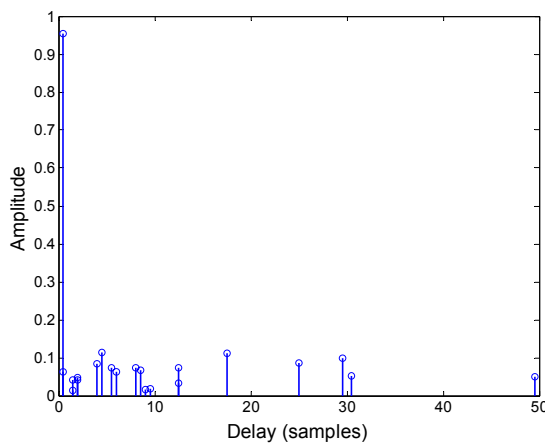
path and all the paths have similar magnitude. Therefore, the frequency selective fading effect in the frequency response of the Rayleigh channel is more serious than that of the Ricean channel.



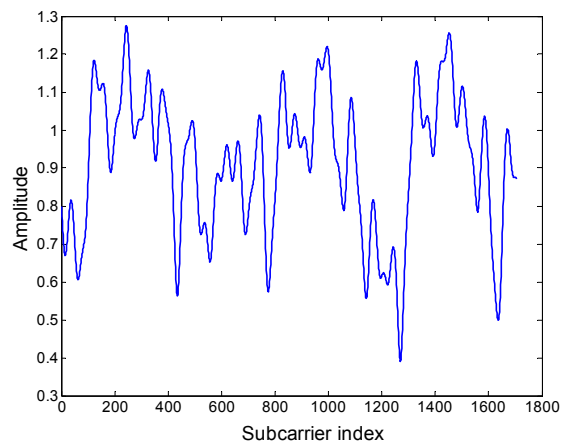
(a) Impulse response of Rayleigh channel



(b) Frequency response of Rayleigh channel



(c) Impulse response of Ricean channel



(d) Frequency response of Ricean channel

Fig. 4.5 Channel response of Rayleigh and Ricean ($K=10\text{dB}$) channel

4.2.2 Mobile channel model

In DVB-T standard, it only provides two static channel models which is described in section 4.2.1. However, the applications in DVB-T/H systems are not only for fixed reception, but also for mobile reception. Therefore, we refer to the channel models Typical Urban 6 (TU6) and Rural Area 6 (RA6) in GSM COST 207 project [23]. The two single-transmitter

profiles come from the set defined by the COST 207 project (GSM transmission). The technical specification of COST207 describes the equipment and techniques used to measure the channel characteristics over typical bandwidths of 10~20 MHz at near 900MHz. Therefore, the COST207 profiles are applicable to the DVB-T transmission situations. The detailed value of these parameters is listed in table 4-1 and table 4-2. The Fig4.6 shows the TU6 model, the Doppler spectrum filter will introduce in next section.

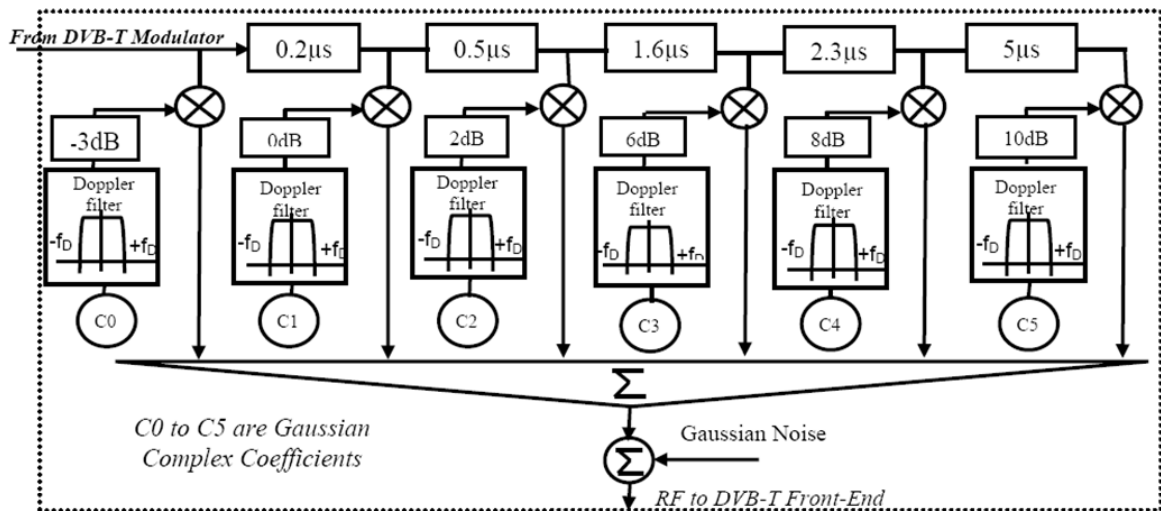


Fig. 4.6 TU6 model

Table 4-1 Typical Urban Reception (TU6) channel model

Tap number	Delay(us)	Power(dB)	Doppler spectrum
1	0	-3	Rayleigh
2	0.2	0	Rayleigh
3	0.5	-2	Rayleigh
4	1.6	-6	Rayleigh
5	2.3	-8	Rayleigh
6	5.0	-10	Rayleigh

Table 4-2 Rural Area Reception (RA6) channel model

Tap number	Delay(us)	Power(dB)	Doppler spectrum
1	0	0	Rice
2	0.1	-4	Ricean
3	0.2	-8	Rayleigh
4	0.3	-12	Rayleigh
5	0.4	-16	Rayleigh
6	0.5	-20	Rayleigh

4.2.3 Doppler spectrum types

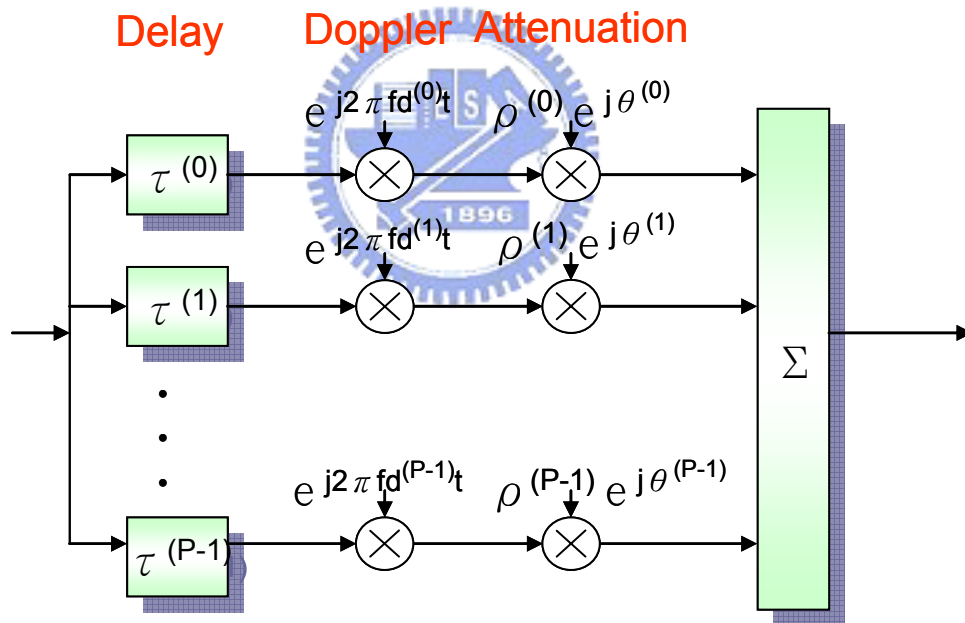


Fig. 4.7 Doppler spread model

A. Pure Doppler

In DVB-T/H system, the reception ability in mobile environment is necessary. Hence a mobile radio channel including Doppler spread must be constructed. A simplified Doppler spread model is shown in Fig. 4.7 [24]. In the beginning, we assume a channel with a known and fixed number of paths P such as Rayleigh or Ricean with a Doppler frequency $f_d^{(k)}$,

attenuation $\rho^{(k)} e^{j\theta^{(k)}}$, and time delay $\tau^{(k)}$. All the parameters are fixed as described in section 4.2.1 except the Doppler frequency. Since each path has its own Doppler frequency, the decision of the statistic distribution of f_d is very important. There are two commonly used Doppler frequency PDFs, uniform and classical, where the former exploits uniform distribution to model Doppler spread, and the later uses Jake's Doppler spectrum [25], respectively. The PDF of the Jake's Doppler spread can be expressed as

$$p(f_d) = \frac{1}{\pi \cdot f_{d\max} \cdot \sqrt{1 - \left(\frac{f_d}{f_{d\max}}\right)^2}}, \quad \text{where } |f_d| \leq f_{d\max} \quad (4-4)$$

After transformation of random variable, each f_d can be obtained by the following equation

$$f_d = \cos(2\pi \cdot \text{rand}(1)) \cdot f_{d\max} \quad (4-5)$$

The type of Doppler spread (uniform or Jake's) affects the system performance enormously. Because each path gets different f_d in each simulation case with different $f_{d\max}$, the value of $f_{d\max}$ should be fixed for each simulation and comparison.

B. Rayleigh fading

In wireless communication, the multi path effect will cause the frequency selective fading problems. If the transmitting environment is without the main direct path, according to central limit theory the amplitude will be Rayleigh distribution and the phase will be uniform distribution. So here we based on the Jake's model to simulate the Doppler effects, in concept, the Jake's model will produce the complex signal with the same statistic characteristics [25-27].

Simulating a multipath fading channel often requires the generation of multiple independent Rayleigh faders which can be modeled as complex-valued random processes. Ideally the Rayleigh faders should conform to the following criteria. First, the real (or in-phase) and imaginary components of each fader are zero-mean independent Gaussian

processes with identical power spectra or auto-correlation functions. As a result, the envelope is Rayleigh distributed and the phase is uniformly distributed. Second, the cross-correlation between any pair of faders should be zero. Rayleigh fading waveforms can be generated deterministically or statistically. The Rayleigh Doppler spectrum generator is shown in Fig. 4.8. The Rayleigh fading Doppler spectrum is generating by Jake's model which Doppler frequency is 100Hz is shown in Fig. 4.9.

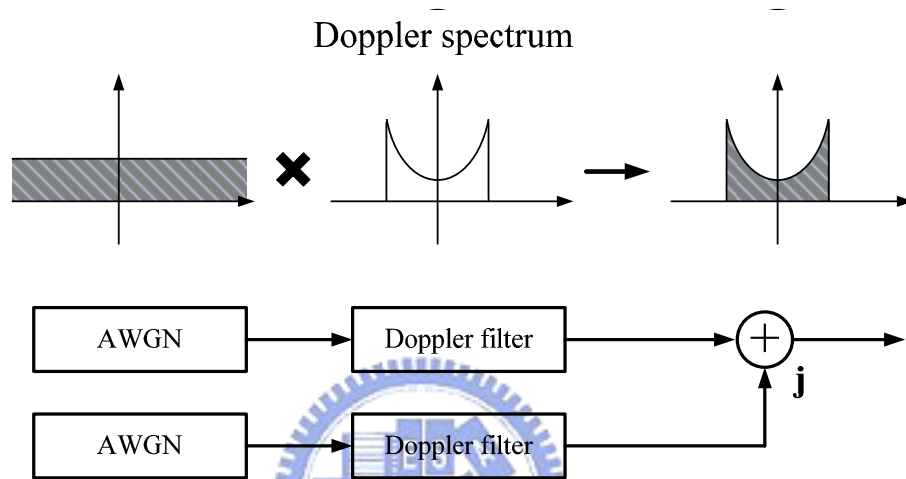


Fig. 4.8 Rayleigh Doppler spectrum generator

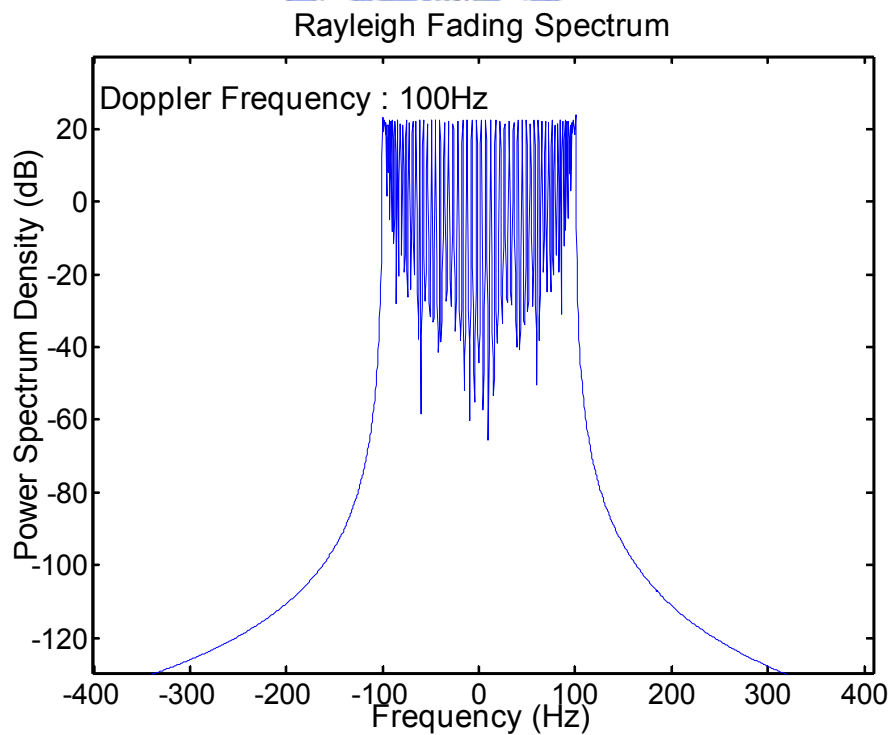


Fig. 4.9 Rayleigh fading Doppler spectrum by jake's model

C. Rice fading

The Rice fading spectrum is similar to Rayleigh fading spectrum, but there are one direct path between the transmitter and the receiver. This direct path with Doppler effects is like pure Doppler spectrum, but the other path is similar to Rayleigh fading spectrum.

The Rice fading Doppler spectrum is generating by Jake's model which Doppler frequency is 100Hz is shown in Fig. 4.10.

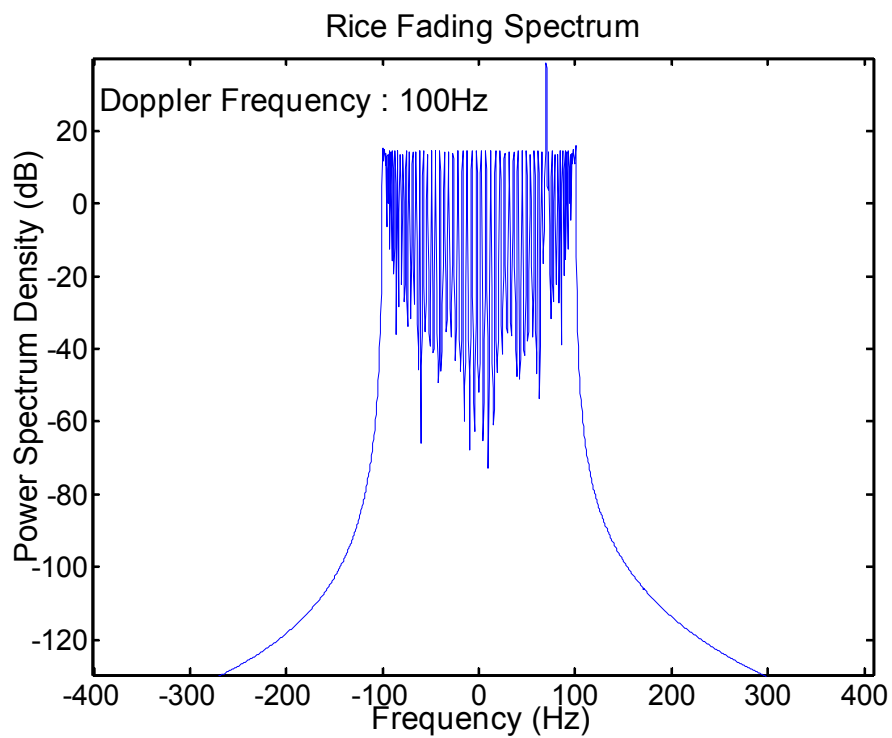


Fig. 4.10 Rice fading Doppler spectrum by jake's model

4.2.4 Additive White Gaussian Noise (AWGN)

The additive white noise is added after multipath fading channel. The SNR in frequency

domain is defined by :
$$SNR = \frac{Es}{N_0} = \frac{Es}{2\sigma^2}$$

In this equation, E_s is the energy of subcarrier, N_0 is the AWGN power density, and the σ^2 is the variance of AWGN. Therefore, the signal in real part and in imaginary part should be

added AWGN which variance is : $\sigma_I^2 = \sigma_Q^2 = \frac{1}{N} \frac{Es}{2 \times SNR}$

N is the size of FFT in OFDM system.

4.2.5 Carrier Frequency Offset and Sampling Clock Offset model

The detailed signal model of CFO is already described in section 2.1.1 and will not be discussed repeatedly in this section. The model of SCO is built based on the concept of sinc interpolation. The input digital signals can be exploited to interpolate the intermediate value between two successive samples by using the shifted value of sic function. Assume that the sampling period is T_s and SCO is ζ . Then the sampling phase can be represented as $nT_s + n\zeta$. The resulting signal after ADC can be expressed as

$$\begin{aligned} r_{ADC}(nT_s) &= r(nT_s) * \text{sinc}\left(\frac{nT_s + n\zeta}{T_s}\right) \\ &= \sum_{k=-N}^N r(nT_s - kT_s) \cdot \text{sinc}\left(k + \frac{n\zeta}{T_s}\right) \end{aligned} \quad (4-6)$$

where $2N+1$ is the taps of the FIR interpolator, k is the sampling point index, $r(\cdot)$ is the received signal with perfect sampling, $r_{ADC}(\cdot)$ is the received signal while SCO is ζ , respectively.

4.3 Performance Analysis

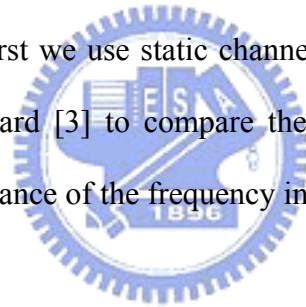
The performance analysis of the proposed channel estimation scheme is illustrated in this section. Except the verification of the proposed algorithms, some performance or computational complexity comparison between different methods and proposed scheme will be made too. We introduced the proposed channel estimation algorithm in chapter 2. The proposed scheme is depicted in Fig. 2.3. First, we do the channel estimator for pilot signal, second, we do the transform domain processing finally do the interpolation process. First we discuss the interpolation process result, then discuss each block finally make the overall

system performance. The simulation environment is 2k mode, GI=1/4, 64-Qam, code rate=2/3. A good compromise between bandwidth efficiency and robustness is 64-QAM with code rate 2/3 (mode used in UK). Furthermore, the performance of the overall system is based on the quasi-error free. The quasi-error free (QEF) condition which corresponds to 2×10^{-4} BER after Viterbi decoder will be the system performance target.

4.3.1 Interpolation in frequency domain

After interpolation in time domain between scattered pilots, we can get estimated CFR every three subcarriers. Here we will make simulation results to verify the algorithm mentioned in section 2.5.2.

Fig.4.11~Fig.4.13 are the simulation results of the different interpolation methods under different channel condition. First we use static channel (Gaussian, Ricean, Rayleigh) which are specified in DVB-T standard [3] to compare the MSE results. Here we use the MSE criterion to discuss the performance of the frequency interpolators.



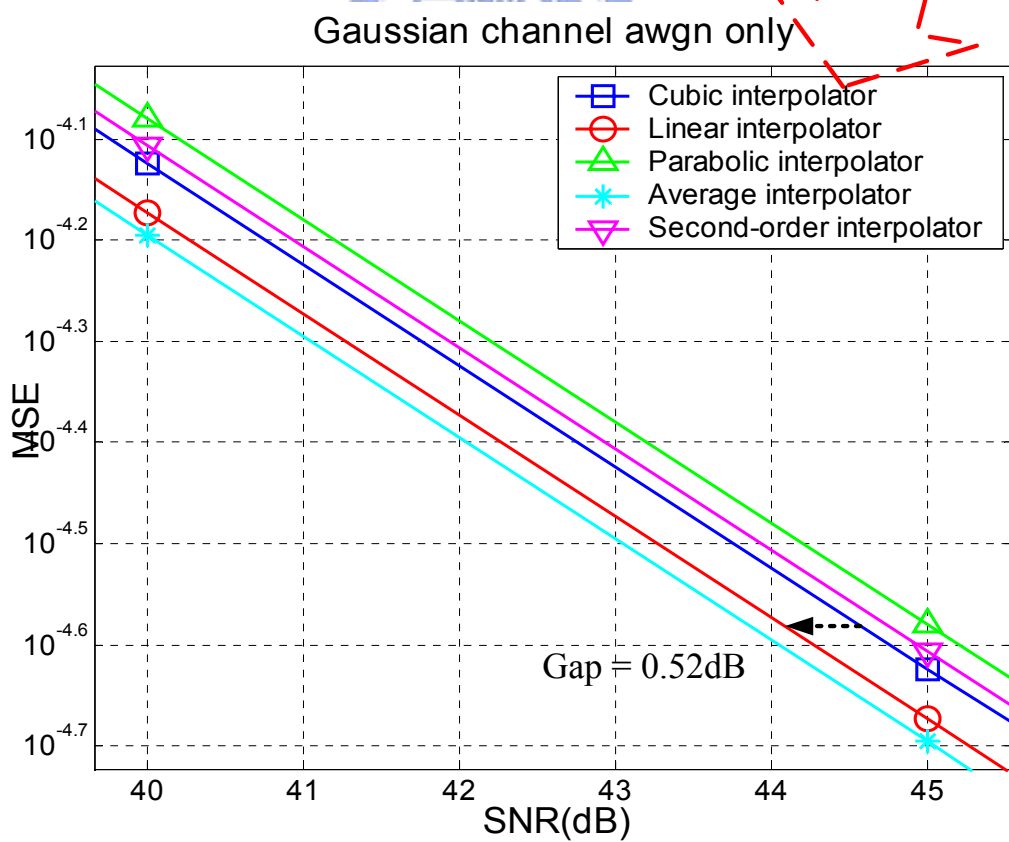
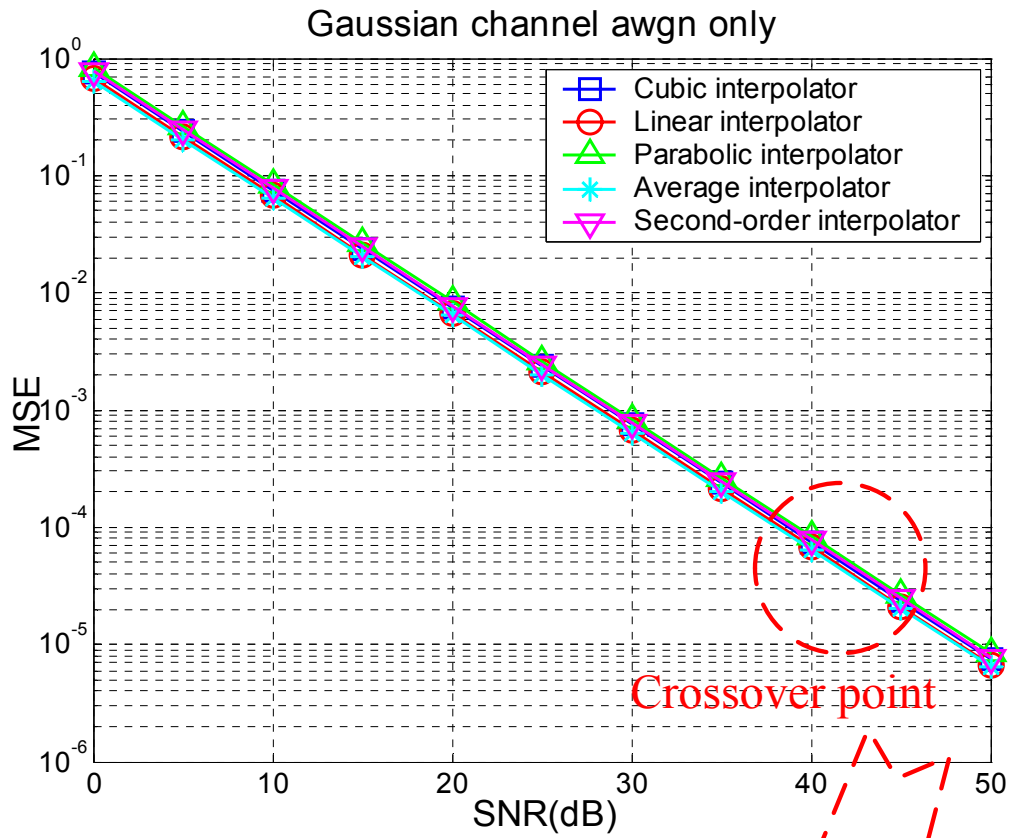


Fig. 4.11 MSE of different frequency interpolator in Gaussian channel

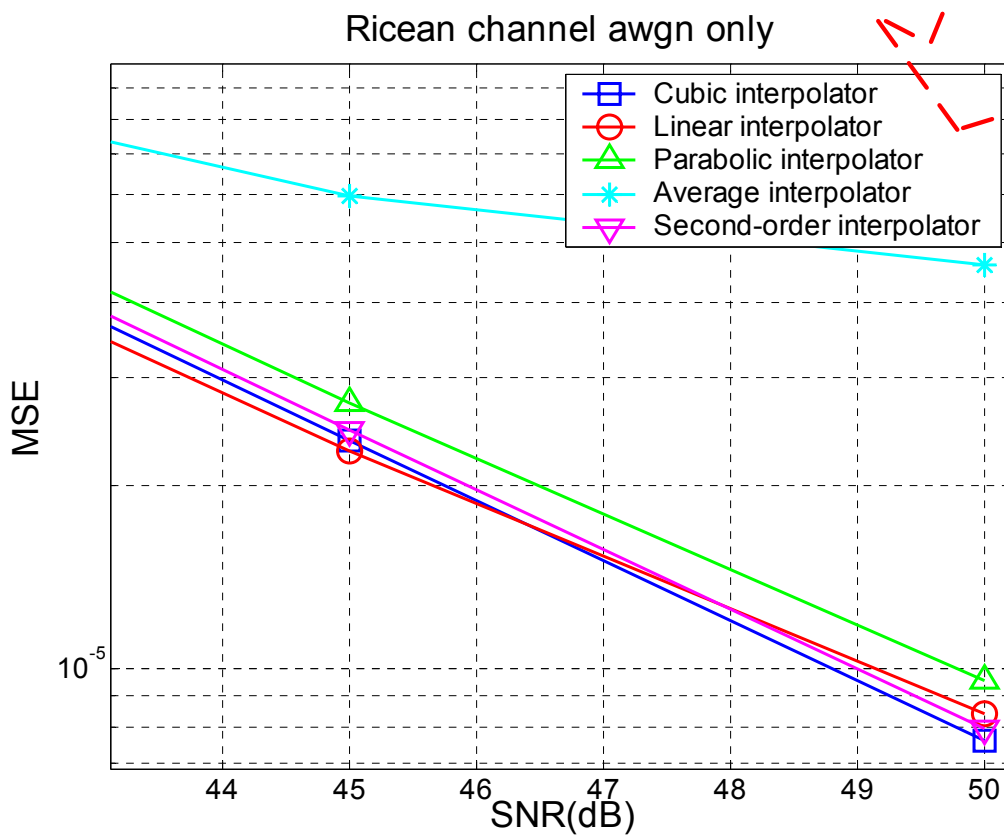
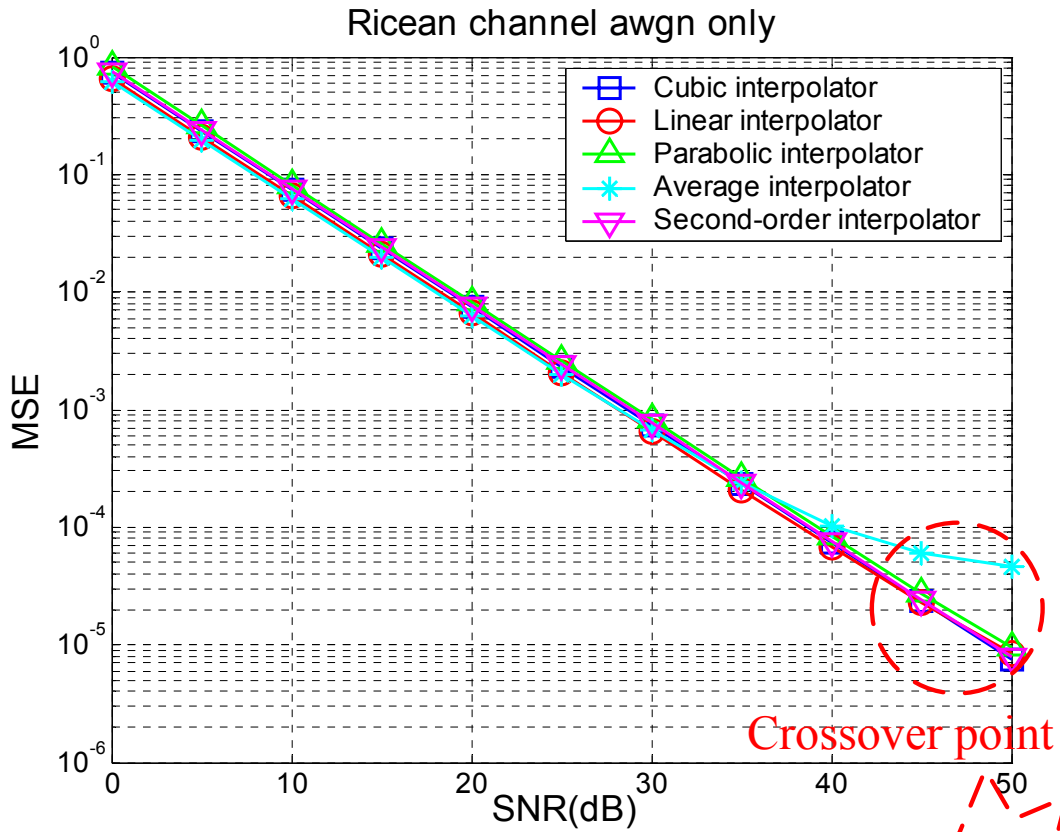


Fig. 4.12 MSE of different frequency interpolator in Ricean channel

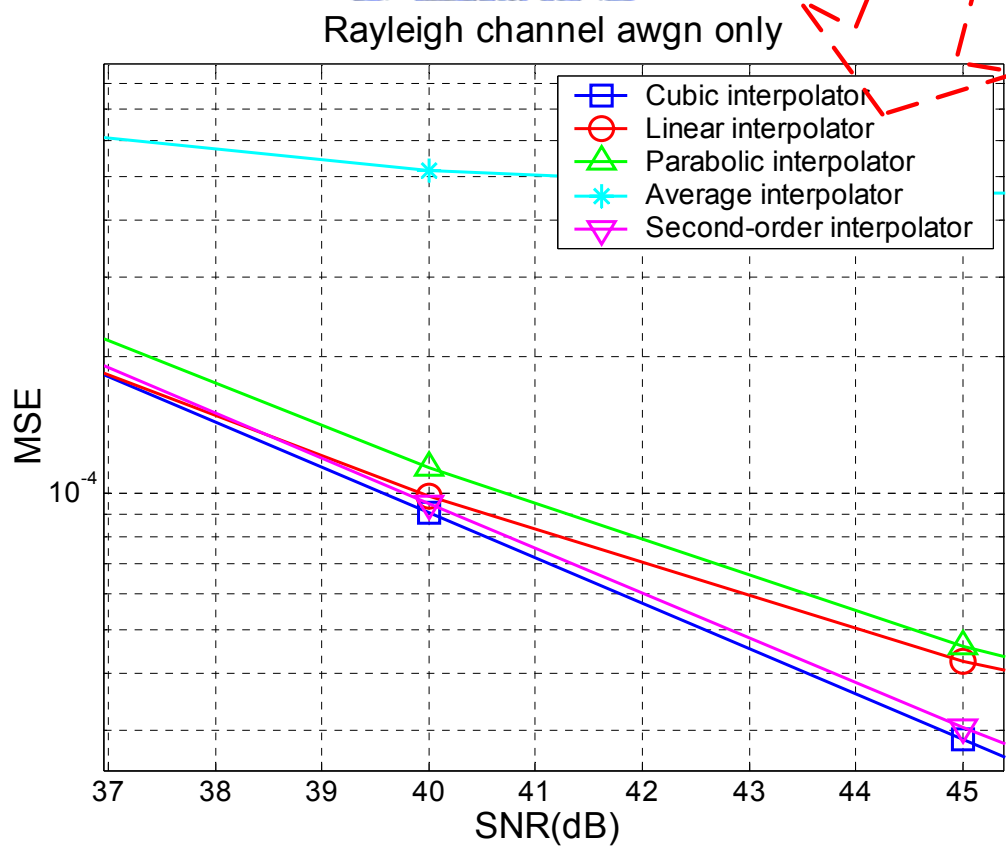
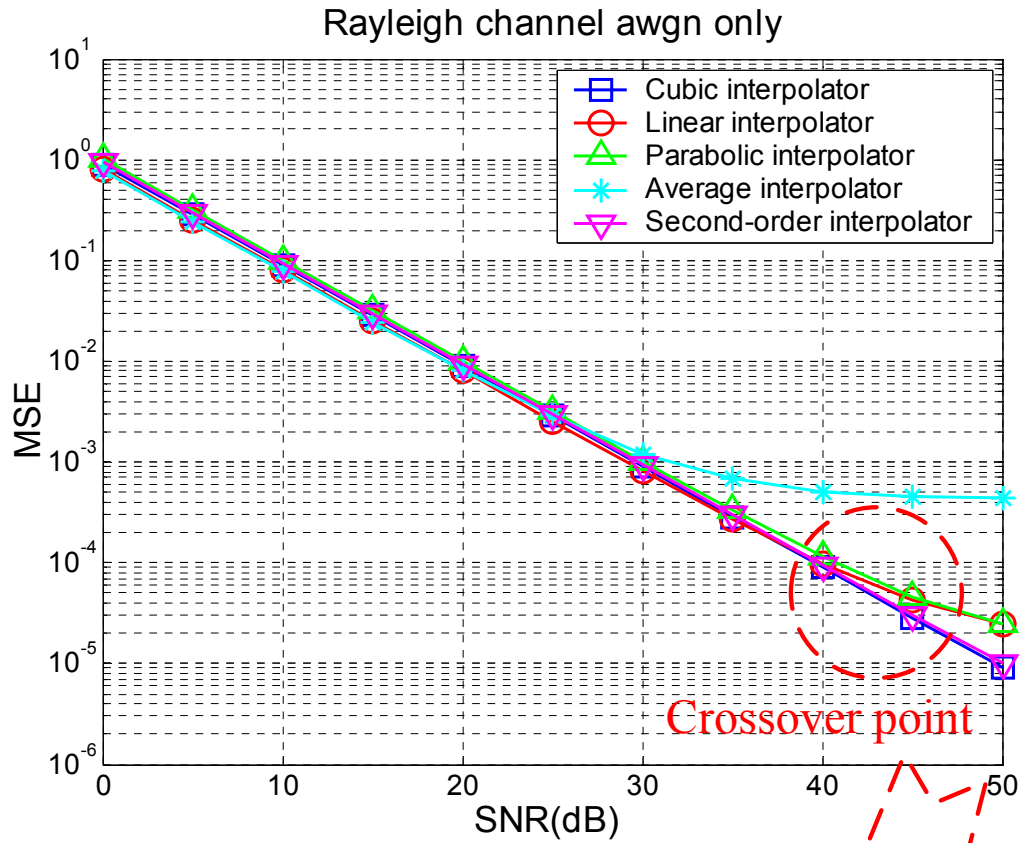


Fig. 4.13 MSE of different frequency interpolator in Rayleigh channel

Here, we define the MSE is the sum of MSE expectation at all subcarriers which is expressed by

$$MSE = \frac{\sum_{k=1}^N E(\hat{H}_k - H_k)^2}{N} \quad (4-7)$$

where N is the total number of subcarriers. Here we use 2k mode for explanation, in 2k mode we can get estimated CFR every three subcarriers after time interpolation. So there are only 1705 subcarriers and 569 (1705/3) subcarrier is estimated by time interpolation. Here they are the same in every interpolation methods which MSE is the $\sum_{k=p} VAR_sample$ term in (4-8).

So the MSE (4-7) becomes to (4-8), where $p \in \{1:3:1705\}$ which are total 569 subcarriers.

$$MSE = \sum_{k=p} VAR_sample + \sum_{k \neq p} E(\hat{H}_k - H_k), p \in \{1:3:1705\} \quad (4-8)$$

In Gaussian channel, the CFR is only effect by AWGN noise. Furthermore, the CFR is the same at every subcarrier ($H_k = 1$), so we can use this AWGN to verify the noise term effects in different interpolation method. From equation (2-21), the MSE can be reduced to (4-9).

$$\begin{aligned} MSE &= E\{|\hat{H} - H_k|^2\} = E\{|\sum_j C_j \times (H_j + N_j) - H_k|^2\} \\ &= (\sum_j C_j^2)E[N_j^2] + \sum_j C_j^2 E[H_j^2] + \sum_{i \neq j} (2C_i C_j \times E[H_i]E[H_j]) - \sum_j (2C_j \times E[H_j]) \times H_k + H_k^2 \\ &\xrightarrow{\text{Gaussian_channel}} (\sum_j C_j^2)E[N_j^2] + (\sum_j C_j^2 + \sum_{i \neq j} 2C_i C_j - \sum_j 2C_j + 1) \end{aligned} \quad (4-9)$$

So we can find $(\sum_j C_j^2 + \sum_{i \neq j} 2C_i C_j - \sum_j 2C_j + 1)$ are zero in each interpolation methods which are listed in Table 2-3. So the MSE of each subcarrier becomes to (4-10).

$$MSE = E\{|\hat{H} - H_k|^2\} = (\sum_j C_j^2)E[N_j^2] \quad (4-10)$$

So the MSE of Linear interpolation is expressed by

$$\begin{aligned} MSE_linear &= \sum_{k=p} VAR_sample + \sum_{k \neq p} E(\hat{H}_k - H_k) \\ &= 569 \times E(N^2) + 1136 \times 0.5555 \times E(N^2) = 1200 \times E(N^2) \end{aligned} \quad (4-11)$$

The MSE of cubic interpolation is expressed by

$$\begin{aligned}
MSE_cubic &= \sum_{k=p} VAR_sample + \sum_{k \neq p} E(\hat{H}_k - H_k) \\
&= 569 \times E(N^2) + 1136 \times 0.6921 \times E(N^2) = 1355.2 \times E(N^2)
\end{aligned} \tag{4-12}$$

So the gap between linear interpolation and cubic interpolation is 0.52dB. (4-13)

$$\begin{aligned}
MSE_cubic &= MSE_linear \times \frac{1200}{1355.2} \\
gap &= -10 \log_{10}\left(\frac{1200}{1355.2}\right) = 0.52dB
\end{aligned} \tag{4-13}$$

In Fig. 4.11, we can find the simulation results can be proven the noise effects will enhanced by different interpolation methods, which is mentioned in section 2.5.2. In Fig. 4.11 we will find there are only AWGN noise effects, so there is no crossover point, even at high SNR region. The performance is AVG > Linear > Cubic > Second-order > Parabolic.

In the other channel types we can still use the MSE criteria to calculate the cross point between linear and cubic interpolation methods. From simulation results, we can find the crossover point is at about SNR=46.5dB in Ricean channel (Fig. 4.12), and at about SNR=38.5 dB in Rayleigh channel (Fig. 4.13). The crossover points are all in the high SNR region, but the system requirement QEF are about less than 30dB [3]. Fig. 4.14 is the simulation results under dynamic channel environments. We can find the uncoded BER are almost the same in each frequency interpolator. In Ricean, Rayleigh, TU6 channel model, we can find the linear interpolator is the best.

So the Linear interpolation in frequency direction is the proper choice than the other interpolation methods which mentioned in section 2.5.2.

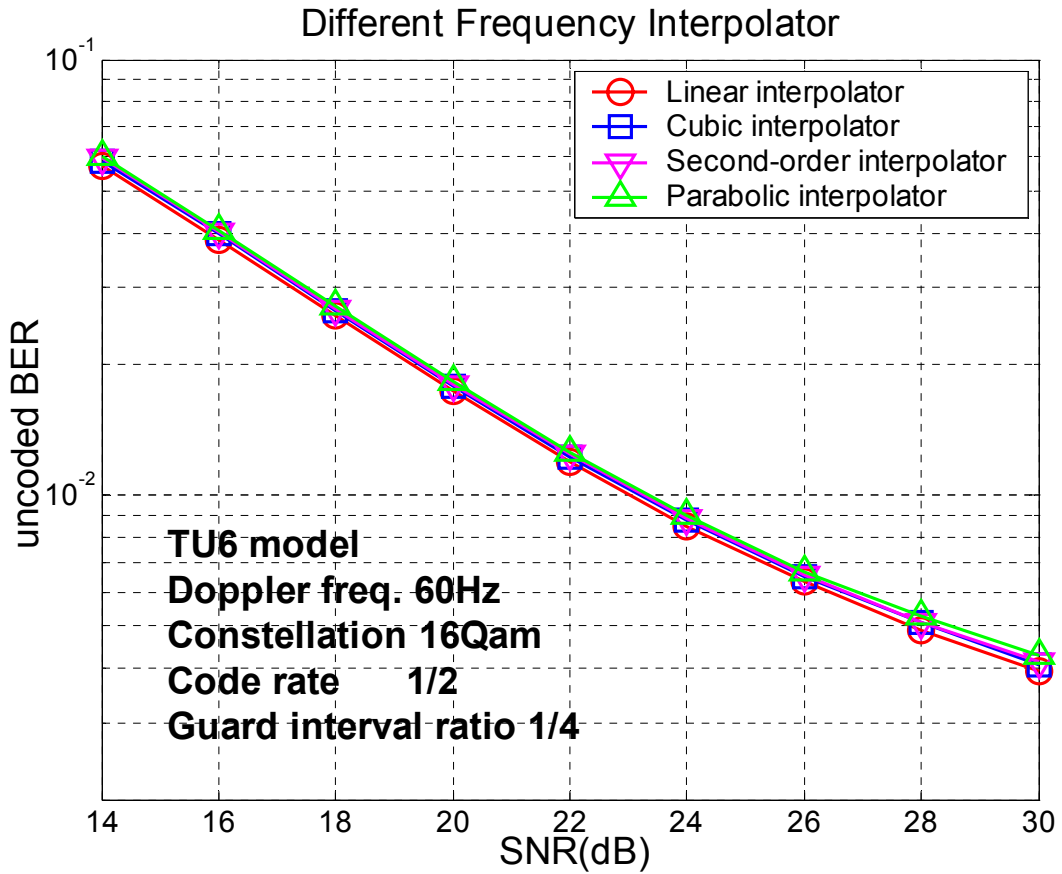


Fig. 4.14 Comparison different frequency interpolator in dynamic channel



4.3.2 Interpolation in time domain

Fig. 4.15 ~ Fig. 4.16 are the simulation results of different time interpolators under different Doppler effects and channel models. In Fig.4.15 we use 2k mode, 64Qam, GI=1/4 and Doppler frequency are 0, 50, 70 Hz under Rayleigh channel. In Fig.4.16 we use 2k mode, 16Qam, GI=1/4 and Doppler frequency are 60, 90 Hz under TU6 channel. The solid line is the linear interpolation method, and the dashed line is the 1st-order extrapolation methods which are mentioned in section 2.5.1. Furthermore, the BER performance achievement is based on the uncodded BER equal to 10⁻².

From the simulation results we can find the 1st order extrapolation is much worse than linear interpolation method, although 1st order extrapolation can save large memory for three OFDM symbols. Cost is trade off to the performance. Table 4-3 and Table 4-4 show that the

1st order extrapolation equalizers can tolerate Doppler frequency 60Hz under dynamic channel. Though 2.5dB to 5dB SNR losses compared with linear interpolators, but 78% storage can be saved by using 1st-order extrapolation.

We can find the performance is much sensitive to the interpolation in time directions. However, for mobile reception, we still propose the linear interpolation in time direction.

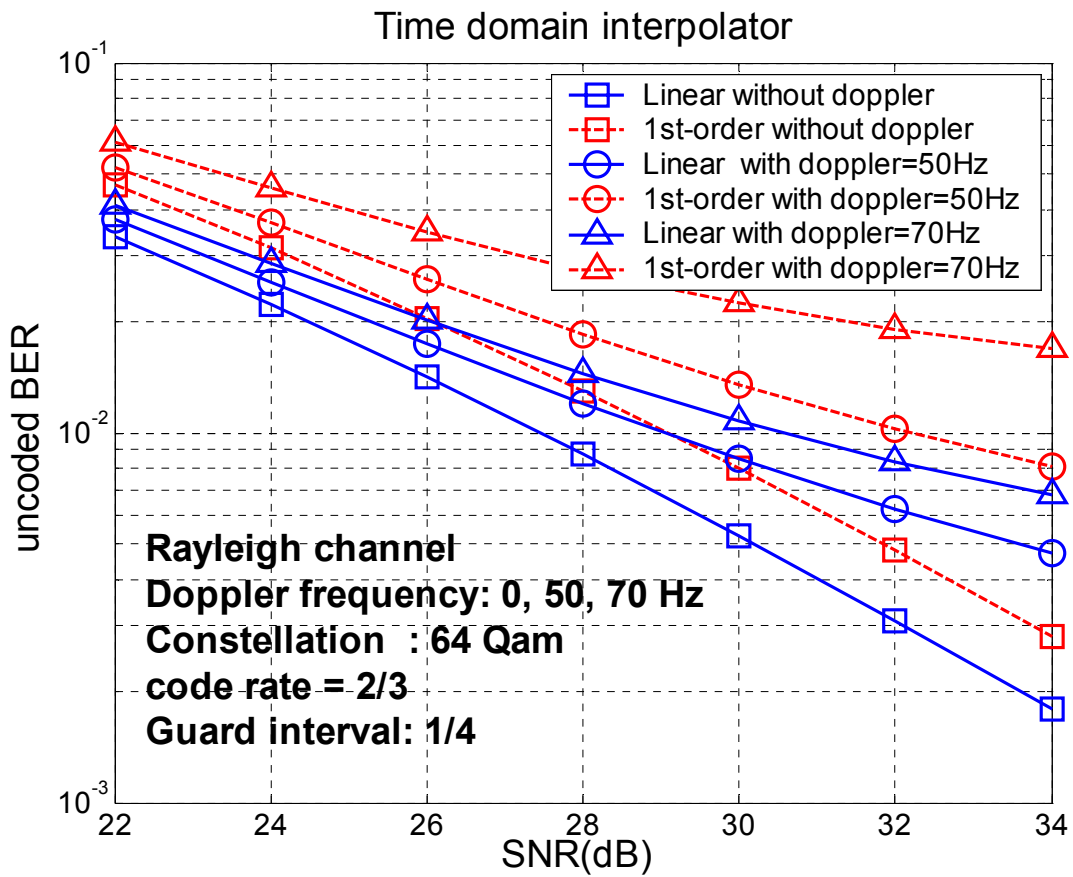


Fig. 4.15 Different time interpolator under Rayleigh channel

Table 4-3 Comparison on performance and cost under Rayleigh channel model

Time interpolator	Doppler range	SNR loss *	Storage requirements(2K)
1 st -order	60	2.5 dB@55Hz	1138 carriers
Linear	>80	0dB	5115 carriers

(* compared with linear interpolator)

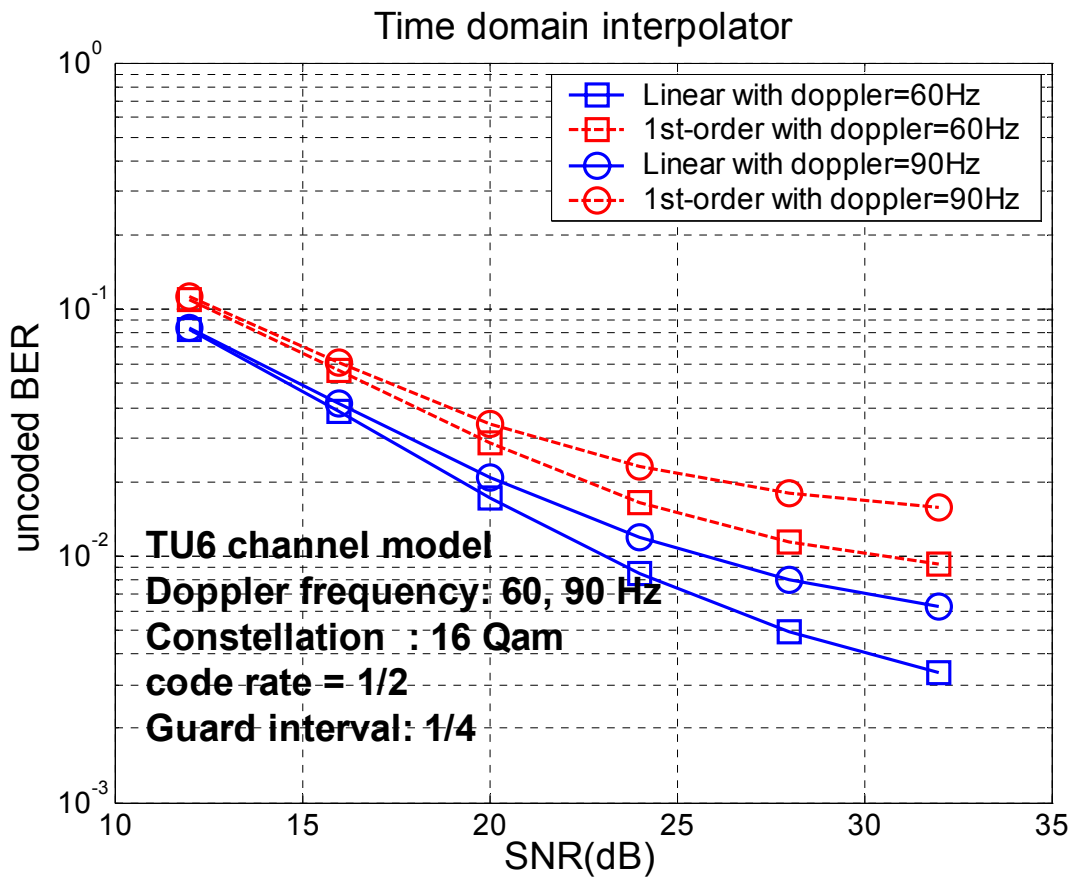


Fig. 4.16 Different time interpolator under TU6 channel

Table 4-4 Comparison on performance and cost under TU6 channel model

Time interpolator	Doppler range	SNR loss *	Storage requirements(2K)
1 st -order	60	6 dB@60Hz	1138 carriers
Linear	>90	0dB	5115 carriers

(* compared with linear interpolator)

4.3.3 Transform domain processing

In section 2.4 we use transform domain processing to implement the low pass filter [11]. The transform domain processing is depicted in Fig. 2.11. There are an M-point FFT, and need to decide the cutoff frequency p_c . In fact, we can do the transform domain processing

after interpolation in time direction, so we can get better accuracy. In 2K mode, there are only 142 (1705/12) CFR for scatter pilots, and we can get 568 (1705/3) after interpolation in time direction. So the resolution is increasing, but more point FFT we need.

Furthermore, the cutoff frequency p_c of the transform domain low-pass filter is an important parameter that affects the accuracy of the channel estimation. Therefore the p_c can be determined from (2-13). The energy ratio R is suggested by [11], $R \in [0.9, 0.95]$.

Fig. 4.17 shows the simulation results of different $R \in [0.8, 0.85, 0.9, 0.95]$ under static channel, and Fig. 4.18 shows the simulation results under dynamic channel. Here we can find the best performance is $R=0.9$ and it can get 0.25 dB in static channel and 0.2dB in dynamic channel. However, it needs a 568 point FFT and IFFT in 2K mode, but the hardware cost is very high. So this method is not efficient in DVB-T/H systems.

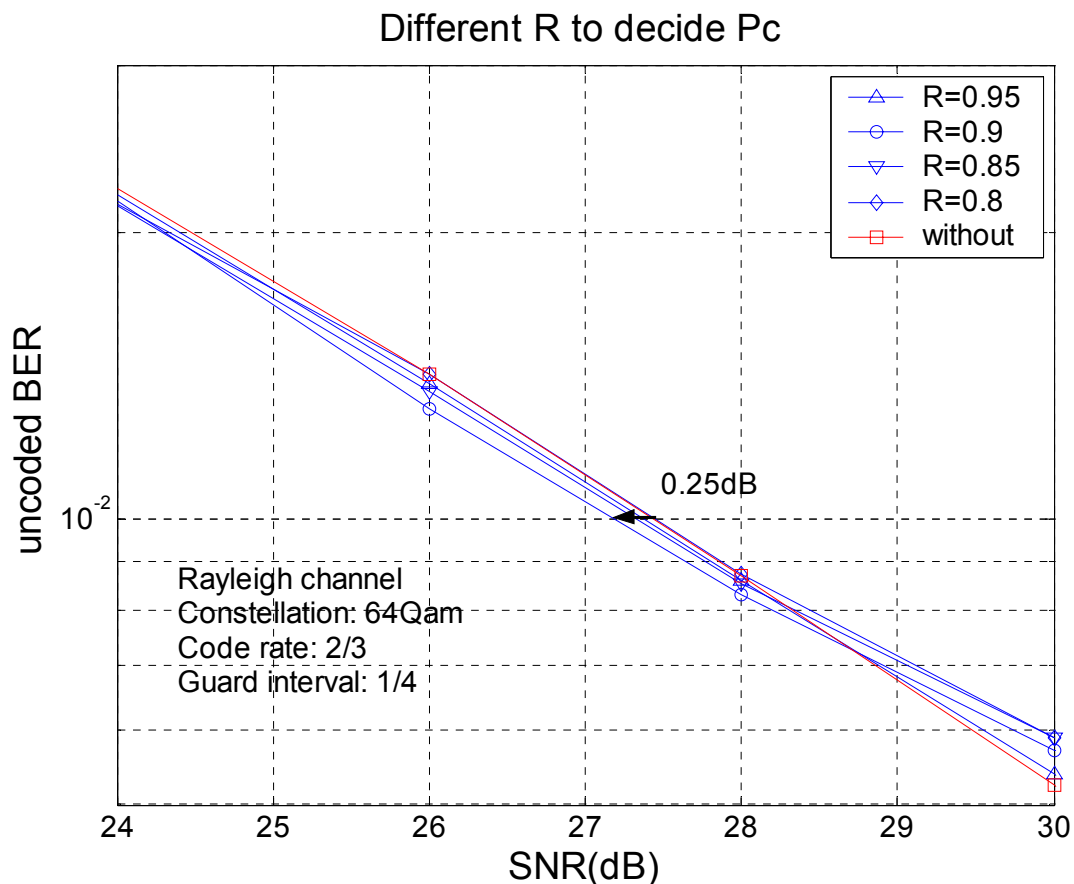


Fig. 4.17 Performance between different R under Rayleigh channel

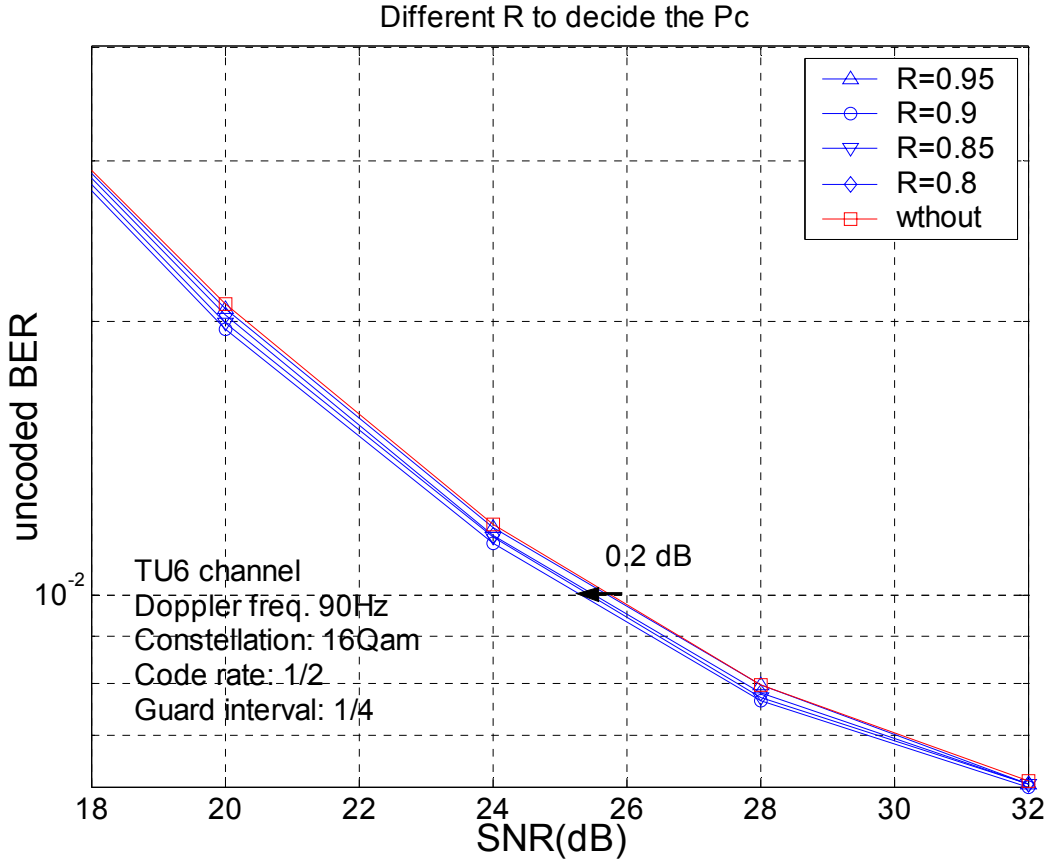


Fig. 4.18 Performance between different R under TU6 channel



4.3.4 Channel estimator for pilot signal

We proposed an adaptive channel estimator for pilot signal in section 2.3. The adaptive weights for estimator in (2-8) are based on MSE criterion in (2-9). Here, we based on the low hardware cost issue, so we assume the weights $\beta \in \{0, 0.25, 0.5, 0.75\}$ four kinds. In equation (2-9), we rewrite it again in (4-14). There are two parameters $E(D^2)$ and $E(N^2/X^2)$ are estimated roughly by a simple algorithm, and the implementation methods are described in next Chapter 5.2.

$$\begin{aligned}
 MSE &= E(\hat{H}_0 - H_0)^2 \\
 &= E(D_1(1-\beta)\beta + D_2\beta^2)^2 + E\left(\frac{N^2}{X^2}\right) \left[(1-\beta)^2 + (1-\beta)^2\beta^2 + \beta^4 \right] \\
 &\xrightarrow{D_2=2D_1} E(D_1^2) [\beta^2 + 2\beta^3 + \beta^4] + E\left(\frac{N^2}{X^2}\right) [1 - 2\beta + 2\beta^2 - 2\beta^3 + 2\beta^4]
 \end{aligned} \tag{4-14}$$

In this section, we show the simulation results between fixed weights [14-16] and

proposed estimator with adaptive 4 kinds of weights $\beta \in \{0, 0.25, 0.5, 0.75\}$. We list the simulation results of static channel and dynamic channel under different frequency effects on table 4-5. Furthermore, Fig. 4.19.~Fig.4.21. show the performance between different β . We can find the $\beta=0.75$ is the best choice in static channel without Doppler effects. As Doppler increasing, the time dependency of channel is less, so the performance will be better with lower β . However, the channel can't be static, so if we fix β to some value, we can find that, when channel with high Doppler frequency effects, the performance will degrade seriously. But in proposed adaptive β estimator, it will let β equal to zero which only use the current symbol information without the previous symbol information. Therefore, it will not to degrade the performance when channel with high Doppler effects.

From simulation results, we can find the proposed estimator could select the proper β at each subcarrier. Here, we will show the performance of the overall system. We list the required SNR for QEF condition which corresponds to 2×10^{-4} BER after Viterbi decoder. We can find in the proposed estimator method we can achieve $f_d = 70$ Hz under Rayleigh channel and $f_d = 150$ Hz under TU6 channel.

From table 4-5, we can find the proposed method can gain 0.3dB in Ricean channel under Doppler frequency 30 Hz, 0.2 dB in Rayleigh channel under Doppler frequency 10 Hz, and 0.2dB in TU6 under Doppler frequency 60 Hz. So the proposed adaptive estimator can get a little improvement under middle Doppler frequency effects environment, it can't degrade the performance in high Doppler frequency effects.

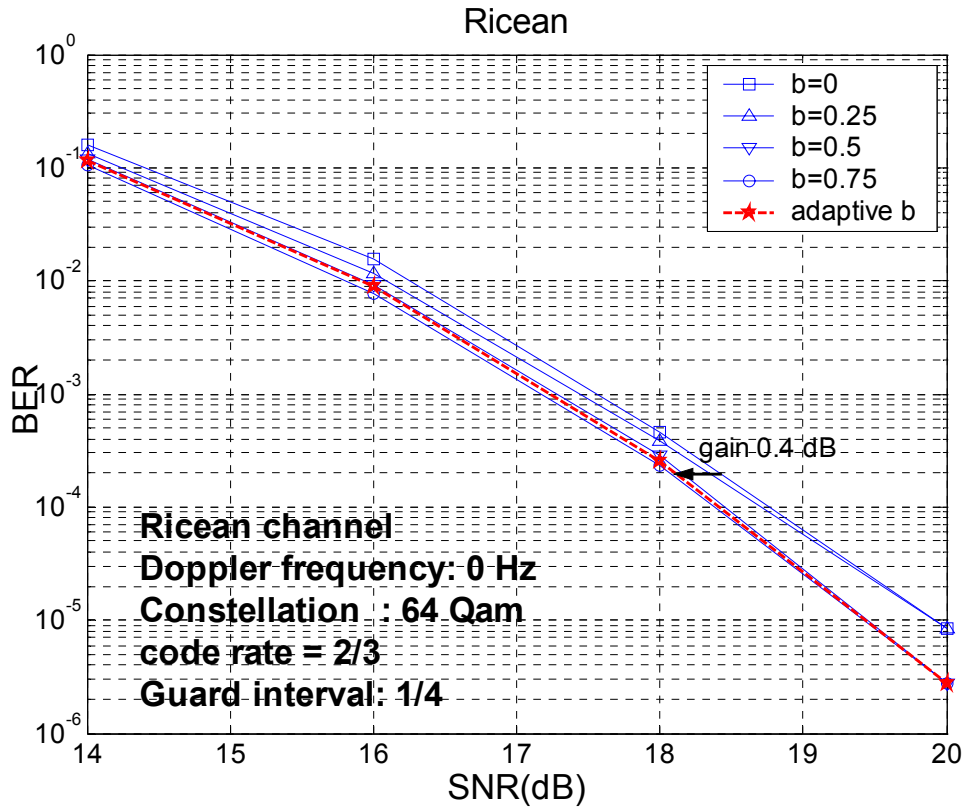


Fig. 4.19(a) Performance under static Ricean channel

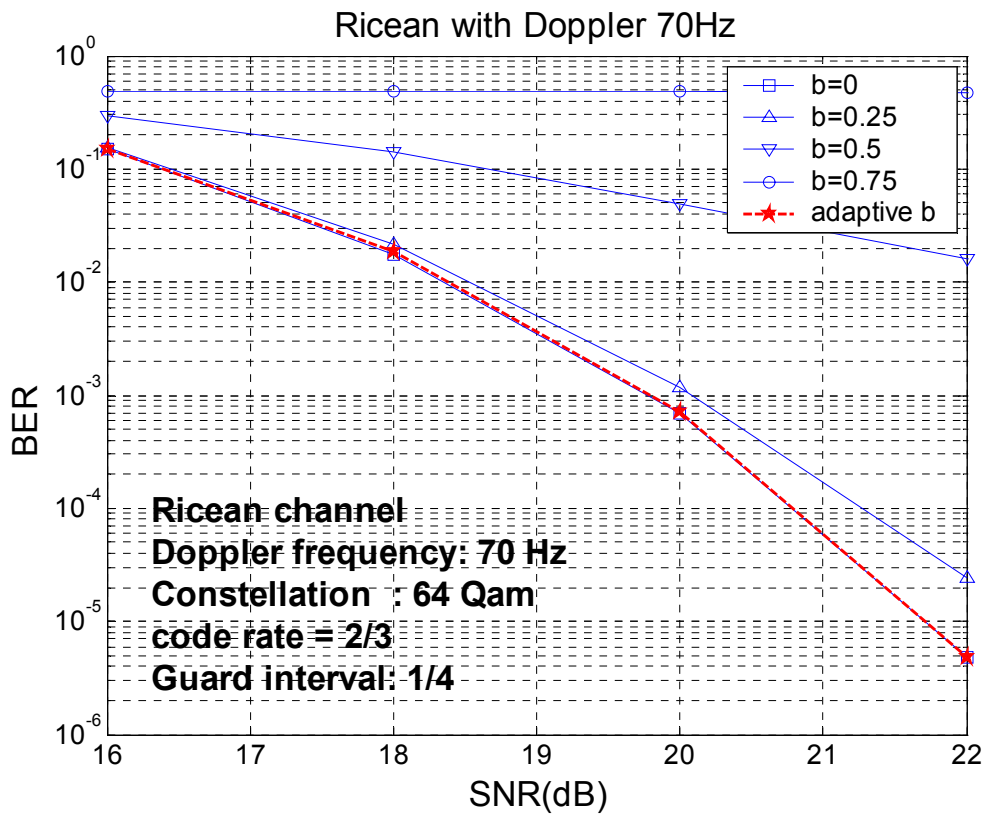


Fig. 4.19(b) Performance under Ricean channel with 70Hz Doppler

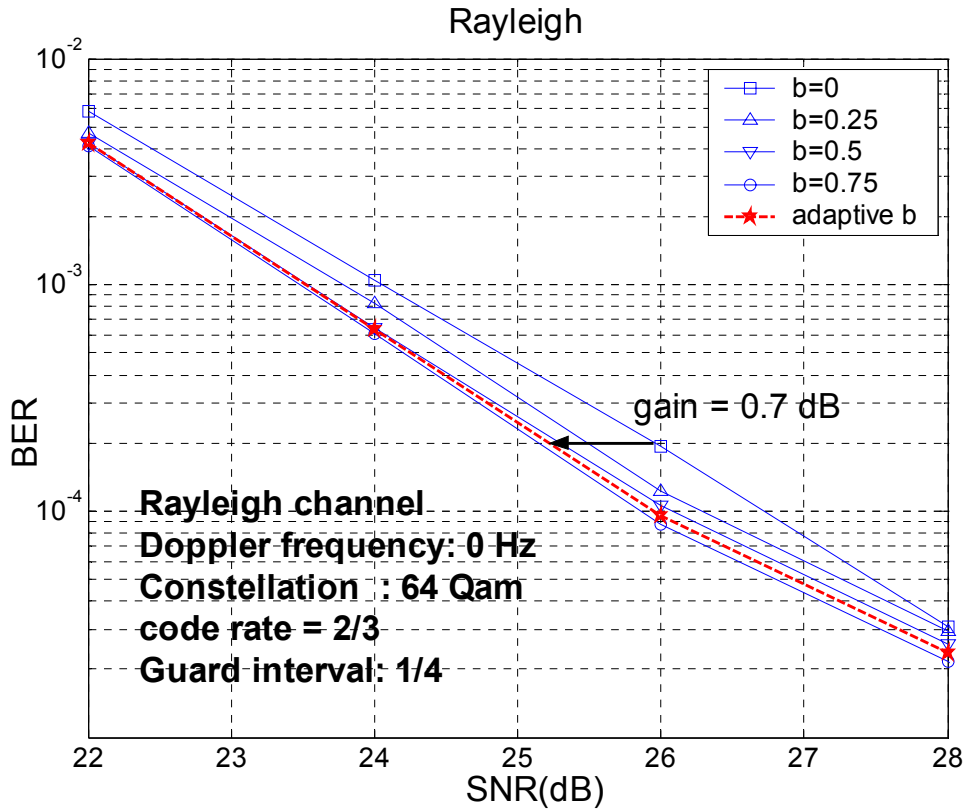


Fig. 4.20(a) Performance under static Rayleigh channel

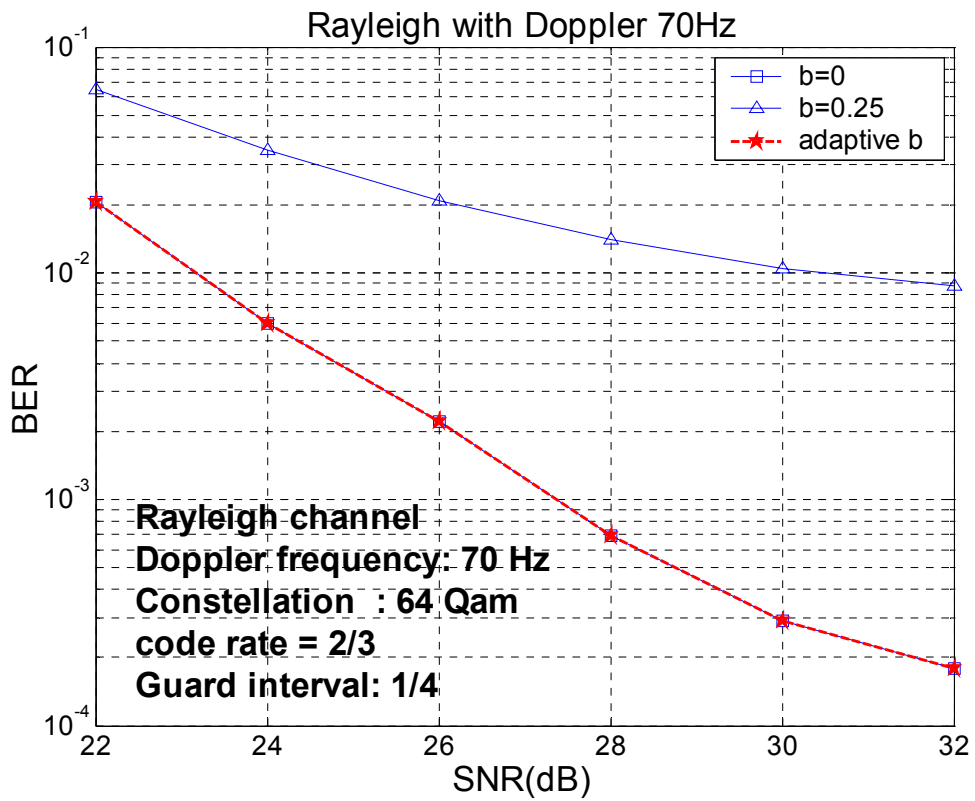


Fig. 4.20(b) Performance under Rayleigh channel with 70Hz Doppler

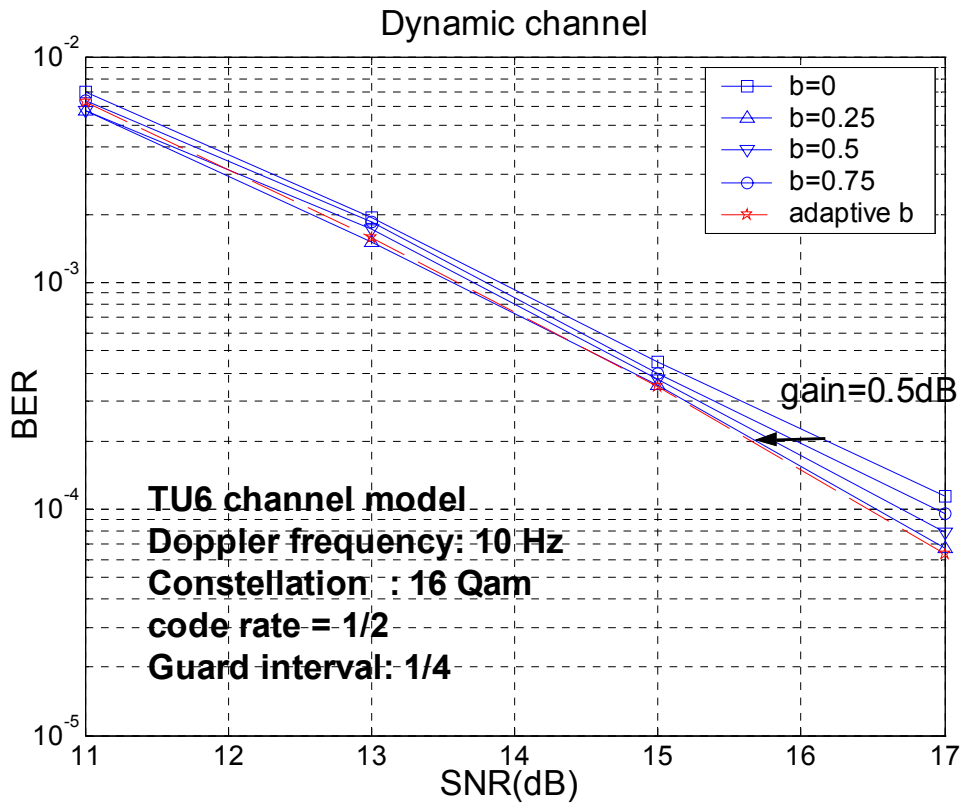


Fig. 4.21(a) Performance under TU6 channel with 10Hz Doppler

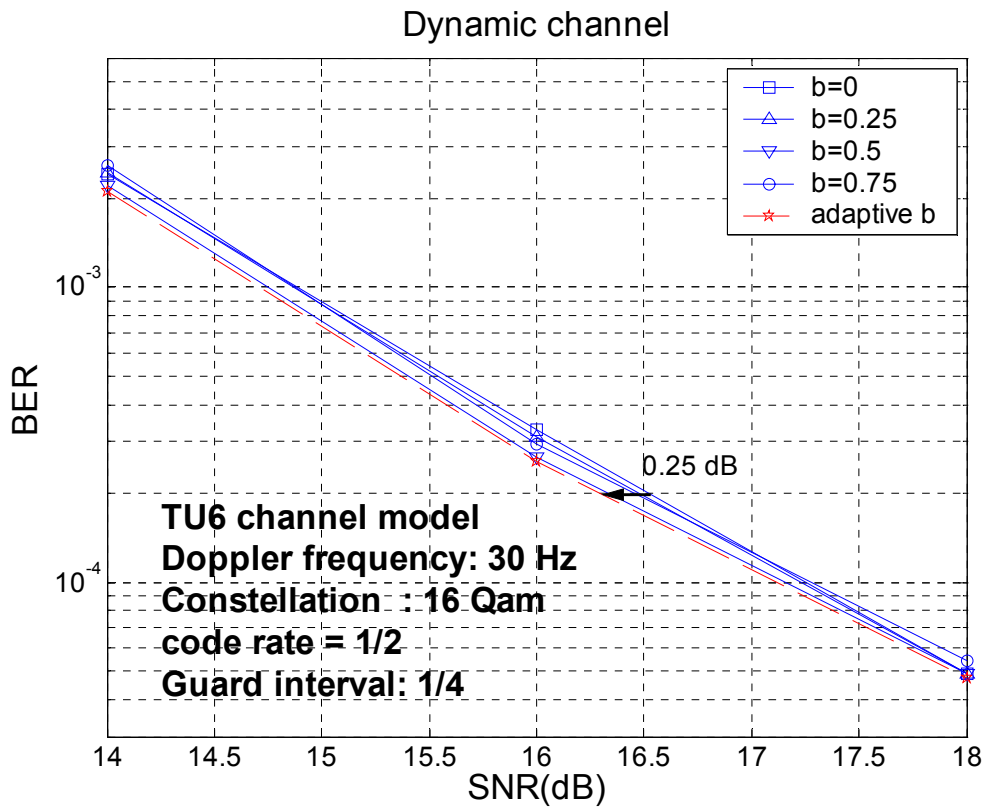


Fig. 4.21(b) Performance under TU6 channel with 30Hz Doppler

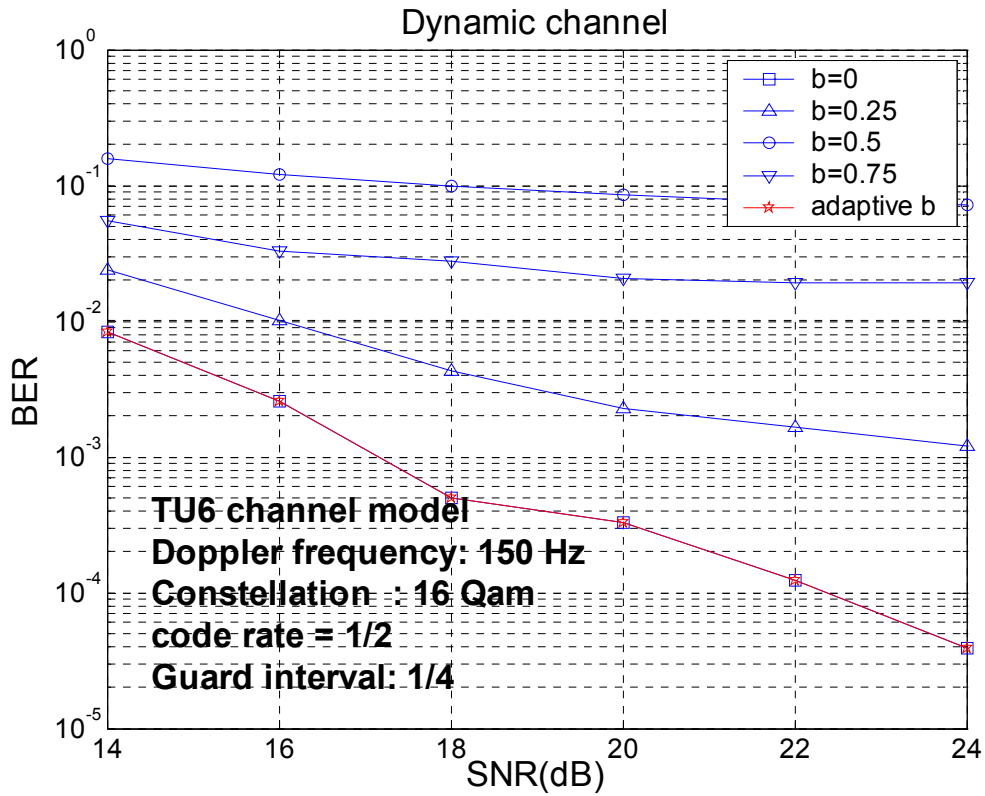


Fig. 4.21(c) Performance under TU6 channel with 150Hz Doppler

Table 4-5(a) Comparison on performance between different β

<i>Ricean channel with different Doppler effects: 2K mode, 64Qam, code rate=2/3, GI=1/4</i>						
<i>required SNR (dB) for BER=2x10⁻⁴ after Viterbi</i>						
Doppler(Hz)	$\beta=0$	$\beta=0.25$	$\beta=0.5$	$\beta=0.75$	Adaptive β	Gain (*)
0	18.5	18.35	18.15	18.05	18.1	0.4
10	19.15	18.8	18.75	18.85	18.75	0.4
30	19.62	19.38	19.45	22.2	19.32	0.3
50	20.14	21.5	NA	NA	20.14	0
70	20.5	20.9	NA	NA	20.5	0

(* compared to $\beta=0$, NA : can't achieve BER=2x10⁻⁴)

Table 4-5(b) Comparison on performance between different β

<i>Rayleigh channel with different Doppler effects: 2K mode, 64Qam, code rate=2/3, GI=1/4</i>						
<i>required SNR (dB) for BER=2x10⁻⁴ after Viterbi</i>						
Doppler(Hz)	$\beta=0$	$\beta=0.25$	$\beta=0.5$	$\beta=0.75$	Adaptive β	Gain (*)
0	25.95	25.5	25.3	25.2	25.25	0.7
10	28.2	28	NA	NA	28	0.2
30	29	40	NA	NA	29	0
50	29.65	NA	NA	NA	29.65	0
70	31.5	NA	NA	NA	31.5	0

(* compared to $\beta=0$, NA : can't achieve BER=2x10⁻⁴)

Table 4-5(c) Comparison on performance between different β

<i>Dynamic channel (TU6) with different Doppler effects: 2K mode, 16Qam, code rate=1/2,</i>						
<i>GI=1/4 required SNR (dB) for BER=2x10⁻⁴ after Viterbi</i>						
Doppler(Hz)	$\beta=0$	$\beta=0.25$	$\beta=0.5$	$\beta=0.75$	Adaptive β	Gain (*)
10	16.2	15.7	15.8	15.95	15.7	0.5
30	16.55	16.45	16.3	16.4	16.3	0.25
60	18.2	18	NA	NA	18	0.2
90	18.5	19.4	NA	NA	18.5	0
150	21	NA	NA	NA	21	0

(* compared to $\beta=0$, NA : can't achieve BER=2x10⁻⁴)

Chapter 5 .

Architecture and Implementation

In this chapter, the platform based design methodology will be introduced first. Then the architecture of the implemented DVB-T/H receiver will be illustrated. The architecture of the proposed channel equalizer design, hardware synthesis information and chip summary will be shown in the following sections.

5.1 Design Methodology

The trend of IC technology is towards to System-on-Chip (SoC). System-level simulation becomes very important in today's design flow. Our design methodology from system simulation to hardware implementation can be shown in Fig. 5.1. First, the system platform and channel modals should be established according to the system specification with MATLAB language, which ensures the design in the practical condition. Algorithm research and architecture development of each function block should be verified in the system platform to ensure the whole system performance. Fixed-point simulation is applied before hardware implementation to make the trade-off between system performance and hardware cost. In hardware implementation, the Verilog HDL modules are verified with the test benches dumped from the equivalent Matlab blocks to ensure the correctness. Finally, once the verification between HDL modules and fixed-point MATLAB platform is finished, the HDL based platform will be synthesized and translated to circuit level by place and route (P&R) tools.

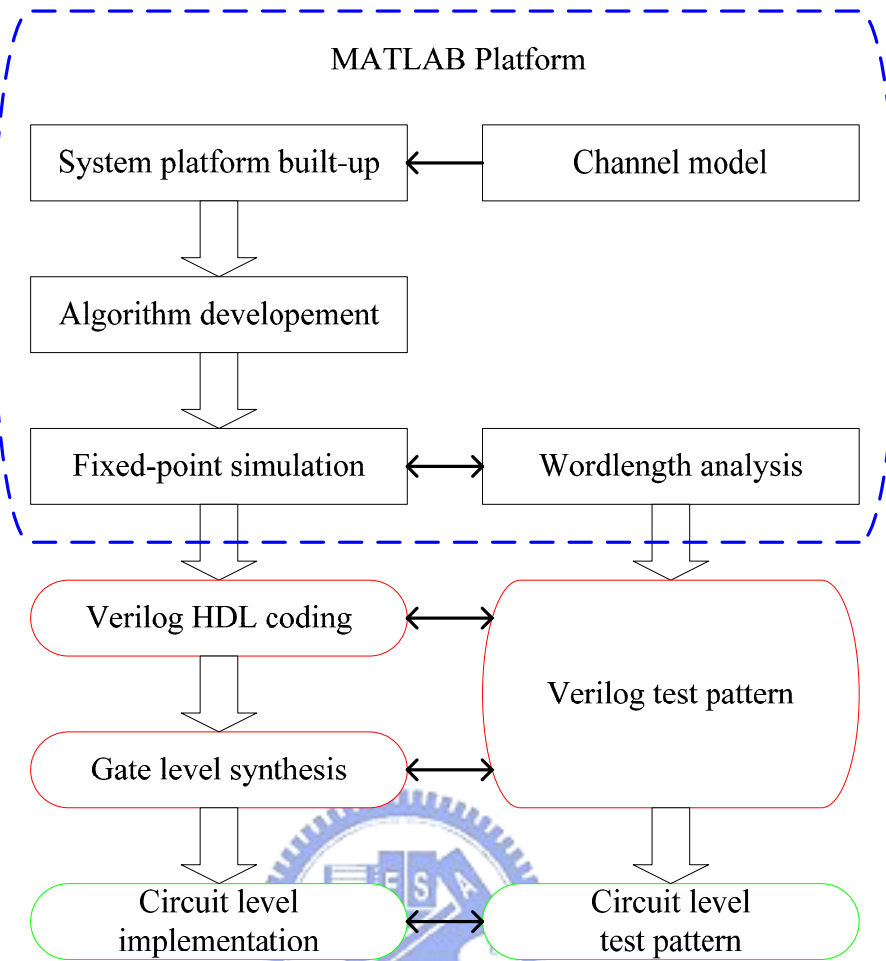


Fig. 5.1 Platform-based design methodology

5.2 Architecture of the DVB-T/H Baseband Receiver[28]

Based on the 2x1D linear interpolation channel estimation scheme and other low power designs such as high speed FEC decoder and dynamic scheduling FFT processor [29], a DVB-T/H baseband receiver is implemented and tapped out in Jun. 2005. The detailed structure in OFDM demodulator is shown in Fig.5.2. In the initial phase, the timing synchronizer estimates Operation Mode (2K/4K/8K), Guard Interval length, and symbol boundary with auto-correlation and power detection. Then the received signal is sent to FFT and the CFO integer is estimated with a monitor of frequency-domain signal drift. The FFT is realized with radix-8 butterfly units, a dynamic wordlength-scaling (DWC) method, and a cache-based architecture to provide 2K/4K/8K modes with less memory power. After FFT

operation, both time-variant CFR and CFO are estimated and tracked by a 2D linear EQ. The equalized signal is sent to symbol deinterleaver. Different from the general approaches, the symbol interleaving is done before QAM demapping. That is because the developed 64-level QAM soft-demapping is designed with a 24-bit input and a 36-bit output to achieve low BER of DVB-T/H. After the de-QAM constellation, the clock rate is raised up to six times of the original data rate to satisfy the bit-level calculation. In DVB-T/H system, different channel bandwidths will correspond to different clock rates. The highest clock rate of the received data is about 9MHz when the 8MHz channel bandwidth is utilized. In order to assure that the implemented chip can work in such condition properly, the basic clock rate of the synthesis result is set at 11MHz.

Power profiling and die photo of the proposal implemented in standard 0.18 μ m CMOS process is shown in Fig.5.3 and Fig.5.4 respectively. Furthermore, chip summary is listed in table 5-1. A 109.71MHz system clock is referenced to provide the working clocks with the frequency division method. Integrating OFDM demodulator and FEC designs, the proposed DVB-T/H baseband receiver consumes 250mW power for the highest data rate 31.67Mb/s with 70Hz Doppler frequency tolerance.

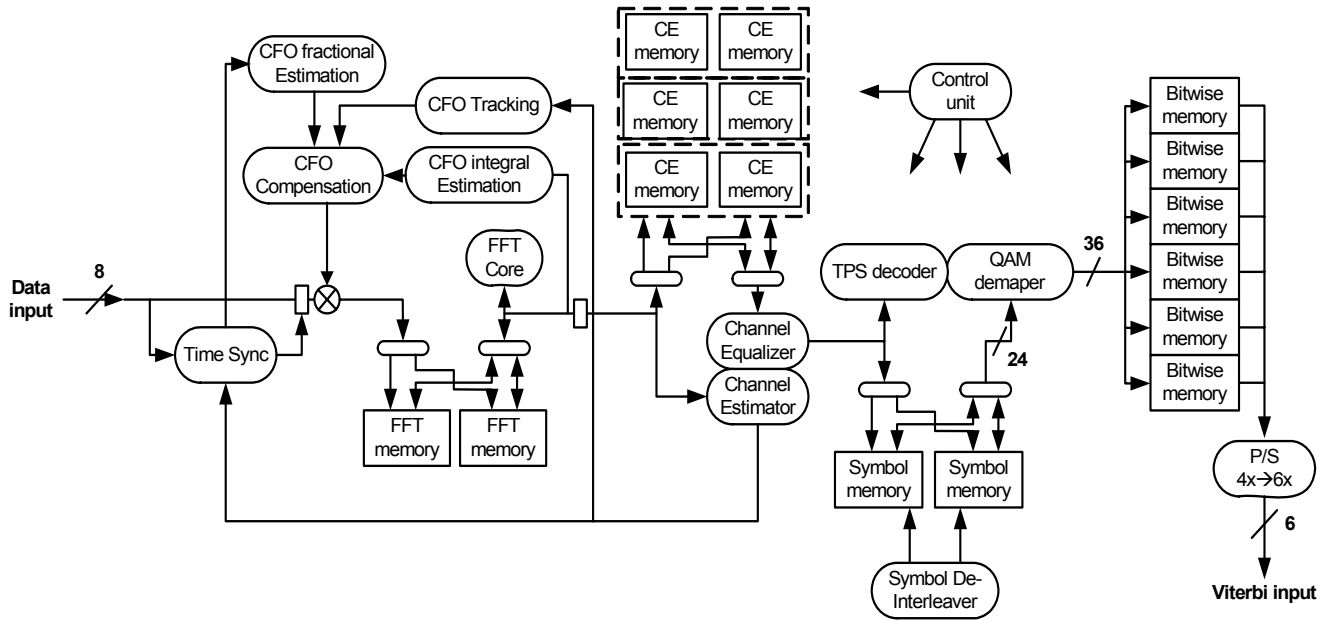


Fig. 5.2 Architecture of the DVB-T/H baseband receiver

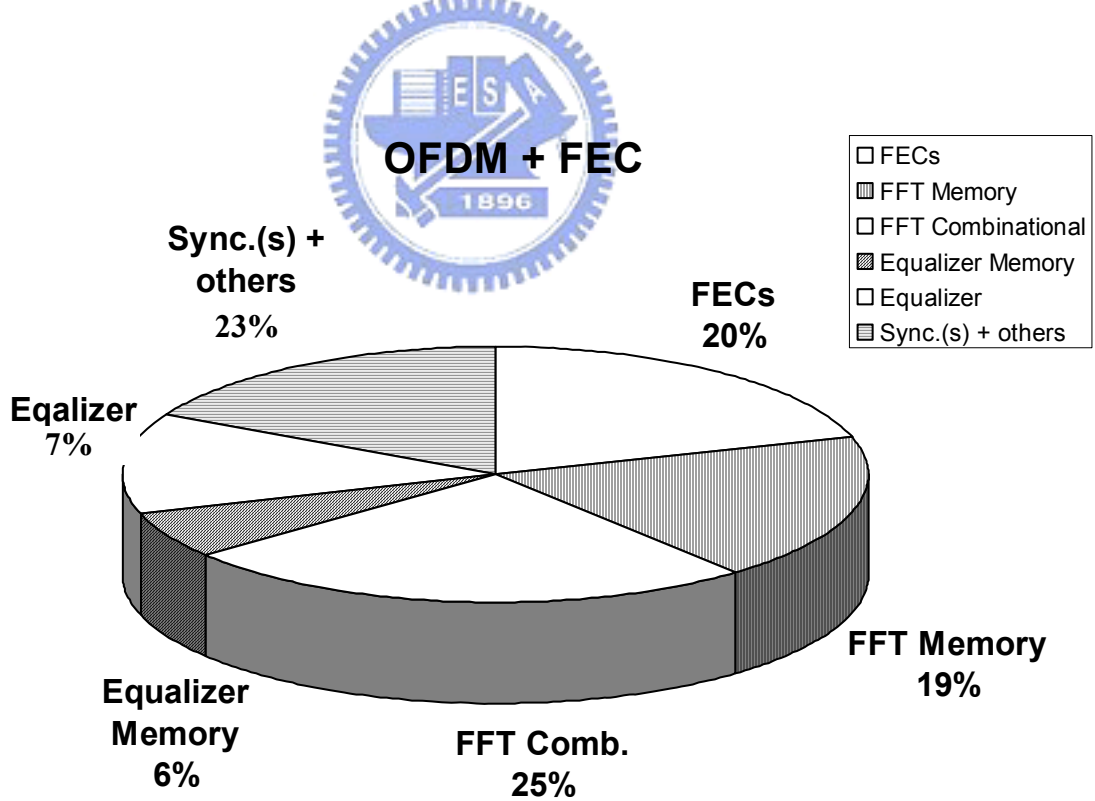


Fig. 5.3 Power profiling

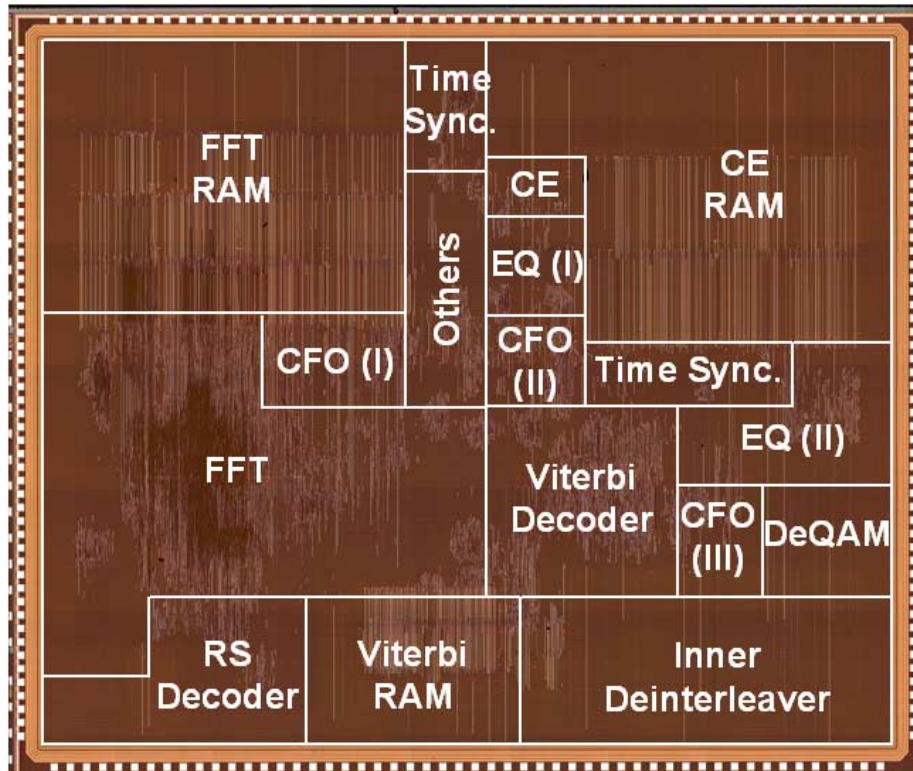


Fig. 5.4 Chip photo

Table 5-1 Chip summary

Process	0.18um CMOS, 1P6M
Logic Gate Count (Excluding SRAM)	371K
Embedded Memory Size	158 K bytes
Package	208-pin CQFP
Die Size	6.9 X 5.8 mm²
Input Clock Speed	109.71 MHz
Supply Voltage	1.8V Core, 3.3V I/O
Power Consumption	250mw@31.67Mb/s with 70Hz Doppler freq.
Supporting Standard	DVB-T/DVB-H
Operation mode	2K, 4K, 8K
Guard Interval ratio	1/2, 2/3, 3/4, 5/6, 7/8
Modulation	QPSK, 16QAM, 64QAM

5.3 *Architecture of Channel Equalizer*

In this section, the detailed architecture of channel equalizer scheme will be illustrated. First, we show the proposed estimation architecture which based on the existing hardware cost and take a little additional cost, which can get about 0.3 dB gain. Second, we modified the equalization architecture, and we can save a lot of hardware cost and power in division model. Finally, we will show the hardware comparisons between proposed method and the implemented DVB-T/H receiver chip which is tapped out in Jun. 2005 [28].

5.3.1 Channel estimation architecture

In this section, we will introduce the hardware architecture for proposed estimation scheme. The performance and cost are trade off, so here we proposed efficiency structure. In section 2.3, the adaptive channel estimator for pilot signal will get about 0.3 dB gain below 30Hz Doppler effects. The simulation results of rough estimation for $E[D^2]$ and $E[N^2/X^2]$ are listed in section 4.3.4. Here we will introduce the rough estimation and it only takes few hardware cost. Furthermore, the transform domain processing [11] is not efficiency in DVB-T/H applications. Because, it needs take 568 points FFT and IFFT in 2K mode and only gain smaller than 0.2 dB which mentioned in section 4.3.3. Here, we will introduce the architecture of 2x1D linear interpolation with proposed adaptive channel estimator.

Fig. 5.5 shows the architecture for 2x1D linear interpolation. Consider 2K mode, there are 3x1705 RAM for storing three OFDM symbols to implement the non-causal property, and 569 RAM for storing previous pilots. Linear interpolation can only use shift and adder based method to implement, so the hardware cost is low. In this architecture, we can find the cost is dominant by memory. The critical path and combinational cost are dominant by complex division operation. We will propose the modified architecture for complex division by low

cost and low power issue.

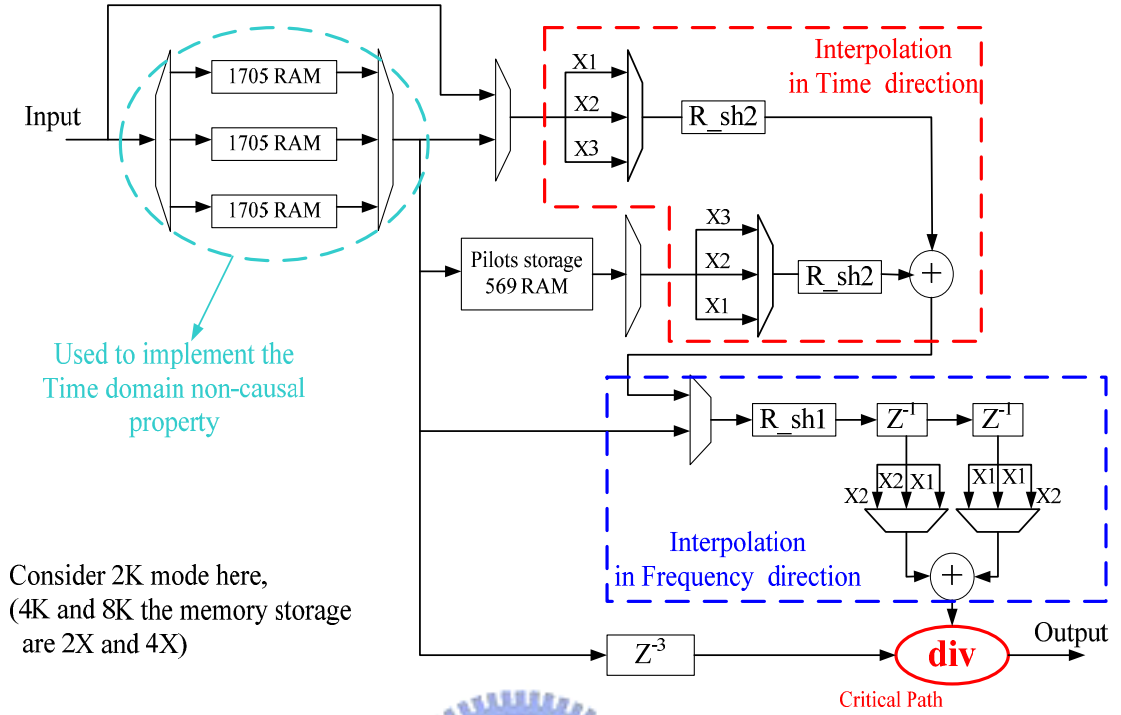


Fig. 5.5 The architecture for 2x1D linear interpolation channel equalization

Based on the Fig. 5.5 channel estimation architecture, Fig. 5.6 shows the estimation for $E[N^2/X^2]$, we estimate the noise variance by continuous pilots. We take all continuous pilots in memory, so there are 4x45 samples (45 CP subcarriers in 2K mode). We calculate each variance by four samples of CP sub-carrier, and then we average the $E[N_i^2/X^2]$ to get the rough estimation for $E[N^2/X^2]$. The ideal value for $E[N^2/X^2]$ is $10^{-(SNR-2.5)/10}$ because of the boosted pilots amplitude $\pm 4/3$. The $E[D_i^2]$ is estimated by the previous three samples at SP sub-carrier, and we calculate the variance of these tree samples to be estimation for $E[D_i^2]$, which shows in Fig. 5.7. Based on the MSE (2-9) we can simplify it to (5-1).

$$\begin{aligned}
 MSE &= E(\hat{H}_0 - H_0)^2 \\
 &\xrightarrow{D_2=2D_1} E(D_1^2)[\beta^2 + 2\beta^3 + \beta^4] + E\left(\frac{N^2}{X^2}\right)[1 - 2\beta + 2\beta^2 - 2\beta^3 + 2\beta^4] \quad (5-1) \\
 &= E(D_1^2) \times C1 + E\left(\frac{N^2}{X^2}\right) \times C2
 \end{aligned}$$

In (5-1), the $C1$ and $C2$ are constants for $\beta \in \{0, 0.25, 0.5, 0.75\}$, so we can save the coefficients into registers in advance. The coefficients are listed in table 5-2. The adaptive estimators for pilot signal architecture is shown in Fig. 5.8. In Fig. 5.8, the hardware architecture, we can find the additional hardware cost are the $E[N^2/X^2]$ and $E[D^2]$ detection, one MSE comparator, several MUXs, shifter and adders, which are all combinational logic. Furthermore, the SP distance is 12 sub-carriers, which means, we can make one β_i every 12 received-data, so the hardware can be reused by efficient scheduling. In addition, the performance is mentioned in section 4.3.4.

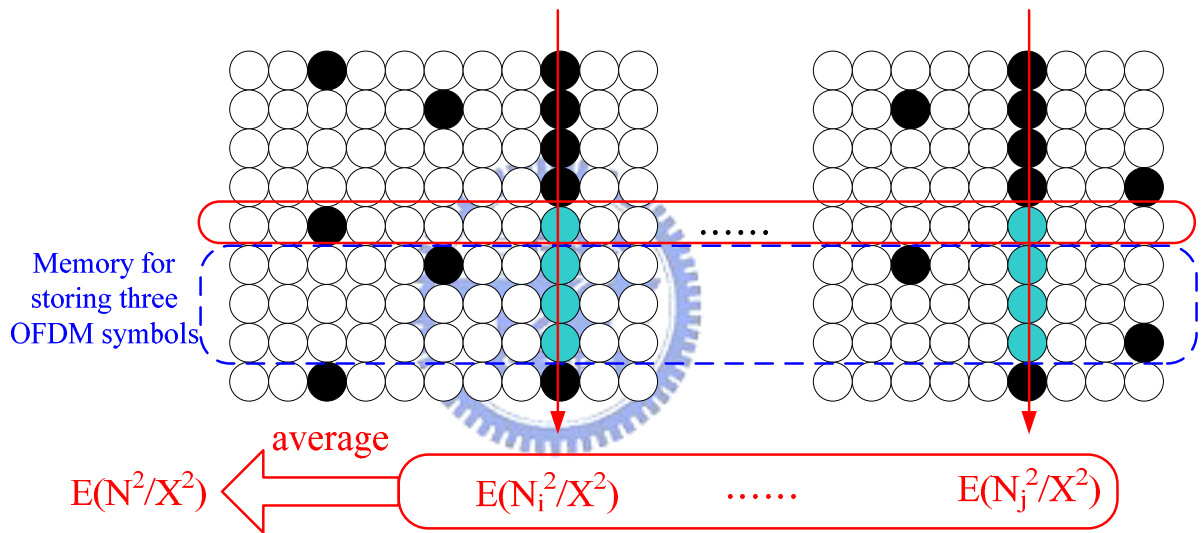


Fig. 5.6 $E[N^2/X^2]$ estimation by continuous pilots

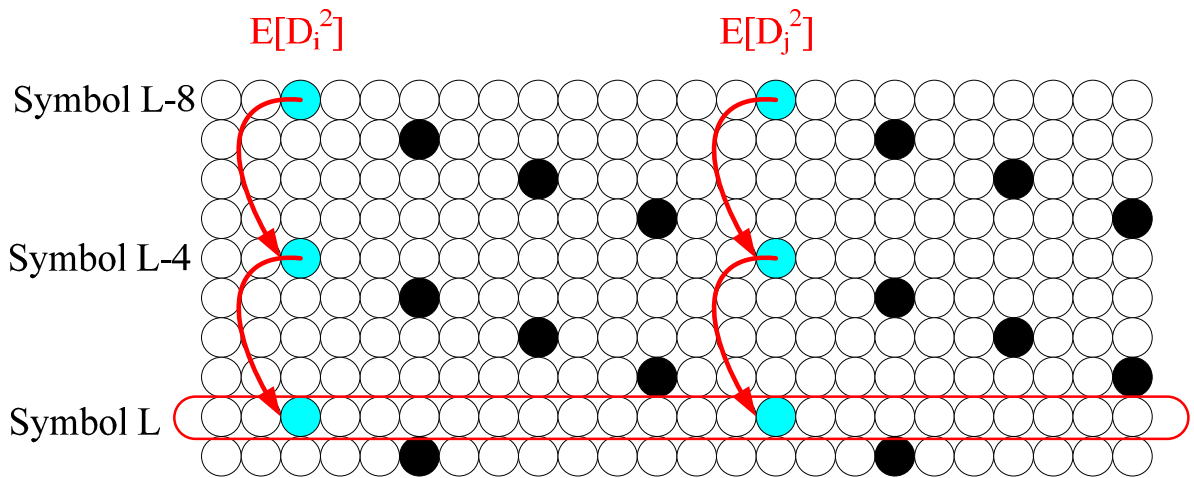


Fig. 5.7 $E[D^2]$ estimation by previous 3 samples

Table 5-2 Coefficients table for C1 and C2

β	0	0.25	0.5	0.75
C1	0	0.0977	0.5625	1.7227
C2	1	0.6016	0.3750	0.4141

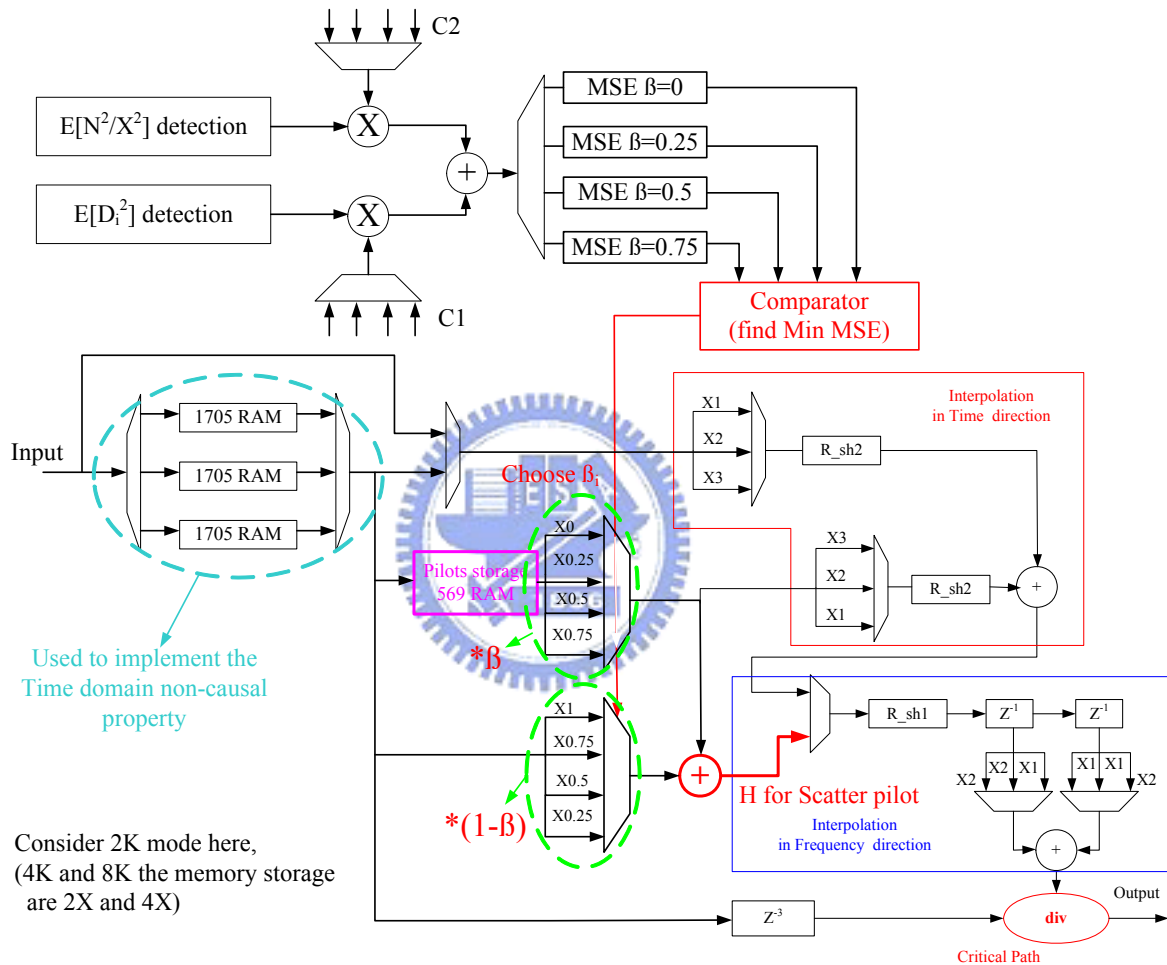


Fig. 5.8 Architecture for proposed estimation

5.3.2 Channel equalization architecture

The hardware architecture of the proposed channel equalization is shown in Fig. 5.9. In the proposed algorithm, the hardware consists of one $(2m_1)$ bits subtractor, and $(2m_1 + m_2)$ bits registers. One register updates the minuend every cycle. The other register is for keeping output stable. The minuend is selected from the dividend after shifting $(m_2 - n_2 - 1)$ bits right,

($A \ll 1$), and ($sub \ll 1$) (the result of subtraction) by MUX1 and MUX2. The subtrahend is the divisor. The control signals of MUX1 and MUX2 are depends on each state and sign bit of sub . The $q[k]$ is inverse of the sign bit of sub . Furthermore, the $q[k]$ is one bit output per cycle, so it will through an S/P after m_2 cycles to become an m_2 bits output. The ratio of working clock rate and symbol rate is $\{1:m_2\}$.

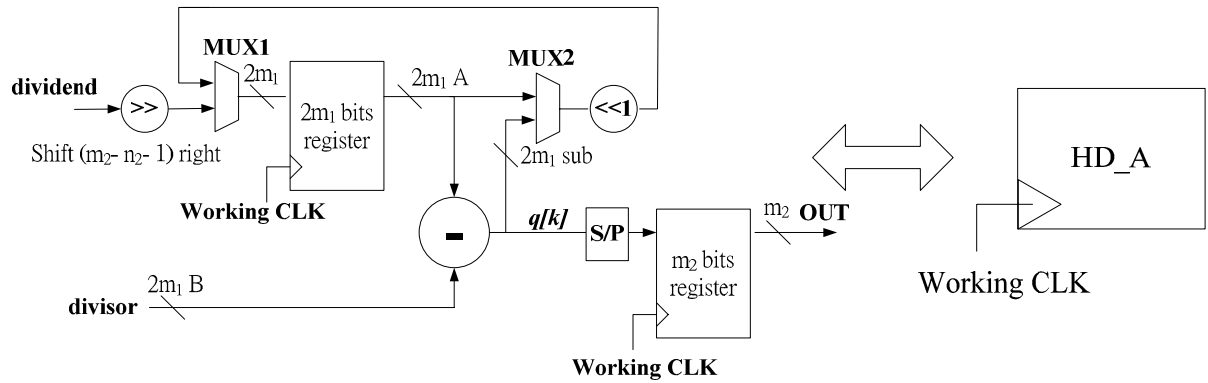


Fig. 5.9 Hardware architecture for proposed channel equalization

According to implementation loss is less than 0.15dB in equalization, we define the input and output formats are (12, 10) [28]. So we need 12 cycles for one division operation. Furthermore, in DVB-T/H system, because of 64-Qam, it will provide a 6 times clock rate (about 54.8 Mhz) for Viterbi decoder in general design. In our design, because of other function needed, it already provides a 12 times clock rate (about 109MHz). Here we provide two structures for comparisons. One is 12 cycle architecture, and it is the proposed design in paper. The other is 6 cycle architecture, but it still needs 12 cycles for one symbol division. The clock rate is not fast enough, so we can execute parallel to achieve enough through put. Here we can double the hardware and add some muxs to achieve the throughput.

The 12 cycle architecture is shown in Fig. 5.10, and the 6 cycle architecture is shown in Fig.5.11.

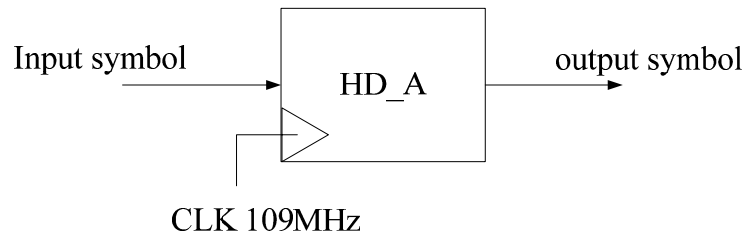


Fig. 5.10 Proposed architecture for 12 cycle

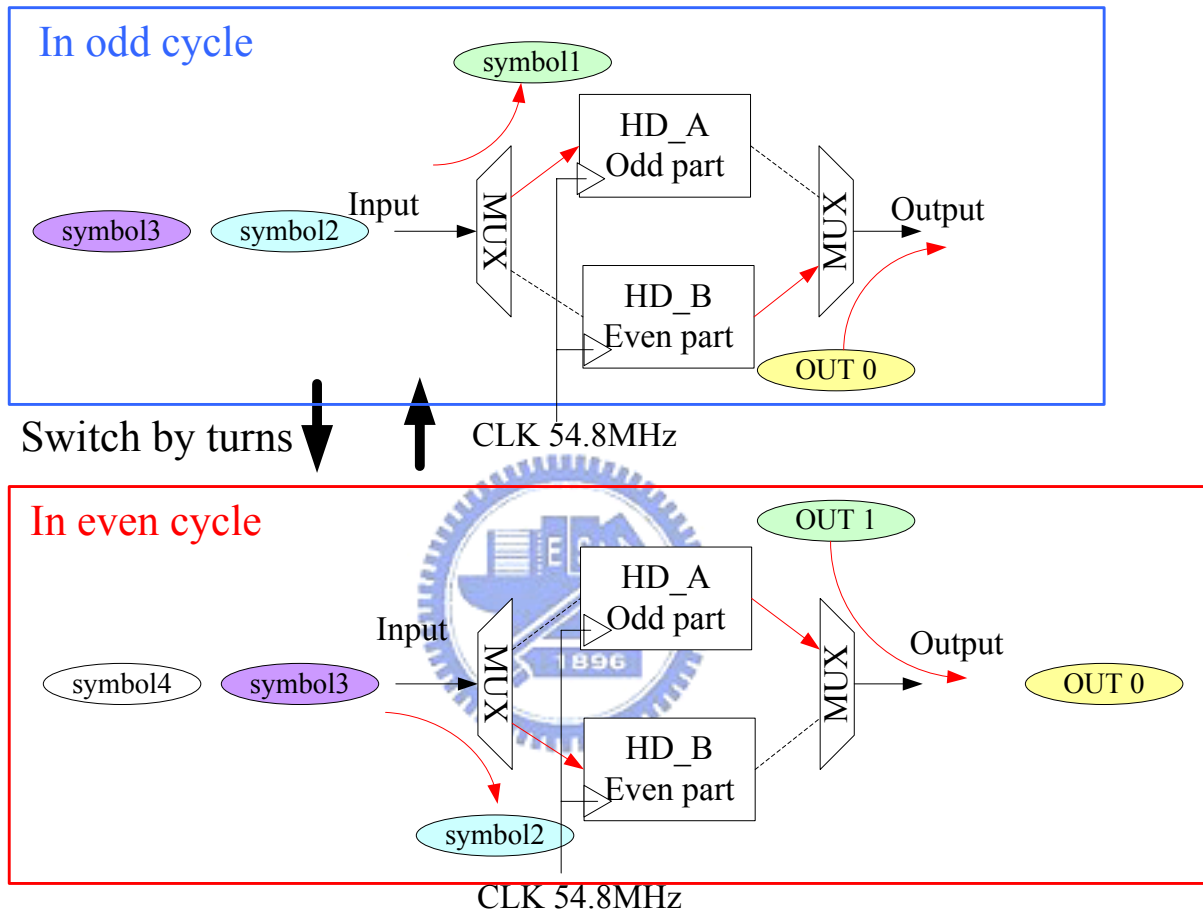


Fig. 5.11 Proposed architecture for 6 cycle

The timing diagram of these two structures is shown in Fig. 5.12. We can find the output latency is one symbol in 12 cycle architecture, but the latency is two symbols in 6 cycle architecture. We can find each operation is twice times in 6 cycle architecture. But it can be chosen by HD_A and HD_B. So it is still serial in and serial out.

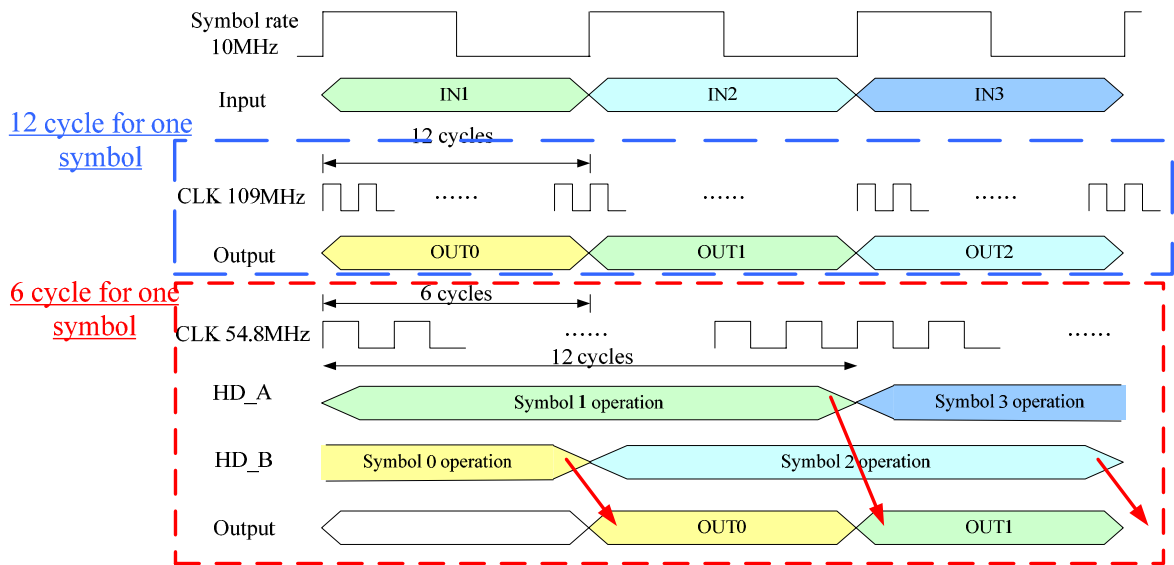


Fig. 5.12 Timing diagram

The synthesis results and gate-level simulation results by Prime-power with UMC 0.18um cell library of divider model are shown in Table 5-3. In this table we can find in our proposed design the hardware cost can be saved 90.5%, even in 6 cycle architecture, it still can be saved 81% of the original design. Furthermore, the power consumption can be reduced 59.9%, and it still can be reduced 59% in 6 cycle architecture. And the functions are consistent in three cases.

In Table 5-4, it shows the improvements ratio in the equalizer. We can find the hardware ratio of dividers in equalizer. In original design, division gate count is 62.8% of equalizer. In proposed design, we can find the division gate count is 13.9% of equalizer. So the equalizer gate count can be reduced to 43% of original design. The hardware cost is saved by 57% and power is reduced by 17% in equalizer.

Table 5-3 Synthesis and gate-level simulation results

Divider architecture	Single cycle division model	6 cycles	12 cycles (proposed in paper)
Clock rate	9.1 (64/7) Mhz [1]	54.8 Mhz	109 Mhz
Clock period	109 ns	18.16 ns	9.08 ns
Gate count (*1)	5901	1122 (561 x 2)	564
Gate count ratio of original design	100%	19%	9.5%
Power per symbol (*2)	2.184 mW	0.686 mW (0.343 mW x 2)	0.658 mW
Power ratio of original design	100%	31.4%	30.1%

Table 5-4 Comparisons for cost and power

Equalizer	Gate count (excluding SRAM)	Power consumption
Proposed design	8103	14.92 mW
Original design[28]	18777	17.98 mW
Improvements ratio	57% (10674)	17% (3.06 mW)

Chapter 6 .

Conclusion and Future Work

After the algorithm and performance analysis, the proposed low complexity adaptive weight channel estimator for pilot signal can improve the performance 0.3dB under dynamic channel with Doppler 60Hz. Furthermore, it will not degrade the performance, but the fixed weight estimator will failed in high Doppler effects.

In choosing interpolation methods, we analyze the noise term effect between polynomial interpolation methods. In noise floor region, high order interpolation methods will get better performance. However, we should focus on the QEF region. We can find the linear interpolation will better than cubic interpolation in QEF region under channel which specified by standards.

As we know the dividers cost are dominant the equalizer cost. The area and power can be further saved by exploiting add-shift divider structure. The modified division structure will save 90.5% hardware cost and 59.9% power consumption in divider itself. The hardware saved by 57% and power reduced by 17% in equalizer. Furthermore, this method can be used not only DVB-T/H system, but also the system which working clock rate is not the critical design issue.

Bibliography

- [1] Recharad Van Nee, and Ramjee Prasad, "OFDM for Wireless Multimedia Communications", pp.20-51, 2000.
- [2] Salzberg, B.R, "Performance of an Efficient Parallel Data Transmission System," *IEEE Trans. Comm.*, Vol. COM-15, pp.805-813, Dec. 1967.
- [3] ESTI EN 300 744 V1.5.1, "Digital Video Broadcasting (DVB); Framing Structure, Channel Coding and Modulation for Digital Terrestrial Television," Nov. 2004.
- [4] ESTI EN 300 401 V1.3.3, "Radio Broadcasting Systems; Digital Audio Broadcasting (DAB) to Mobile, Portable and Fixed Receivers," May 2001.
- [5] IEEE 802.11a IEEE Standards for Wireless LAN Medium Access Control and Physical Layer Specifications, Nov. 1999.
- [6] IEEE P802.15 Working Group, "Multi-band OFDM Physical Layer Proposal for IEEE 802.15 Task Group 3a," July 2003.
- [7] ESTI EN 302 304 V1.1.1, "Digital Video Broadcasting (DVB); Transmission System for Handheld Terminals (DVB-H)," Nov. 2004.
- [8] ETSI EN 301 192 V1.4.1, "Digital Video Broadcasting (DVB); DVB specification for Data Broadcasting," Nov. 2004.
- [9] P.Hoehner, S. Kaiser , and P. Robertson, "Two dimensional pilot-symbol-aided channel estimation by Wiener filtering", *IEEE ICSASSP'97*, Munich, Germany, Apr. 1997
- [10] M. Speth, S. Fechtel, G. Fock, and H. Meyr, "Optimum Receiver Design for OFDM-Based Broadband Transmission-Part II: A Case Study", *IEEE Transactions on Communications*, Apr. 2001.
- [11] Y. Zhao and A. Huang, "A novel channel estimation method for OFDM mobile

- communication systems based on pilot signals and transform-domain processing”, *1997 IEEE 47th Vehicular Technology Conference*, May 1997.
- [12] M. Nakamura and et al., “A study on an MMSE ICI canceller for OFDM under Doppler-spread channel”, *in proc. of IEEE 2003 14th International Symposium on Personal, Indoor and Mobil Radio Communication Proceedings*, Sept 2003.
- [13] V. Fischer, A. Kurpiers and D. Karsunkc, “ICI reduction method for OFDM systems”, *8th International OFDM-Workshop 2003*, Hamburg, Germany, Sept 2003.
- [14] J. Rinne, M. Renfors , “Equalization of orthogonal frequency division multiplexing signals”, *IEEE GLOBECOM’94*, Nov 1994.
- [15] T. Kella, “Decision-directed channel estimation for supporting higher terminal velocities in OFDM based WLANs”, *IEEE GLOBECOM’03*, Dec 2003.
- [16] S. Tomasin, A. Gorokhov, H-B. Yang, J-P Linnartz, “Iterative interference cancellation and channel estimation for mobile OFDM”, *IEEE Transaction on Wireless Communications*, Jan 2005.
- [17] T-A. Lin, C-Y. Lee, “Predictive Equalizer Design for DVB-T System”, *IEEE ISCAS2005*, May 2005.
- [18] L. Erup, F.M. Gardner, “Interpolation in Digital Modems-Part II: Implementation and performance”, *IEEE Transactions on Communications*, June 1993.
- [19] F.B. Hildebrand, “Introduction to Numerical Analysis”, New York:McGraw-Hill,1956, Section 2.5.
- [20] R.S. Sherratt, S.L. Linfoot, “Deterministic equalization and results of a DVB-T multipath equalizer for both 16-QAM and 64-QAM operation”, *Consumer Electronics, IEEE Trans.* Vol.49, Issue 1, Feb. 2003.
- [21] Miloš D. Ercegovac, Tomás Lang, “Digital Arithmetic”, *MK publishers*, 2004, ch.5.
- [22] Cheng-Wei Kuang, “Timing Synchronization for DVB-T System,” *MS Thesis, NCTU*,

Sep. 2004.

- [23] MOTIVATE report to the 36th DVB-TM meeting, 26,27 January 2000.
- [24] P. Robertson and S. Kaiser, "The Effects of Doppler Spreads in OFDM(A) Mobile Radio Systems," *IEEE Vehicular Technology Conf.*, Vol. 1, pp. 329-333, Sep. 1999.
- [25] W. C. Jakes, "Microwave Mobile Communications," *John Wiley & Sons Inc.*, 1974.
- [26] M. Patzold and F. Laue, "Statistical properties of Jakes' fading channel simulator", *1998 IEEE 48th Vehicular Technology Conference*, May 1998.
- [27] P. Dent, G.E. Bottomley, and T.Croft, "Jakes fading model revisited", *IEE Electronic Letters*, June 1993.
- [28] L-F. Chen, Y. Chen, L-C. Chien, Y-H. Ma, C-H. Lee, Y-W. Lin, C-C. Lin, H-Y. Liu, T-Yi. Hsu, C-Y. Lee, "A 1.8V 250mW COFDM Basedband Receiver for DVB-T/H Applications", *ISSCC Digest of Technical Papers*, Feb. 2006.
- [29] Yu-Wei Lin, "The Matrix Prefetch Buffer Based FFT Processor," *MS Thesis, NCTU*, Jun. 2003.
- [30] Y-H. Ma, L-F. Chen, C-Y. Lee, "A Channel Equalizer Design for COFDM System", *IEEE VLSI-DAT'06*, April 2006.

作者簡歷

姓名：馬英豪

出生地：台灣省桃園縣

出生日期：1981. 12. 02

學歷：1988. 9 ~ 1994. 6 新竹縣立長安國民小學

1994. 9 ~ 1997. 6 新竹縣立湖口國民中學

1997. 9 ~ 2000. 6 國立新竹高中

2000. 9 ~ 2004. 6 國立交通大學 電子工程學系 學士

2004. 9 ~ 2006. 7 國立交通大學 電子研究所 系統組 碩士



得獎事績

2005/05 2005 全國 IC 設計競賽優等獎

2006/05 2006 全國 IC 設計競賽佳作獎

發 表 論 文

- Lei-Fone Chen, Yuan Chen, Lu-Chung Chien, **Ying-Hao Ma**, Chia-Hao Lee, Yu-Wei Lin, Chien-Ching Lin, Hsuan-Yu Liu, Terng-Yin Hsu, Chen-Yi Lee, “**A 1.8V 250mW COFDM Basedband Receiver for DVB-T/H Applications**”, *ISSCC Digest of Technical Papers*, pp. 262-263, San Francisco, USA, Feb. 2006.
- **Ying-Hao Ma**, Lei-Fone Chen, Chen-Yi Lee, “**A Channel Equalizer Design for COFDM System**”, *2006 IEEE International Symposium on VLSI Design, Automation, and Test (VLSI-DAT'06)*, pp. 75-78, HsinChu, Taiwan, April 2006.
- Chia-Hao Lee, Lei-Fone Chen, **Ying-Hao Ma**, Chen-Yi Lee, “**Phase Alignment with 2D Channel Estimation Method for DVB-T/H Application**”, *accepted by 17th VLSI Design/CAD Symposium*, Aug. 2006.

